Doctoral theses at NTNU, 2013:263

Tung Manh

Development of High Frequency Miniature Ultrasound Transducers

Doctoral thesis

Tung Manh

ISBN 978-82-471-4652-1 (printed ver.)
ISBN 978-82-471-4653-8 (electronic ver.)
ISSN 1503-8181

NTNU – Trondheim
Norwegian University of
Science and Technology

Doctoral theses at NTNU, 2013:263

NTNU
Norwegian University of
Science and Technology
Thesis for the degree of
Philosophiae Doctor
Faculty of Medicine
Department of Circulation and Medical Imaging

NTNU – Trondheim
Norwegian University of
Science and Technology

Tung Manh

Development of High Frequency Miniature Ultrasound Transducers

Thesis for the degree of Philosophiae Doctor

Trondheim, October 2013

Norwegian University of Science and Technology
Faculty of Medicine
Department of Circulation and Medical Imaging

NTNU – Trondheim
Norwegian University of
Science and Technology

NTNU
Norwegian University of Science and Technology

Thesis for the degree of Philosophiae Doctor

Faculty of Medicine
Department of Circulation and Medical Imaging

ISBN 978-82-471-4652-1 (printed ver.)
ISBN 978-82-471-4653-8 (electronic ver.)
ISSN 1503-8181

Doctoral theses at NTNU, 2013:263

Printed by NTNU-trykk

Utvikling av høyfrekvente miniatyr ultralydtransdusere

Diagnostisk ultralydavbildning benytter vanligvis frekvenser i området fra 2 til 10 MHz. Men i moderne ultralydteknologi ser vi nå økende bruk av høyere frekvenser, over 10 MHz, da dette gjør det mulig å avbilde mikrostrukturen i bløtt vev, eksempler er små tumorer eller veggen i blodårene. Disse teknikkene krever små høyfrekvente ultralydtransdusere med stor båndbredde, for å gi bilder med høy oppløsning der avstanden til objektet er kort. Lav kostnad er også ønskelig, spesielt for engangsutstyr. I denne oppgaven er det sett på en ny metode for å produsere slike transdusere, basert på mikromaskinering av silisium. Metodene som benyttes er veletablerte for masseproduksjon av identiske komponenter på en enkelt silisiumskive, for eksempel innen produksjon av mikrosensorer.

Transduseren er den delen av ultralydsystemet som sender ut og tar i mot lydbølgene. De fleste av dagens transdusere benytter en piezoelektrisk plate for å generere og motta lydbølger. For å overføre lydenergien effektivt mellom det piezoelektriske elementet og vevet legges det inn flere akustiske tilpasnings-lag. Når frekvensene blir høye og dimensjonene små byr dette på to utfordringer: Tykkelsen av lagene kan være vanskelig å styre nøyaktig nok, og det kan være vanskelig å finne eller framstille materialer med de ønskede akustiske egenskapene.

Denne oppgaven ser spesielt på den siste av disse utfordringene. Materialer med definerte akustiske egenskaper er framstilt som kompositter av silisium og polymer. To forskjellige metoder for mikrofabrikasjon av silisium er prøvd ut for å få materialer med de ønskende egenskapene: Anisotrop våt-ets og dyp reaktiv ione ets (DRIE). Teoretiske modeller er utviklet og datamaskinsimuleringer og eksperimentelle målinger er gjort for å forstå de akustiske egenskapene til disse nye kompositttmaterialene. Komplette ultralydtransdusere er produsert og undersøkt, der silisium-polymer-kompositt utgjorde enten det eneste tilpasningslaget, eller inngikk som en del av en struktur med flere lag. Den gode ytelsen til disse transduserne har demonstrert at den nye fabrikasjonsmetoden bør være velegnet til produksjon av ultralydtransdusere.

Kandidat: TUNG MANH
Institutt: Institutt for sirkulasjon og bildediagnostikk, DMF, NTNU.
Veiledere: Førsteamanuensis Tonni F. Johansen, NTNU, og Professor Lars Hoff, Høgskolen i Vestfold.
Finansieringskilde: Norges forskningsråd, prosjekt nr. 176540, 191282 og 181712/I30.

Ovennevnte avhandling er funnet verdig til å forsvares offentlig
for graden PhD i Medisinsk Teknologi.
Disputas finner sted i Auditoriet, Medisinsk-teknisk forskningssenter,
fredag 15. november 2013, kl. 12.15.

Abstract

Small, high frequency ($\geq$ 10MHz) broadband ultrasound transducers are required in modern medical imaging systems to provide short range, high resolution images for studying of microstructures in soft tissues, such as the composition of small tumors or a vessel wall. The manufacturing of these probes using conventional methods, i.e. lapping and dicing, becomes difficult and expensive for high frequency applications and there is a need to produce small ultrasound transducers with low cost and high reliability. Being identified as one of the key technologies that has produced μ-scale, high volume products in a wide variery of markets such as electronics, telecommunications, automobiles, etc..., Micro-Electro-Mechanical-Systems (MEMS) technology seems to deliver a good solution.

This thesis presents the development of novel small-sized, high frequency broadband ultrasound transducers based on silicon processing borrowed from the MEMS industry. We have categorized the work in this thesis within two main themes:

1. The modeling, fabrication and characterization of silicon-polymer composite acoustic matching layers formed by MEMS techniques. Two different micromachining approaches have been employed: Deep Reactive Ion Etch (DRIE) and Anisotropic Wet Etch. The modeling of the micromachined composite materials was carried out both by analytical and finite element method (FEM) simulations. The properties of the fabricated composites were extracted via electrical impedance and pulse-echo measurements of air-backed transducers.
2. The design, fabrication and characterization of high frequency (15 MHz) broadband ultrasound transducers, where the composite materials described above were used as an intermediate layer in the stack of multiple matching layers.

The main contributions are:

1. Fabrication and testing of silicon-polymer composites made by an advanced technique, DRIE, used as matching layers for 15 MHz ultrasound transducers. A method for extracting the composite properties via inversion scheme from electrical impedance measurements of air-backed transducers with composites as single matching layers was proposed.
2. Modeling of silicon-polymer composite materials and ultrasound transducers under different circumstances, i.e. in contact with fluid/solid media. This provides the understanding of the dynamic behavior of the silicon-polymer composite, helps to define the maximum allowable period sizes and properties of the composites without influence the transducer's performance. The modeling was carried out by analytical calculations and FEM simulations.
3. Development of an in-house anisotropic wet etching process of silicon to form well-defined size, high aspect ratio, vertical sidewall trenches. This process is benificial for constructing of many MEMS devices for various applications such as biological, optical and energy harvesting sensors.
4. Development of an in-house fabrication process to manufacture high frequency broadband ultrasound transducers based on micromachining techniques, i.e. photolithography and anisotropic wet etch of (110)-oriented silicon wafers.

Preface

This doctoral thesis is submitted in partial fulfilment of the requirements for the degree of Philosophiae Doctor at the Faculty of Medicine, Norwegian University of Science and Technology (NTNU), Norway.

The PhD work was carried out at the Department of Micro and Nano Systems Technology (IMST), Faculty of Technology and Maritime Sciences, Vestfold University College (HiVe) in Horten, Norway and in collabration with the Department of Circulation and Medical Imaging, Faculty of Medicine, NTNU (Trondheim, Norway) and SINTEF ICT (Oslo, Norway) under the supervison of Professor Lars Hoff, HiVe, and Associate Professor Tonni Franke Johansen, NTNU.

The study is funded by the Research Council of Norway under Grants No. 176540, 191282 and 181712/I30.

Acknowledgements

First of all, I would like to express my sincere gratitude to my supervisors, Professor Lars Hoff and Associate Professor Tonni F. Johansen, for the guidance and support throughout my PhD research.

Professor Lars Hoff has been invaluable for the success of my PhD work. His advices and encouragements have helped me keeping neccesary progression and his positive attitude has always inspired my morale.

Associate Professor Tonni F. Johansen has been very important to my PhD project. His fruitful discussions and practical experience in manufacturing and characterization of ultrasound transducers help me a lot during my PhD research duration.

My deep gratitude also goes to the staffs at SINTEF MiNaLab, Dag Wang, Geir Uri Jensen, and Lars Geir Whist Tvedt, who have been involved in my PhD project. Special thanks to Geir Uri Jensen for fabrication of the etched structures by deep reactive ion method and giving constructive comments for improving the research.

I would like to thank Professor Bjønrn Angelsen and my colleagues at the Department of Circulation and Medical Imaging, NTNU, for the discussions and contributions to my PhD work. Specical thanks to Tarjei Rommetveit, Martijn E. Frijlink, and Jochen Deibele for the interesting conversations and practical assistance during the unforgetable time I spent in Trondheim.

I am also grateful to my colleagues at IMST, HiVe, for the meaningful discussions and contributions to my thesis. Special thanks to Zekija Ramic, Tormod Vinsand, Ragnar Dahl Johansen and Svein Mindrebøe for the constant support in the labratory. Great thanks to Tone Gran for the devoted assistance with the administrative process. Many thanks also go to Anh-Tuan Thai Nguyen and Suong Thi Thu Vo, who had worked with me during their Master projects. Working with you was a great pleasure and I have learned uncountable experiences from all of you.

The Research Council of Norway is thankfully acknowledged for the financial support for this PhD study. The Norwegian PhD Network on Nanotechnology for Microsystems is also deeply acknowledged for granting the travel supports to the international conferences.

Finally, I would like to thank my family and friends for the support, understanding and encouragement during these years.

Contents

List of Tables

List of Figures

Chapter 1

Introduction

1.1 Background and motivation

1.1.1 Micro-Electro-Mechanical-Systems

Micro-Electro-Mechanical-Systems (MEMS) has experienced remarkable growth since the early 1950's. The term MEMS refers to the use of tools and techniques developed for the integrated circuit industry such as microlithography, etching, etc...to create miniaturized sensors and actuators with the feature sizes in the range from a few micrometers to millimeters [1,2]. Though developed from microelectronics, MEMS now is a distinct field with market value exceeding 1 billion US dollars and predicted average annual growth of 13% in revenues (reported by Yole Dévelopment, France in 2012) [3]. Being identified as one of the most promising technologies for the 21st century, high volume MEMS products now can be found in a wide variety of applications across multiple markets such as automotive, aerospace & defense, optical/telecommunications and biomedical systems [3, 4]. Some examples of MEMS-based devices that have been developed at the Department of Micro and Nano Systems Technology (IMST), Vestfold University College (HiVe) are summarized in Fig. 1.1 including micro2phone [5], MEMS energy harvesting device [6], optical de-speckle modulator [7], fluidic device [8], miniature ultrasound transducer [9] and miniature heart monitoring sensor [10].

The reasons prompting the development of MEMS technology can be classified into three categories [11]:

1. Miniaturization of existing devices.
2. Using physical principles not working at larger scale.
3. Developing tools for operation in the micro-world.

Among of them, miniaturization is the most critical factor [11]. Size reduction brings performance benefits such as higher speed, lower power consumption, and more com-

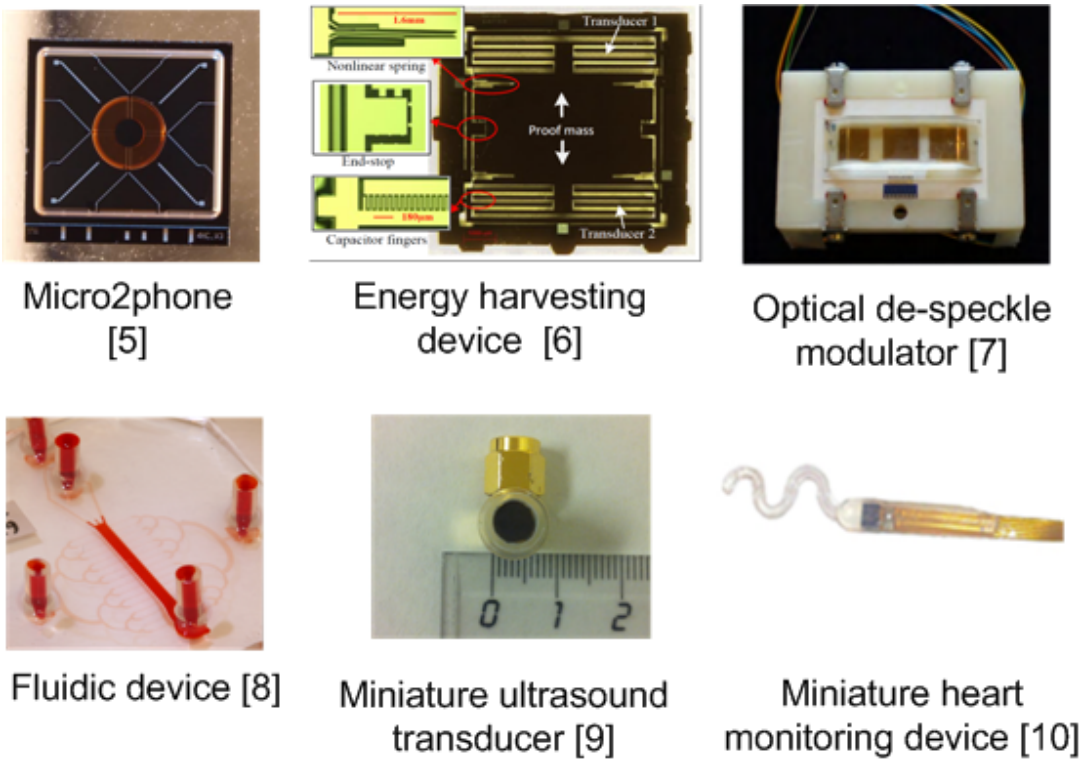

Figure 1.1: Examples of MEMS-based devices developed at IMST, HiVe [5–10]

plexity (higher intergration applicability) [12]. But, above all, economy is an important driver behind as size reduction decreases material consumption and allows batch fabrication [11, 12]. Moreover, MEMS on silicon can also be integrated directly with the electronics on the same chip, and can be packed in the same package. This increases realibily and decrease assembly cost, bringing new application opportunities, including those in medical ultrasound imaging.

1.1.2 Medical ultrasound imaging

Ultrasound technology involves the use of sound waves in the frequency range above the audible range, i.e. from 20 KHz to a few hundreds MHz, to detect/image target objects. The first use of sound waves for ranging measurements was in sonar systems during World War I to fulfill the need of locating the submarines and mines, etc... [13, 14]. This technology is also a well-established method in the nondestructive testing (NDT) community to find flaws in materials and measure thickness of objects [15]. However, the most well-known applicability of ultrasound is in the field of medicine where the backscattered signals can be used to image the tissue structures or, using the Doppler effects, to measure and image the velocity of blood [16]. Initially used in therapy in the 1920's, ultrasound was first realized as a potential diagnostic imaging tool as early as the late 1940's [14, 17]. Since then, medical ultrasound imaging has grown up tremendously and now is a popu-

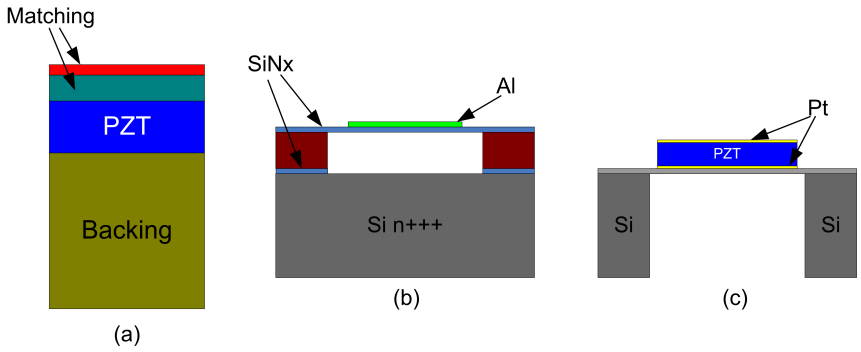

Figure 1.2: A schematic of a typical (a) piezoelectric transducer, (b) CMUT, and (c) pMUT.

lar diagnostic tool in many areas in medicine such as echocardiography, abdominal and obstetric ultrasonography and intravascular applications. From the first commercial contact B-mode static scanners in the early 1960's [14], modern ultrasound imaging systems nowadays can be found in pocket/laptop-sizes [17], be able to produce three-dimensional (3D) images in real-time [18–20], and image structures as small as a couple tens of micrometers [21]. Compared with other modalities such as X-ray, Computed Tomography (CT) , and Magnetic Resonance Imaging (MRI), ultrasound is considered as a preferred imaging method due to its low cost, non-invasiveness, and portability [14].

1.1.3 High frequency ultrasound transducers

An ultrasound transducer is one of the most important components in a medical ultrasound imaging system. This sensing device interacts with the load medium by conversing eletrical energy to mechanical waves transmitted to the human tissue and transforming backscattered waves to electrical signals. Most ultrasonic transducers are currently based on a multilayer structure of one piezoelectric ceramic/piezocomposite as active element, operating in thickness mode; one heavy/soft backing on the backside and several matching layers on the other side of the piezoelectric plate to effectively couple energy from the active element to the human tissue. A schematic of a typical piezoelectric transducer is shown in Fig.1.2(a). Table 1.1 shows some piezoelectric materials used as active layers in ultrasound transducer designs, where ϵ_{33}^{S} is the material permittivity at constant strain in the thickness direction; ϵ_0 is the vacuum permittivity; k_t is the electromechanical coupling factor in the thickness direction presenting the efficiency of converting electric energy to acoustic energy and vice versa; and Z denotes the acoustic impedance, i.e. the product of material density and longitudinal wave velocity.

Diagnostic ultrasound usually operates in the range 2-10 MHz for transcutaneous measurements, but a trend in ultrasound imaging technology is to move to higher frequency applications ($\geq$ 10 MHz) for studying of microstructures in soft tissues, such as the composition of small tumors or a vessel wall. Some of the high frequency ($\geq$ 10 MHz)

Material	$\epsilon_{33}^{S}/\epsilon_0$	k_t	**Z (MRayl)**	**References**
PVDF	5-13	0.12 - 0.15	3.92	[22]
P(VDF-TrFE)	6-9	~ 0.30	4.00	[23]
$LiNbO_3$ 36° Y-cut	39	0.49	34.00	[23]
$KNbO_3$ 49.5° X-cut	45	0.67	34.70	[22]
$PbTiO_3$	200	0.50	36.00	[23]
PMN-PT	680-800	0.58	37.10	[22]
PMN-33% PT single crystal 1-3 composite	500	0.71	20.00	[23, 24]
PZT-5A (bulk ceramic)	830	0.48	33.70	[16]
PZT-5H (bulk ceramic)	1470	0.51	34.40	[16]
Thick-film Pz29 (Tape-casting)	1055-1250	0.41-0.45	33.70-35.90	[25]
Thick-film PZT (Screen-printing)	370	0.49	17.90	[26]
Thick-film PZT (Sol-gel)	680	-	22.00	[27]

Table 1.1: Piezoelectric materials used in ultrasound transducer designs

medical imaging applications are intravascular imaging of coronary arteries [28, 29], intravascular imaging of cartilage [30], imaging of the eye [31–34], and imaging of the skin [32,35]. In such a high frequency medical imaging system, a small, broadband transducer is required to provide short range, high resolution images in both lateral and axial directions. Miniaturization is therefore required to produce small-size, reliable ultrasound imaging probes with low cost and MEMS technology seems to deliver a good solution.

The MEMS-based transducers which have been received extensive interest in the field recently are the Capacitive Micromachined Ultrasound Transducers (CMUTs) [36–46]. Instead of using piezoelectric principle as in most of the conventional ultrasonic transducers, the CMUTs employ the electromechanical transduction mechanism based on capacitance changing. A typical CMUT consists of a thin membrane suspended on an air-filled gap, a metallized layer on top of the membrane as the top electrode, and the silicon substrate serving as the bottom electrode [Fig.1.2(b)]. When bias DC voltage is applied between the metallized membrane and the substrate, the electrostatic force attracts the membrance towards the substrate, whereas the mechanical force due to the stiffness of the membrane balances the attraction. If an AC signal is superposed on the biased electrodes, the membrane will vibrates to transmit sound waves and vice versa. Possessing some advantages compared to traditional piezoelectric transducers such as no matching layers required, wide achieveble bandwidth (>100%), improved radial resolution, contrast enhanced, and integrated electronics capability, the CMUTs are believed the future probes [39–41]. However, the CMUTs have not been widely released in commercial market yet. Some of the drawbacks that pospone the public use of the CMUTs are their low sensitivity, i.e. limited penetration depth [42, 43], low signal to noise ratio [42], charging

effects [45, 47] and cross-talk [44].

Another approach to apply micromachining on transducer manufacturing is the piezoelectric Micromachined Ultrasonic Transducers (pMUTs) [48–50] . The pMUTs share the same structure as the CMUTs, i.e. consisting of a large number of micromembranes; but their operation is based on piezoelectric effect in a flextensional mode. A typical pMUT is shown in Fig.1.2(c), where a transversally poled piezoelectric layer is bonded on a clamped metal plate. As an electric field is applied across the piezoelectric layer, it attempts to deform in the lateral direction due to the transversal coupling, causing flexural vibration and hence, the vibration of the membrane. Compared with the CMUTs, the pMUTs show advantages as lower electrical impedance and better matching with the front-end electronics, and reducing parasitic capacitance influence to the sensitivity of the transducer [50]. However, the pMUTs is are just at the early stage of development and their potential still needs to be proven. Some challenges associated with the pMUTs are the PZT deposition is time-consuming, the fabricated PZT layer is easily cracked and the process is not fully compatible with the standard MEMS techniques [50].

Besides the trends of manufacturing devices based on novel working principles as the two mentioned approaches, there are also many efforts to produce conventional piezoelectric transducers at high frequency range (10-100 MHz). In fact, two major challenges when manufacturing these devices are obtaining the correct thickness of the active layer and matching the high acoustic impedance of this layer to that of the human tissue. As the thickness of the active layer is inversely proportional to the transducer's center frequency, this layer must be in between 20-200 μm to operate in the range 10-100 MHz. However, the common lapping technology to manufacture plates with correct thickness becomes difficult and expensive at thicknesses in ranges below 50-60 μm, corresponding to frequencies above 30-40 MHz. Piezoelectric polymers such as polyvinylidene fluoride (PVDF) or poly(vinylidene fluoride-trifluoroethylene) P(VDF-TrFE) are often the choice for high frequency transducers due to their flexible mechanical properties, low acoustic impedance and thin thicknesses that can be obtained by current technology (covering a wide range of frequency from 20 to over 100 MHz) [26, 51]. However, the relatively low thickness coupling factor (k_t=12-30%, see Table 1.1) causes low transducer sensitivity. Another solution receiving enormous attention recently to produce active layers working at high frequency range is to use piezoelectric ceramic thick films. Several manufacturing approaches have been proposed such as tape casting [52], screen-printing [26], and sol-gel or sol-gel composites [27, 53, 54]. The first method can produce thick films with thicknesses in the range 0.1-2 mm [25] and the material properties are comparable with those of bulk ceramic (acoustic impedance Z $\geq$ 30 MRayl, k_t=41-45%, see Table 1.1); whereas with the other two, a film with a few tens micron thickness is achievable, but due to the film's porosity, its acoustic impedance is reduced to about that of silicon [26,27,53]. In the last two methods, a temporary substrate is required as a carrier for the films to be deposited on and it is usually removed by delicate steps to obtain operating transducers. Depending on specific process, aluminum (Al), Pt-coated silicon (Si) or porous PZT can be chosen as substrates [26, 27, 52, 53]. Si is the preferable material as it is electronics compatible and can stand high annealing temperature. Therefore, using it as substrate

helps to improve the film qualities [27].

As shown in Table 1.1, except PVDF and P(VDF-TrFE) with acoustic impedances ~ 4 MRayl, the acoustic impedance of the active layer ($\sim$ 18-37 MRayl) is much higher than that of the human tissue ($\sim$ 1.54 MRayl). To effectively couple energy into the human tissue, one or more matching layers with a thickness of a quarter of wavelength are required [55]. These matching layers should have acoustic impedance in between that of the active layer and the load medium. Finding a single-phase material with the required impedance is not allways possible and composites are often used. The most common form of composite matching layers is in 0-3 connectivity, i.e. a mixture of particles in an epoxy resin. Two main concerns about this technique are the uniformity (in one batch and from batch to batch) and its poor performance at high frequencies [55, 56]. To achieve acoustic impedance in the range 8-15 MRayl, a quite large volume fraction of particles is required [55]. This increases the probability of particles to come into contact and change the composite acoustic properties, especially at high frequencies. Some solid materials such as glass and graphite have also been considered as matching layers. However, there is the classical problem of assembling these pre-fabricated matching layers into the transducer's stack since the bonding line may destroy the effectiveness of the matching layers [57]. In the early 1990's, M. Haller and Khuri-Yakub [56, 58] demonstrated a technique borrowed from micromachining industry to fabricate a 2-2 composite matching material from silicon, using anisotropic wet etch along the crystal planes. This formed deep long trenches into (110)-oriented silicon wafers, which were subsequently filled with epoxy resin. The method can produce small structures with controlled volume fraction and should be appropriate for transducers operating at high frequencies. However, the method requires accurate alignment of the long straight line features to the $\{111\}$ planes in the silicon within 0.1°, which can be demanding if structures are less than 2 μm wide [59]. Though the method was introduced, the theoretical background was not well investigated. The work was lie on the iso-strain model [60], which is only valid as the composite period is much smaller than the wavelength. It is more interesting to see how the composite structures behave as the lateral dimension is comparable with the acoustical wavelength. It is also important to find how coarse the structures should be so that it could be used as matching layers in ultrasound transducers without degrading the transducers' performance. Moreover, the fabrication process to produce the etched trenches was not fully described in these previous studies. The obtained materials were manufactured for transducers working at 1-5 MHz, which is fairly low compared to the requirements for modern transducers operating above 10 MHz.

1.2 Research goals and tasks

The "High frequency miniature ultrasound transducers"project funded by Norwegian Research Council is intended to develop a miniaturized transducer using MEMS technology. Instead of following the CMUT trend, this Ph.D work focuses on the development of ultrasound transducers based on piezoelectric thick-film on silicon wafer and bulk microma-

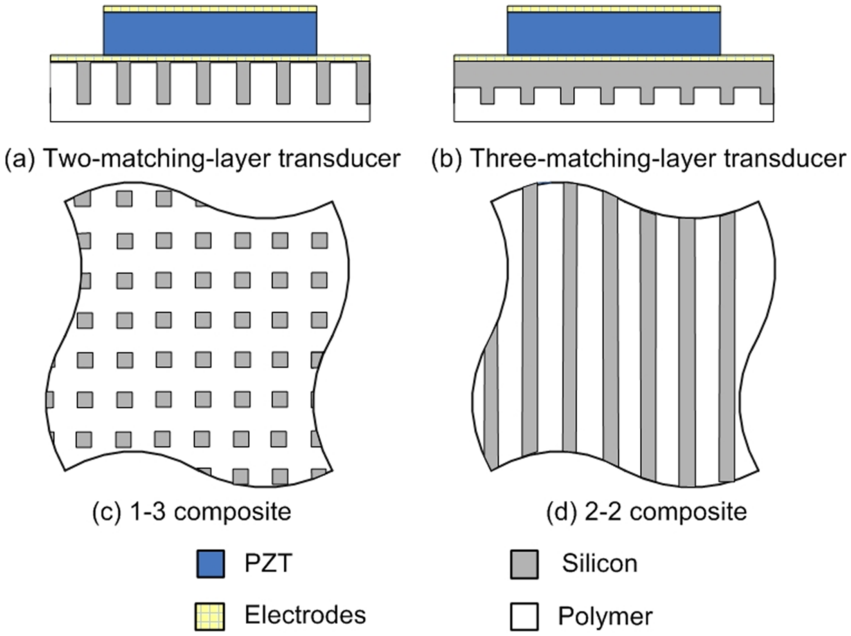

Figure 1.3: Proposed multiple-matching-layer transducers (a) Two-matching-layer transducer (b) Three-matching-layer transducer (c) 1-3 composite (d) 2-2 composite

chining processes [see Fig.1.3(a) and (b)]. The PZT film vibrates in thickness mode and the generated waves are transmitted through the substrate. Applying modern micromachining techniques, e.g. photholithography and etch, the silicon substrate can be formed to a passive acoustic matching layer stack through machining and adding polymer. In this way, the substrate is modified into multiple layers with descending characteristic acoustic impedance from the piezoelectric plate to the load material, so that it performs an acoustic impedance matching between the load material and the piezoelectric plate, to increase the transducer bandwidth, while the transducer is left air backed. Instead of performing alternately deposition and lapping layer by layer as in conventional transducer manufacturing process, the proposed structure allows to build a stack of multiple layers as one, which is advantageous for thin transducers, e.g. less than 100 μm. This method is promising for low cost, mass-production of high frequency broadband transducers.

Following the initial works of Haller and Khuri-Yakub [56, 58, 61, 62] on micromachined composites (tested at 1-5 MHz), the ultimate goal of this project has been to develop mass-product, multiple matching layer micromachined transducers working at higher frequencies, potentially used in intravascular applications. The initial idea was using available thick-film technology from InSensor (Kvistgaard, Denmark) to build thick-film PZT on Pt-coated silicon substrate, and then the proceed substrate would be micromachined with available equipments at IMST, HiVe, Norway. Due to some limitations of available infrastructures, the thick-film PZTs were replaced by bulk ceramics (PZT-5A, Boston Piezo-optics, Bellingham, MA, USA) and the test prototypes were fabricated for operating at the center frequency of 15 MHz, though the initial idea was to manufacture transducers working at higher frequencies ($\geq$ 30 MHz). However, if the method has been

proven to work, it is possible to scale up the working frequency. The project is the combination between analytical and Finite Element Method (FEM) modeling, and experimental work, where the experimental part is the most crucial task. During the course of work, it was found to be a wide topic across multiple fields such as material engineering, ultrasound and micromachining technologies. The following subtasks have been identified and resolved:

1. Formulate an analytical calculation as the basis for the composite design and characterization. The theoretical calculations assist chosing the suitable composite lateral scale and finding appropriate composite properties. This was only achievable for silicon-polymer 2-2 composites where dispersion curves found from partial wave solutions were presented. Due to the mathematical complexity, the analytical calculation for silicon-polymer 1-3 composite was ignored and the FEM simulations were employed instead.

2. Model the behaviors of the composites and the transducers using FEM software, i.e. COMSOL Multiphysics (COMSOL AB, Stockholm, Sweden). This includes eigenvalue calculations of the composites and modeling of the micromachined ultrasound transducers under specific circumstances, e.g. interaction with surrounding load medium such as fluids and solids. Both 2-2 and 1-3 composites were investigated.

3. Design and fabricate 2-2 and 1-3 composites based on two different micromachining techniques: anisotropic wet etch and deep reactive ion etch (DRIE) to form μ-sized structures. The DRIE process was done by Geir Uri Jensen at SINTEF MiNaLab and the wet etching process was performed by the author at HiVe. Testing prototypes were manufactured for transducers working at 15 MHz.

4. Assemble the air-backed transducers.

5. Characterization of the composite materials, the PZT plates and the transducers at high frequencies. The method to extract material properties via inversion scheme was proposed. The pulse-echo measurements were also performed.

The work can be summarized in four below articles:

1. Microfabrication of silicon-polymer 1-3 composite acoustic matching layers for ultrasound transducers based on DRIE method. This includes FEM modeling, fabrication and characterization of the composite materials.

2. Modeling of microfabricated silicon-polymer 2-2 composite materials as matching layers for high frequency ultrasound transducers. This includes analytical calculation, FEM modeling and measurements where the measured results support the analytical calculation and FEM simulations.

3. Fabrication of deep, long, vertical trenches using anisotropic wet etch of silicon. This describes the fabrication process in detail and this recipe can be used as an internal document at IMST lab, HiVe, to fabricate similar structures that might be useful for many other applications such as microfluidic, optical and energy harvest-

ing MEMS structures [59, 63–68].

4. Development of high frequency (15 MHz) ultrasound transducers with multiple matching layers based on micromachining of silicon.

1.3 Silicon-polymer composites

Composites have been widely used in ultrasound transducers as active layers (piezoelectric composite materials) due to its advanced properties such as low characteristic impedance, large dielectric permittivity and high electromechanical coupling factor [24, 60, 69–71]. The work of Newnham *et. al.* [72] classified composite materials according to the connectivity of the constituent phases, and there are 16 composite patterns that can be identified for a bi-phase material. Among them, the 0-3, 2-2 and 1-3 connectivity composites (Figure1.4) are the most practical in transducer engineering.

0-3 composite materials are commonly used as matching layers, whereas the other two, 2-2 and 1-3 composites, are extensively used as active materials. The current method to produce these two last materials is dice-and-fill, where the ceramic plate is diced into small posts, and kerfs are filled with polymer. This technique has difficulties in making structures with ceramic post width and epoxy kerf width below approximately 50 and 10 μm, which limits the operating frequencies to approximately 20 MHz [70]. The work presented in this thesis deals with silicon-polymer composites as passive materials for use as matching layers. Micromachining technology allows fabricating composite material with much smaller period and hence, potentially used at higher frequencies. Using the etching of silicon, deep trenches are etched into a substrate. These trenches are then filled with low impedance polymer. By adjusting the width and period of the silicon trench, the acoustic impedance of the material can be selected. The minimum and maximum obtainable impedances are limited by the impedance of the polymer and silicon, respectively.

1.3.1 Analytical models

Considering the silicon-polymer 2-2 and 1-3 composites as shown in Figure 1.4(b) and (c), where the bright denotes silicon and the dark denotes polymer, respectively. If the structures in the composite are much smaller than the acoustic wavelength, the composite will acoustically behave like one effective medium, and its effective acoustic impedance and speed of sound are described by the iso-strain model [60]. In contrast, if the finite dimensions of the composite are considered, the dynamic model of guided waves [69, 73] provides better estimations of the material properties.

- **Iso-strain model** [60] Assumed the lateral dimensions of the composite unit cell are sufficiently fine, effective parameters of the composite are

$$\bar{c}_{33}^{C} = \Phi^{Si}[c_{33}^{Si} - \Phi^{p}\frac{(c_{12}^{p} - c_{13}^{Si})^2}{\Phi^{p}c_{11}^{Si} + \Phi^{Si}c_{11}^{p}}] + \Phi^{p}c_{11}^{p} \tag{1.1a}$$

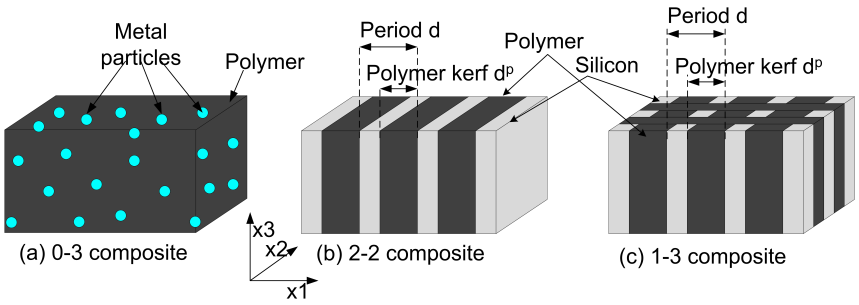

Figure 1.4: Schematic of (a) 0-3 composite (b) 2-2 composite and (c) 1-3 composite

$$\bar{c}_{33}^{C} = \Phi^{Si}[c_{33}^{Si} - \Phi^{p}\frac{2(c_{12}^{p} - c_{13}^{Si})^2}{\Phi^{p}(c_{11}^{Si} + c_{12}^{Si}) + \Phi^{Si}(c_{11}^{p} + c_{12}^{p})}] + \Phi^{p}c_{11}^{p} \tag{1.1b}$$

$$\bar{\rho}^{C} = \Phi^{Si}\rho^{Si} + \Phi^{p}\rho^{p} \tag{1.2}$$

$$\bar{Z}_{iso}^{C} = \sqrt{\bar{c}_{33}^{C}\bar{\rho}^{C}} \tag{1.3}$$

$$\bar{V}_{iso}^{C} = \sqrt{\frac{\bar{c}_{33}^{C}}{\bar{\rho}^{C}}} \tag{1.4}$$

where Eq. (1.1a) and Eq. (1.1b) are applied for silicon-polymer 2-2 and 1-3 composites, respectively. The overbars ($\bar{x}$) with superscript C refers to effective parameters of the composite, superscript p refers to parameters of the polymer, superscript Si to parameters of the silicon. c_{ij} are the elastic coefficients of the materials, ρ are the densities, and Φ^{Si} is the volume fraction of silicon in the composite, with $\Phi^{p} = 1 - \Phi^{Si}$ being the volume fraction of polymer. $\bar{Z}^{C}$ is the effective acoustic impedance and $\bar{V}^{C}$ is the longitudinal wave speed of the composite, both measured in the thickness direction. Note that (100)-silicon is an anisotropic crystal with the stiffness coefficients given below

$$\left[\ c^{Si}\ \right] = \begin{bmatrix} c_{11}^{Si} & c_{12}^{Si} & c_{13}^{Si} & 0 & 0 & 0 \\ c_{12}^{Si} & c_{22}^{Si} & c_{12}^{Si} & 0 & 0 & 0 \\ c_{13}^{Si} & c_{12}^{Si} & c_{33}^{Si} & 0 & 0 & 0 \\ 0 & 0 & 0 & c_{44}^{Si} & 0 & 0 \\ 0 & 0 & 0 & 0 & c_{55}^{Si} & 0 \\ 0 & 0 & 0 & 0 & 0 & c_{66}^{Si} \end{bmatrix} \tag{1.5}$$

where $c_{11}^{Si} = c_{22}^{Si} = c_{33}^{Si} = 166$ GPa and $c_{12}^{Si} = c_{13}^{Si} = 64$ GPa, $c_{44}^{Si} = c_{55}^{Si} = c_{66}^{Si} = 80$ GPa [2].

For two other commercialized silicon wafers: the (110)-oriented and (111)-oriented silicons, new stiffness matrices corresponding to the new coordinate systems must be used and these can be found by performing certain rotations in Euclidean space.

For the (110)-oriented wafers used in this study, the new stiffness matrix is found and shown below

$$\left[\ c'^{Si}\ \right] = \begin{bmatrix} c_{11}'^{Si} & c_{12}'^{Si} & c_{13}'^{Si} & 0 & 0 & 0 \\ c_{12}'^{Si} & c_{22}'^{Si} & c_{23}'^{Si} & 0 & 0 & 0 \\ c_{13}'^{Si} & c_{23}'^{Si} & c_{33}'^{Si} & 0 & 0 & 0 \\ 0 & 0 & 0 & c_{44}'^{Si} & 0 & 0 \\ 0 & 0 & 0 & 0 & c_{55}'^{Si} & 0 \\ 0 & 0 & 0 & 0 & 0 & c_{66}'^{Si} \end{bmatrix} \tag{1.6}$$

where

$$\begin{aligned} c_{11}'^{Si} = c_{11}^{Si} &= 166 \text{ GPa}, \\ c_{22}'^{Si} = c_{33}'^{Si} = \frac{1}{2}(c_{11}^{Si} + c_{22}^{Si}) + c_{44}^{Si} &= 195 \text{ GPa}, \\ c_{23}'^{Si} = \frac{1}{2}(c_{11}^{Si} + c_{22}^{Si}) + c_{44}^{Si} &= 35 \text{ GPa}, \\ c_{12}'^{Si} = c_{13}'^{Si} = c_{13}^{Si} &= 64 \text{ GPa}, \\ c_{44}'^{Si} = \frac{1}{2}(c_{11}^{Si} + c_{22}^{Si}) &= 51 \text{ GPa}, \\ c_{55}'^{Si} = c_{66}'^{Si} = c_{44}^{Si} &= 80 \text{ GPa}. \end{aligned}$$

- **Dynamic model of guided waves** [69, 73] As the lateral dimension of the composite is comparable with the wavelength, the iso-strain model is not sufficient to describe composite behavior. Therefore, the dynamic model should be used. For a periodic 2-2 composite as shown in Figure 1.4(b), the problem can be treated as a two dimensional model in Ox_1x_3 plane where dimension in x_1 direction is treated as infinite, if the dimensions in the x_1 and x_2-directions are much larger than the composite period d and thickness L.

  The dynamical coupled wave equations in an elastic material are [69]

$$\frac{\partial T_1}{\partial x_1} + \frac{\partial T_5}{\partial x_3} = \rho \frac{\partial^2 u_1}{\partial t^2}, \tag{1.7a}$$

$$\frac{\partial T_5}{\partial x_1} + \frac{\partial T_3}{\partial x_3} = \rho \frac{\partial^2 u_3}{\partial t^2} \tag{1.7b}$$

  where T_i are the stress tensor components, u_i are the elastic displacement components, ρ is the density. The constitutive equations between stress tensor $\left[\ T\ \right]$ and strain $\left[\ S\ \right]$ are via the stiffness matrix $\left[\ c\ \right]$.

$$\left[\ T\ \right] = \left[\ c\ \right]\left[\ S\ \right] \tag{1.8}$$

  Combining Eq. (1.7) and Eq. (1.8) leads to two second order diffrential equations,

$$c_{11}u_{1,11} + (c_{13} + c_{55})u_{3,13} + c_{55}u_{1,33} = \rho\ddot{u}_1, \tag{1.9a}$$

$$c_{55}u_{3,11} + (c_{13} + c_{55})u_{1,13} + c_{33}u_{3,33} = \rho\ddot{u}_3 \tag{1.9b}$$

where

$$u_{i,lk} = \frac{\partial^2 u_i}{\partial x_l \partial x_k},$$
$$\ddot{u}_i = \frac{\partial^2 u_i}{\partial t^2}$$

For an unbounded plate, the field solutions to Eq. (1.9) have the form

$$u_1 = A_1 \exp(j(k_1 x_1 + k_3 x_3 - \omega t)), \tag{1.10a}$$
$$u_3 = A_3 \exp(j(k_1 x_1 + k_3 x_3 - \omega t)) \tag{1.10b}$$

where $j = \sqrt{-1}$; A_i are the amplitudes; $\omega = 2\pi f$ is the angular frequency; f is the frequency; k_i are the wave vector components in the x_i directions, respectively.

Substituting Eq. (1.10) into Eq. (1.9) leads to two homogenous equations

$$(c_{11}k_1^2 + c_{55}k_3^2 - \rho\omega^2)A_1 + (c_{13} + c_{55})k_1 k_3 A_3 = 0, \tag{1.11a}$$
$$(c_{13} + c_{55})k_1 k_3 A_1 + (c_{55}k_1^2 + c_{33}k_3^2 - \rho\omega^2)A_3 = 0 \tag{1.11b}$$

A nontrivial solution of the system in Eq. (1.11) requires that the determinant vanishes, which yields to a quadratic equation in k_1^2, i.e.

$$a_0(k_1^2)^2 + a_1 k_1^2 + a_2 = 0 \tag{1.12}$$

where

$$a_0 = c_{55}c_{11},$$
$$a_1 = c_{55}(c_{55}k_3^2 - \rho\omega^2) + c_{11}(c_{33}k_3^2 - \rho\omega^2) + (c_{13} + c_{55})k_3^2,$$
$$a_2 = (c_{55}k_3^2 - \rho\omega^2)(c_{33}k_3^2 - \rho\omega^2)$$

Eq. (1.12) contains four possible eigen-values of k_1, which determine four partial waves in a material. Hence, a complete wave solution is a linear combination of all the partial waves

$$u_1 = \sum_{n=1}^{4} B_n A_{1n} \exp(j(k_{1n}x_1 + k_3 x_3 - \omega t)), \tag{1.13a}$$
$$u_3 = \sum_{n=1}^{4} B_n A_{3n} \exp(j(k_{1n}x_1 + k_3 x_3 - \omega t)) \tag{1.13b}$$

where B_n is the coefficient of the summation for nth partial wave; A_{in} are wave amplitudes depending on wave vector components k_{in} in the x_i-direction.

In transducer engineering, we only deal with symmetric modes. Hence, the symmetric guided wave solutions in the unbounded silicon plate are

$$u_1^{Si} = \sum_{n=1}^{2} jB_n^{Si} A_{1n}^{Si} \sin(k_{1n}^{Si}x_1) \exp(jk_3 x_3), \tag{1.14a}$$
$$u_3^{Si} = \sum_{n=1}^{2} B_n^{Si} A_{3n}^{Si} \cos(k_{1n}^{Si}x_1) \exp(jk_3 x_3) \tag{1.14b}$$

where superscript Si denote the quantities in silicon. Similarly, solutions in polymer can also be written by replacing x_1 in Eq. (1.14) by $(x_1 - d/2)$. Note that the wave vector k_3 in the x_3-direction is for both phases. Four unknowns need to be solved are $B_n^{Si,p}; n = 1, 2$ and they are determined from the boundary conditions requiring continuity in the displacements and stresses at the silicon-polymer interface $x_1 = \Phi^{Si} d/2$.

$$u_1^{Si} = u_1^p, u_3^{Si} = u_3^p, T_1^{Si} = T_1^p, T_5^{Si} = T_5^p \tag{1.15}$$

The equations can be rewritten in the matrix form of a homogeneous linear system

$$\begin{bmatrix} K_{11} & K_{12} & K_{13} & K_{14} \\ K_{21} & K_{22} & K_{23} & K_{24} \\ K_{31} & K_{32} & K_{33} & K_{34} \\ K_{41} & K_{42} & K_{43} & K_{44} \end{bmatrix} \begin{bmatrix} B_1^{Si} \\ B_2^{Si} \\ B_1^p \\ B_2^p \end{bmatrix} = 0 \tag{1.16}$$

where the K_{ij} element is a function of f, k_3, Φ^{Si}, d and the material properties of both silicon and polymer phases. For examples,

$$K_{11} = A_{11}^{Si} sin(k_{11}^{Si} \Phi^{Si} \frac{d}{2}), \tag{1.17}$$

$$K_{13} = -A_{11}^p sin(k_{11}^p (1 - \Phi^{Si}) \frac{d}{2}) \tag{1.18}$$

The condition for the nontrivial solution of this system requires the determinant of the coefficients vanishes, i.e.

$$\begin{vmatrix} K_{11} & K_{12} & K_{13} & K_{14} \\ K_{21} & K_{22} & K_{23} & K_{24} \\ K_{31} & K_{32} & K_{33} & K_{34} \\ K_{41} & K_{42} & K_{43} & K_{44} \end{vmatrix} = 0 \tag{1.19}$$

When the composite volume fraction Φ^{Si} and period d are known, this yields the relations between the wave vector component k_3 and the frequency f, the dispersion curves, in an unbounded 2-2 composite. When these relations are found; considering the frequency range that only thickness mode exists, the effective longitudinal wave velocity can be approximately evaluated from the first branch of the dispersive curves by

$$\bar{V}_{dyn}^C = 2\pi \frac{f}{k_3} \tag{1.20}$$

and the effective acoustic impedance can be approximately evaluated by

$$\bar{Z}_{dyn}^C = \bar{V}_{dyn}^C \bar{\rho}^C \tag{1.21}$$

1.3.2 Fabrication methods

Two different composite types: 2-2 and 1-3 connectivities have been manufactured using micromachining methods. The main fabrication process to form these composites

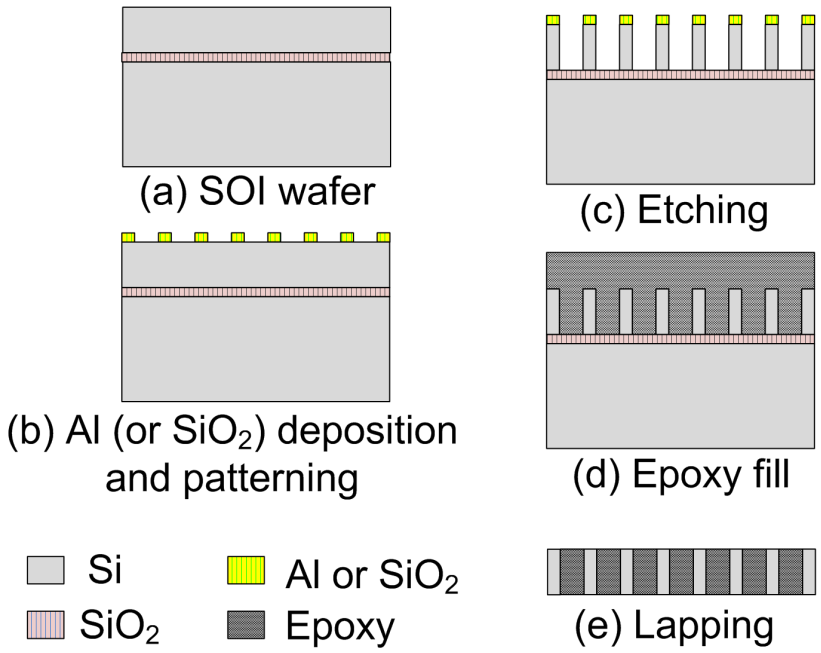

Figure 1.5: Main steps to produce silicon-polymer composites

	Anisotropic Wet Etch	**Deep Reactive Ion Etch**
Method	Chemical Solutions (KOH)	Ion Bombardment and Chemical Reactive
Mask	SiO_2	Al
Wafer	(110)	(100) and (110)
Etching time	Long (40 min. – 110 min.)	Short (~20 min.)
Crystal orientation dependence	Yes	No
Delicate alignment along {111} planes	Yes	No
Composite can be formed	2-2 connectivity	2-2 and 1-3 connectivity
Repeatability	Good	Very good
Etching profile	Smooth, vertical sidewalls	Tapered profile
Equipment cost	Inexpensive	Expensive
Labour cost	Labour consuming	Less labour consuming

Table 1.2: Comparison between two fabrication methods to manufacture composite matching layers used in this study

are summarized in Fig.1.5. Starting with an SOI wafer [Fig.1.5(a)], a thin Al (or SiO_2) layer was deposited on the wafer surface and patterned to form a mask for silicon etching [Fig.1.5(b)]. Etching of silicon was then performed, using either DRIE or anisotropic wet etch in KOH etchant [Fig.1.5(c)]. The etching process stopped at the oxide burried layer. The mask was stripped and epoxy risin was then filled into the etched trenches

[Fig.1.5(d)]. The wafer was cured and diced to separate dies. Then the silicon and polymer layers on each die were lapped off, leaving the composite alone [Fig.1.5(e)].

Two different micromachining methods were used in this study to form μm-sized trenches: anisotropic wet etch which makes use of the differences in etching rates between different crystal orientations; and DRIE, which alternates repeatedly between the plasma etch and passivation mode to achieve high aspect ratio structures. The former requires silicon wafers with (110) crystal orientation and only 2-2 composite can be formed, whereas the latter is not sensitive to the crystal orientation and both 1-3 and 2-2 composites can be made. Both methods have strengths and weaknesses and are summarized in Table 1.2.

1.4 Modeling of piezoelectric ultrasound transducers

Transducer modeling plays an important role in the development of a new product. A reliable model provides good understanding and prediction of a transducer behavior and its performance. Through modeling, new ideas can be designed, tested and optimized before moving to the fabrication step.

In this thesis, modeling of the transducers is divided into one dimensional (1D) model and FEM simulation. The 1D model is a good approximation for layered structures. This model serves as a base for the estimation of the composite materials. The limitation with the 1D model is that it can only capture the thickness vibration mode, and it will also ignore the finite dimensions of the composite structure. Moreover, deviations from a perfect structure, such as tapering of the side-walls from the fabrication process, cannot be captured by a 1D model. To investigate such effects, 2D/3D FEM models of the transducers should be employed.

1.4.1 One-dimensional model

In many cases, a 1D equivalent circuit model is sufficient to describe a piezoelectric transducer, as long as there is one dominant resonant mode. There are several existing models, but the most commonly used are the approaches of Mason [74], RedWood [75] and Krimholtz, Leedom and Matthaei [76]. By cascading the piezoelectric layer, modeled by an equivalent three-port circuit, and the passive layers, modeled by transmission lines (two-port), the overall layered transducer structure can be fully described. In this work, the three-port Mason model (Figure1.6) is employed as an equivalent circuit of the piezoelectric active layer, where the two acoustic back and front ports are represented by the pressures P^{BW} and P^{FW} and the vibration velocities U^{BW} and U^{FW}. The electrical port is represented by the voltage V and current I between the two electrode surfaces. The lumped circuit parameters are given as follow

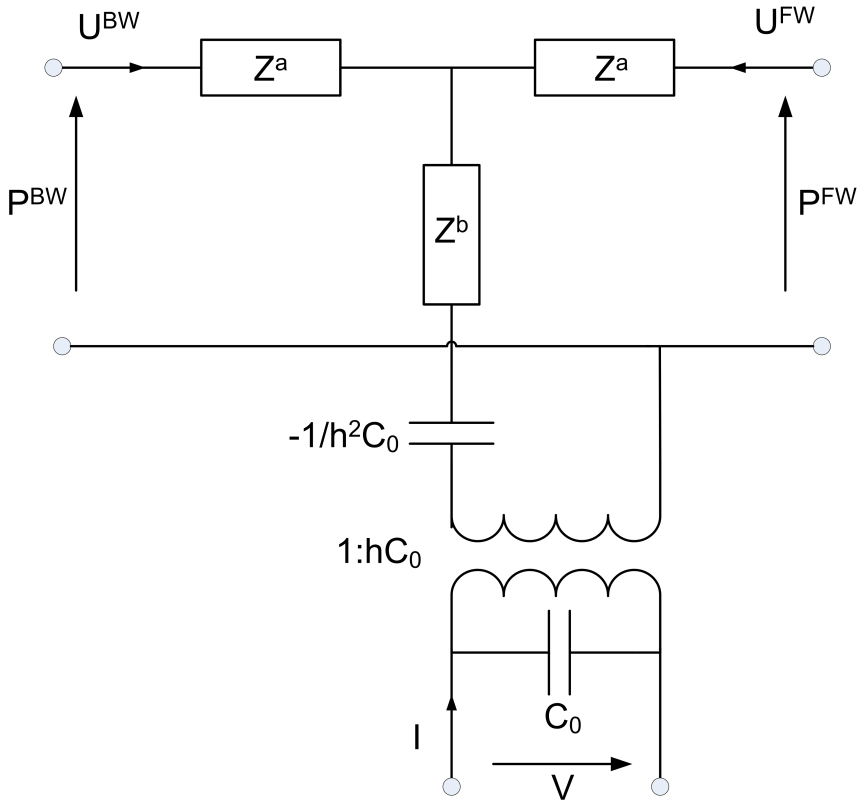

Figure 1.6: Mason model for a piezoelectric disc

$$\begin{aligned} C_0 &= \epsilon_{33}^{S,r}\epsilon_0/L^{PZT}, \\ Z^a &= jZ^{PZT}tan(k_3^{PZT}L^{PZT})/2, \\ Z^b &= -jZ^{PZT}/sin(k_3^{PZT}L^{PZT})/2, \\ h &= e_{33}/\epsilon_{33}^{S,r}\epsilon_0 \end{aligned} \tag{1.22}$$

where $Z^{PZT} = \rho^{PZT}V^{PZT}$ is the characteristic impedance, ρ^{PZT} is the density and V^{PZT} is the longitudinal velocity, $k_3^{PZT} = \omega/V^{PZT} = 2\pi f/V^{PZT}$ is the wave number in the thickness direction of the piezoelectric element; e_{33}, $\epsilon_{33}^{S,r}$ are the coupling coefficient and relative dielectric constant in the thickness direction, $\epsilon_0 = 8.85e{-}12(F/m)$ is the vacuum permittivity.

The block diagram for an overall piezoelectric transducer including one active layer, one backing and three matching layers is shown in Figure1.7 where losses in materials are also taken into account as linear attenuation, i.e.

$$k_3^n = \frac{\omega}{V^n}(1 - j\frac{1}{2Q^n}) \tag{1.23}$$

where $j = \sqrt{-1}$, the superscript $n = B, PZT, 1, 2, 3$ denotes the layer n in the diagram;

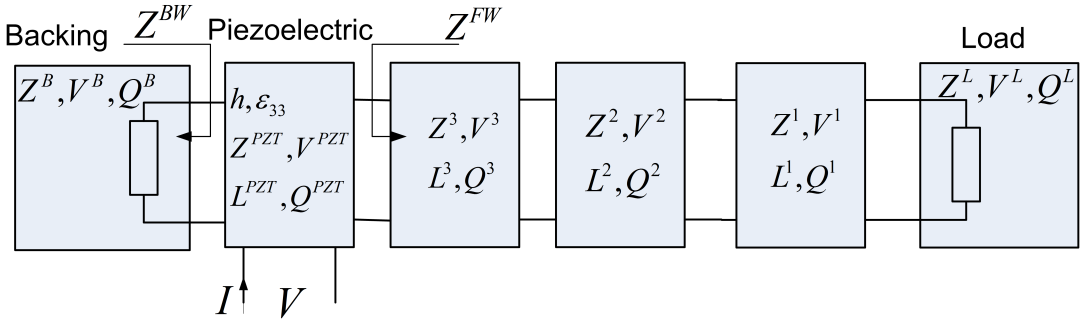

Figure 1.7: Block diagram

ω is the angular frequency, V^n is the longitudinal velocity, Q^n is the mechanical loss. Assume harmonic variables are used, the acoustic impedance seen forward (Z^{FW}) from the piezoelectric layer can be iteratively calculated using the formula [77]

$$Z_{AI}^n(\omega) = Z^n \frac{Z_{AI}^{n-1} + jZ^n tan(k_3^n L^n)}{Z^n + jZ_{AI}^{n-1} tan(k_3^n L^n)} \tag{1.24}$$

where Z_{AI}^n, Z^n, k_3^n, and L^n are the spatial dependent acoustic impedance seen from layer n, the characteristic impedance, wave number and thickness of layer n. Note that the initialize iteration starts from the load, i.e., $Z_{AI}^0 = Z^L$. The acoustic impedance seen backward is $Z^{BW} = Z^B$. The total electrical impedance of the transducer, Z^e, seen from the electrical port is calculated as

$$Z^e(\omega) = (Z^{C_0} \parallel Z^M)/A \tag{1.25}$$

where operator $\parallel$ denotes the two impedances in parallel; A is the area of the piezo-layer while Z^M is the impedance of the components above the transformer referred to the primary side given by

$$Z^M(\omega) = [-h^2 C_0/(j\omega) + Z^b + (Z^{FW} + Z^a) \parallel (Z^{BW} + Z^a)]/(hC_0)^2 \tag{1.26}$$

The transfer function from voltage to velocity at the transducer-load interface is defined as the ratio between the velocity on the transducer surface, U^L, and the applied voltage on the two electrodes, V, i.e.

$$H_{tt}(\omega) = \frac{U^L}{V} \tag{1.27}$$

1.4.2 Finite Element Method simulations

FEM is a powerful and comprehensive tool for modeling of a transducer's behavior, especially in the case where analytical and/or simple 1D model is not able to valid the performance of the transducer. However, to achieve consistent results, one should have reliable material data as well as good understanding of the physics behind the model. In the current work, FEM modeling was utilized to explore the anisotropic/dispersive behavior of the composite layer. Moreover, the FEM is especially useful to inspect non-ideal effects from the micromachining process, which cannot be captured by the 1D model. The simulations were time harmonic analysis, i.e. the model was solved at every single harmonic excitation at different frequencies.

In the piezoelectric layer, the constitutive matrix equations relating the mechanical and electrical quantities that are the basis for the derivation of the finite element method are given by

$$\left[\ T\ \right] = \left[\ c^E\ \right]\left[\ S\ \right] - \left[\ e\ \right]\left[\ E\ \right] \tag{1.28}$$

$$\left[\ D\ \right] = \left[\ e\ \right]\left[\ S\ \right] + \left[\ \epsilon^S\ \right]\left[\ E\ \right] \tag{1.29}$$

In the 3D case, $\left[\ T\ \right]$ is the 6x1 stress vector, $\left[\ S\ \right]$ is the 6x1 strain vector, $\left[\ E\ \right]$ is the 3x1 electric field vector and $\left[\ D\ \right]$ is the 3x1 electric displacement field vector; $\left[\ c^E\ \right]$, $\left[\ e\ \right]$ and $\left[\ \epsilon^S\ \right]$ are the 6x6 piezoelectric elasticity matrix, the 3x6 coupling matrix and the 3x3 permittivity matrix of the PZT material, respectively. The superscript E indicates a constant electric field; the superscript S indicates a constant strain field.

The silicon layer was modeled as an anisotropic material, the isotropic material was employed for polymer layer. The mechanical damping is given as a loss factor, $1/Q^n$ where $n = B, 1, 2, 3$.

The triangular element was used to mesh the structures in 2D, whereas the tetrahedron element is used in the 3D models. The maximum mesh size should be at least 1/6 of the minimum wavelength, i.e. at the highest frequency and the lowest speed of sound in the material.

In order to compare the FEM and the 1D models, we are interested in the electrical impedance seen from the electrodes of the active element; and the transfer function, as defined in Eq. 1.27. When a voltage V applied over the electrodes of the active element, the current density, J, was developed. The total current is then calculated by performing boundary integration over the electrode as

$$I = \int J \mathrm{d}A \tag{1.30}$$

where A is the area of the piezoelectric element.

The electrical impedance seen from the electrodes is

$$Z^e = \frac{V}{I} \tag{1.31}$$

The transfer function from voltage to velocity at the transducer-load interface is found by

$$H_{tt} = \frac{\frac{1}{A}\int u_n^L \mathrm{d}A}{V} \tag{1.32}$$

where V is the applied voltage, A is the transducer area in contact with the load, and u_n^L is the particle velocity normal to the transducer-load interface.

1.5 Thesis structure

In addition to the introductory chapter, four technical articles covering the entire PhD work are included in this thesis. Contributions from these articles are summarized in section 1.6. For already published papers, slight corrections may have been made according to the journal papers. As each article should be possible to be read independently, some contents may be repeated several times.

1.6 Summary of contributions

This subsection contains a summary of the contributions included in this thesis.

Paper A: Microfabricated 1-3 Composite Acoustic Matching Layers for 15 MHz Transducers

This paper presents a new fabrication method to manufacture silicon-polymer 1-3 composites to be used as matching layers in high frequency transducers. Unlike the anisotropic wet etching of (110) silicon wafer method, which is crystal orientation dependence, the proposed Deep Reactive Ion Etch (DRIE) approach does not require delicate alignment along {111} planes and hence, is promising for mass production. Through Finite Element Method (FEM) simulations, the period size of the composite was carefully chosen to avoid unwanted resonances and maintain the desired acoustical properties of the composite. The imperfection from fabrication process, i.e. the tapering profile of the etched sidewalls, was also investigated by FEM. To characterize composite materials at high frequency, a method to estimate the composite parameters was also proposed by curve-fitting the electrical impedance measurements of air-backed transducers with composite as matching layers to the corresponding theoretical Mason models. The estimated parameters of composite with different volume fractions showed good correspondence to the FEM simulations.

Most of the work in this paper was conducted by the candidate. The Deep Reactive Ion Etching process was done at SINTEF Minalab by Dr. Geir Uri Jensen. The pulse-echo measurements were performed at the Medical Imaging laboratory, NTNU by the candidate with the assistance of Asc. Prof. Tonni Franke Johansen.

This paper was published in Ultrasonics, vol. 53, issue 6, 2013.

Paper B: Modeling of micromachined silicon-polymer 2-2 composite matching layers for 15 MHz ultrasound transducers

This paper discusses the modeling of the silicon-polymer 2-2 composite materials. When working with composites, determining of the maximum allowance lateral dimensions to avoid unwanted resonance is crucial. Moreover, being used as matching layers in ultrasound transducers, the composite acoustical properties might change with frequency, composite dimensions and surrounding contact media and therefore, these circumstances must be considered. Both theoretical and FEM modeling were employed and results were compared with experiments. It is shown that lateral resonance in silicon-polymer 2-2 composite is defined by composite period and the maximum allowable lateral dimensions can be increased by at least a factor 1.2 compared to what was found in piezo-polymer composite. It is also shown that when only thickness mode is excited in the composite, the curve-fitting the electrical impedance measurements to the theoretical Mason models method (proposed in Paper A) is sufficient to characterize the composite acoustical properties.

Most of the work in this paper was conducted by the candidate. The Deep Reactive Ion Etching process was done at SINTEF Minalab by Dr. Geir Uri Jensen. The pulse-echo measurements were performed at the Medical Imaging laboratory, NTNU by the candidate with the assistance of Asc. Prof. Tonni Franke Johansen.

This paper has been submitted for publishing in Ultrasonics.

Paper C: Fabrication of deep, long, vertical trenches using anisotropic wet etch of silicon

In this paper, the fabrication process to form deep, long, vertical trenches using anisotropic wet etching of (110) silicon wafers is presented. This process is beneficial for many applications such as optical MEMS, microfluidic and energy harvesting systems. The paper provides a technical document for in-house use at IMST lab, HiVe. The process might be useful for one who would like to reproduce these structures for other MEMS applications.

This work was initially developed by Anh-Tuan Thai Nguyen during his master project at IMST, HiVe in collaboration with the candidate. The candidate took over the process and implemented it with some modifications on the mask design, the etchant concentration, the use of wafers to improve the uniformity of the silicon bars, the repeatibility of the process and achieving the desired dimensions for the composite structures used in Paper D.

This paper is being prepared as a technical report for internal use at IMST, HiVe.

Paper D: Microfabrication of Stacks of Acoustic Matching Layers for 15 MHz Ultrasonic Transducers

This paper presents the development of novel multiple matching layer ultrasound transducers working at high frequencies based on micromachining technology. The tested transducers with single composite matching layers in Paper A and Paper B were not sufficient for practical applications in terms of bandwidth and multiple matching configurations were required. A 2-2 silicon polymer composite material based on anisotropic wet etch of silicon was developed from the fabrication process described in Paper C. This composite was used as an intermediate matching layer in a stack of multiple-matching layer structures. Two matching configurations were tested: The two layer matching approach where the inner layer is silicon-polymer composite and the outer layer is polymer, and the three layer matching design where the inner layer is silicon, the intermediate layer is silicon-polymer composite and the outer layer is polymer. The measured results showed the - 6 dB relative bandwidths and two-way insertion loss ranging from 70 to 93% and 18.4 to 25.4 dB, respectively. These results show the feasibility of manufacturing high frequency ultrasound transducers using silicon micromachining techniques. However, in order for a transducer manufactured by these techniques can be used in intravascular applications, the transducer fabrication process needs to be further optimized to fulfill the requirement of transducer's size, operating frequency, reliability, electronics compatibility and mass production.

Most of the work was conducted by the candidate. The anisotropic wet etching process was initially developed by Anh-Tuan Thai Nguyen during his master project at IMST, HiVe in collaboration with the candidate. The pulse-echo measurements were performed at the Medical Imaging laboratory, NTNU by the candidate with the assistance of Asc. Prof. Tonni Franke Johansen.

This paper has been accepted and available online in Ultrasonics, 2013.

1.7 General discussion and future work

The current work has been categorized into two main themes: the silicon-polymer composite and the micromachined broadband ultrasound transducers. In relation to the former, paper A focuses on the silicon-polymer composite in 1-3 connectivity where this composite was designed by FEM, manufactured using the DRIE method to form the trenches and these trenches were filled with epoxy resin. The composite properties were characterized by electrical impedance and pulse-echo measurements. The imperfection in the DRIE process due to high local loading effect leads to non-vertical trenches, which reduces the composite acoustic impedance and velocity. The achieved tapered angle of the silicon sidewall is about 0.3°, but might be further improved by doing research to find the optimal parameter set to fulfill this particular application. The effective acoustical properties of the fabricated composites are lower than values calculated from the iso-strain model,

and these deviations are attributed to the finite dimensions of the composite structure and the tapering profile of the etched structures.

The silicon-polymer composite is dispersive, i.e. the material properties are frequency dependent. Understanding the acoustic behavior of the composite materials is essential for using them as one of several layers in multilayered structures. This was investigated for silicon-polymer 2-2 composites in Paper B. The analytical calculations based on partial waves solutions and FEM modeling of the silicon-polymer 2-2 composite show that for a composite operating in the condition without influence by the lateral resonance, the lateral allowed dimensions of the silicon-polymer 2-2 composite can be enlarged at least by a factor 1.2 compared to that of piezo-composite. The acoustical impedance of the composite varies with frequency, composite dimensions and the material that the composite is in contact with. When a composite is in contact with soft materials such as air or water, its effective impedance is lower than the values predicted from the analytical dynamic model of guided waves due to high dispersion. When a composite is between two solid materials, lower dispersion is predicted by FEM simulations and therefore, theoretical dynamic model may be used to estimate the composite properties.

When the lateral dimensions of a composites are chosen so that the transducer bandwidth is below the lateral resonance of the composites, a 1D equivalent model, e.g. Mason model, can be used to characterize the composite properties, though the FEM simulations provide better fit to the measurement data in prediction of lateral resonance. By fitting the measured electrical impedance of an air-backed transducer including a PZT active layer and a composite matching layer to an equivalent 1D model, the effective acoustical properties of the composite (acoustic impedance, longitudinal wave velocity and loss tangent) can be deduced. This method is simple and easy to apply, suitable to be used to characterize the thin matching layer at high frequency. However, the method is sensitive to the bonding layer between the PZT active plate and the composite layer: The thicker the bonding layer, the lower estimated parameters. The bonding thickness in this work is estimated to be less than 1 μm, based on the assumption that the measured roughness of the active PZT and composite layers defines the bonding thickness. This thin thickness is confirmed by cross-section observation and is not included in the fit as it is much smaller compared to the wavelength at the operating frequency. If the method is used for transducers working at higher frequency, this layer must be taken into consideration. The method is also sensitive to predict the loss tangent, as the composite dispersion depends on the surrounding contact materials. When an air-backed transducer working in air, the measured electrical resistance at the resonance peaks are very large compared to the bias resistance of the electrical circuit formed by the connector and the poor electrical connection between the transducer and the connector. Hence, the biased influence from the electrical circuit into the fitted results can be neglected in this circumstance. However, due to higher dispersion when composite is in contact with air, the estimated results will give slightly high loss tangent estimates. In contrast, fitting of the the electrical impedance of the air-backed transducer working in water to the 1D model suffers the influence from the electrical loss. Therefore, further work should be performed to improve the method. A modified 1D model where disperison and electrical loss are included should be ap-

plied to provide better estimation of the loss tangent. To better avaluate the robustness of the fitting method, a different characterization approach, e.g. the method based on the impedance matching principle by H. Wang [78], should also be considered and the results from this method should be compared with those from our fitting approach. However, the method proposed by H.Wang requires complicated set up, high frequency transducer for transmitting the waves and the composite area must be much bigger than that used in this work to ensure that the incoming waves from the transmitted transducer hit a uniform composite material and not diffracted from the outer silicon frame. This method is also sensitive to predict the loss tangent of the characterized material. It should be noted that the method proposed by H. Wang might just be applied to the composite fabricated by anisotropic wet etch of silicon (Paper C), since the properties of the composites with big and small areas are expected to be similar. The method might not be implemented to the composite manufacted by the DRIE process. The resulting structures with big etched area are sufferred higher loading effect and hence, more tapering profile of the etched posts is expected. Therefore, the composite material properties of the composites with big etched area might be very different from those with small etched area.

The non-vertical sidewall trenches caused by high loading effect in the DRIE method might significantly influence the transducer performance when the etched features are smaller (or the transducer works at higher frequencies). However, this can be overcome by using anisotropic etching of (110)-oriented silicon wafers, as described in Paper C. The method is cost effective and able to produce high aspect ratio structures with vertical sidewalls. With good mask resolution, e.g. critical dimension feature about 1 μm, and more sophiticated lithography method such as electron beam, it is possible to achieve composites with sub-micron silicon bars, suited to be used as matching layers in ultrasound transducers at frequencies above 100 MHz. However, this method involves many delicate fabrication steps and hence, it is labor expensive. To be able to fabricate trenches with vertical sidewalls, the long line features must be accurately aligned to the <111> planes in the silicon within 0.1°, which can be demanding if structures are less than 2 μm wide [59]. This can be done by a pre-alignment step where fan-shaped patterns [59] or circles features [79] are etched to find the correct $\{111\}$ planes. Our experiment results show that using the circle patterns, which turn to be hexagons after the pre-alignment step, is easier than using fan-shaped patterns to perform appropriate alignment to ensure forming vertical sidewall trenches. A different alignment feature should be considered is the diamond-shaped pattern [80], which may even better reveal the $\{111\}$ plane. The anisotropic etching method also requires chosing appropriate silicon wafers, etchant solutions, etching conditions (etching concentration and temperature), etc ... to ensure high etching rate, high selectivity between etching surfaces, high reproducibility, low surface roughness, good etching uniformity, etc ...This study shows that using SOI wafers and with KOH solution 40 wt% at 70°C, structures that meet the mentioned requirements about the etching selectivity, the surface roughness, the uniformity of the structures, etc...can be fabricated. Hence, the fabricated composites from the chosen recipe are sufficient to be used as matching layers for transducers working at 15 MHz. It is believed that much smaller structures can be fabricated with available infrastructures at IMST lab.

This will be the future work to produce either matching layers for transducers working at higher frequencies or structures for different applications such as optical MEMS, energy harvesting com-driver structures, or bioMEMS channels.

In this work, the SiO_2 layer patterned by BOE 7:1 was used as mask to etch silicon due to the limited facilities available at IMST lab. Patterning the SiO_2 layer by RIE is recommended for smaller structures. Patterning profile also should be investigated. If it is possible to use a low pressure chemical vapor deposition process (LPCVD), silicon nitride (Si_3N_4) is recommended to replace SiO_2 due to the higher selectivity etching ratio between mask and silicon (Si_3N_4 is almost not attacked by KOH [2]). Since KOH is not highly compatible with the CMOS technology, it is also advised to use different etchants, i.e. tetramethyl ammonium hydroxide (TMAH) based solutions, if the electronics part is integrated on the same silicon substrate of the transducers. The work could be further improved by detailed inspection of the influence of the doping concentration on the process, measuring the roughness of interested surfaces, etc... Due to the limited duration and the fact that these evaluations are not the targets for this work, they were not investigated in details.

With the results from Paper C, transducers with multiple matching layers where silicon-polymer composite was an intermediate layer in these multilayered structures, were fabricated and tested, as presented in Paper D. The two matching layers configuration shows large - 6 dB bandwidth (70.2%), low insertion loss (18.4 dB) and short pulse (196 ns). The three matching layers shows large - 6 dB bandwidth (90-93%) but displays long pulse duration (326-446 ns) due to high ripple level in the frequency passband. This configuration can be improved by optimizing the matching impedances and thicknesses under constraints to bandwidth, ripple and loss [81]. The performance of these transducers demonstrate the feasibility of using silicon micromachining to manufacture high frequency broadband ultrasound transducers. However, in order for a transducer manufactured by these techniques can be used in intravascular applications, the transducer fabrication process needs to be further optimized to fulfill the requirement of transducer's size, operating frequency, reliability, electronics compatibility and mass production.

In the begining of the project, it was an aim to develop a high frequency (> 30 MHz) broadband transducer based on thick-film PZT and silicon micromachining for intravascular application. However, the need of thorough understanding of the silicon-polymer composite materials quickly lead to much work related to modeling, fabrication and characterization of these biphase materials. This left little time for manufacturing and testing of the broadband transducers with multiple matching layers. The idea of using the PZT thickfilm on silicon was also left behind and normal bulk ceramics were used as the PZT film might contaminate the chamber in the DRIE process of silicon. Hence, the fabricated transducers only demonstrate the feasibility of manufacturing of the ultrasound transducers based on micromachining of silicon. The prototypes were fabricated to operate at a relatively low frequency (15 MHz) compared to the need for intravascular imaging applications. However, when the concept is proven to work, it is possible to scale up the operating frequency. The manufacturing process was still partly based on conventional

lapping process. A new fabrication process which is more MEMS-friendly should be developed for transducers working at higher frequencies.

Using anisotropic wet etching of (110)-oriented silicon wafers to form long trenches with vertical sidewalls is a great advance to manufacture an "ideal" silicon-polymer 2-2 composite with vertical sidewalls, which are used as intermediate layer in the multiple matching layer structures. However, this method has two weaknesses that must be considered. First, the method requires accurately alignment of the feature lines to the {111} planes, as mentioned above. Second, the stacks of multiple layers formed from (110)-oriented wafers are more fragile under the grinding process than those from (110)-oriented wafers, especially when the stacks become too thin, because the structure tends to crack along the etched 111 lines. Hence, delicate fabrication process with careful manipulating steps must be applied. For transducer working at higher frequencies (> 15 MHz), using SOI wafers with double device layers could be used to avoid the grinding process.

Controlling the bonding layer between the PZT plate and the matching stack is a critical task that should be addressed in manufacturing of the ultrasound transducers operating at higher frequencies (> 15 MHz). With the epoxy bonding technology in this study, it is not applicable for manufacturing transducers working at higher frequencies, e.g. for a transducer working at frequency of 100 MHz, the required thickness for the epoxy layer should be less than 0.15 μm. To resolve this, thermo-compression bonding with indium could be used [82]. As indium has higher acoustic impedance than epoxy, a thicker bonding layer will be tolerated. Alternatively, the bonding layer problem will be eliminated by using a PZT thick-film printed directly on a platinum-coated silicon wafer [26, 27, 52, 53].

1.8 Publication lists

What follows is a list of all publications made during the time as a Ph.D candidate.

Peer reviewed papers

1. **Tung Manh**, Lars Hoff, Tonni F. Johansen, and Bjørn .A. J. Angelsen, "A New Design for a High Frequency Broadband Ultrasound Transducer using Micromachined Silicon, "in *IEEE Wearable Micro and Nano Technologies for Personalized Health (pHealth), 2009 6th International Workshop*, Oslo, Norway, pp.33-36, 2009.

2. **Tung Manh**, Geir U. Jensen, Tonni F. Johansen, and Lars Hoff, "Microfabricated 1-3 Composite Acoustic Matching Layers for 15 MHz Transducers,"*Ultrasonics*, vol. 53, issue 6, 2013.

3. **Tung Manh**, Anh-Tuan Thai Nguyen, Tonni F. Johansen, and Lars Hoff, "Microfabrication of Stacks of Acoustic Matching Layers for 15 MHz Ultrasonic Transducers,"accepted and available online in *Ultrasonics*, 2013.

Submitted for publication

1. **Tung Manh**, Geir U. Jensen, Tonni F. Johansen, and Lars Hoff, "Modeling of Micromachined Silicon-Polymer 2-2 Composite Matching Layers for 15 MHz Ultrasound Transducers,"submitted to *Ultrasonics*.

Conference proceedings

1. Anh-Tuan Thai Nguyen, **Tung Manh**, and Lars Hoff, "Acoustic Matching Layer for High Frequency Ultrasound Transducers Made by Anisotropic Wet Etching of Silicon, "in *Proc. of IMAPS Nordic*, Goteburg, Sweden, 2010.

2. **Tung Manh**, Anh-Tuan Thai Nguyen, Geir U. Jensen, Tonni F. Johansen, and Lars Hoff, "Design of High Frequency Ultrasound Transducers using Micromachining,"in *Proc. of 33rd Scandinavian Symposium on Physical Acoustics*, 2010.

3. Anh-Tuan Thai Nguyen, **Tung Manh**, Geir U. Jensen, Tonni F. Johansen, and Lars Hoff, "Fabrication of Silicon-polymer Composite Acoustic Matching Layers for High Frequency Transducers, "in *Proc. IEEE Ultrasonics Symposium*, pp. 2064-2067, 2010.

4. **Tung Manh**, Geir U. Jensen, Tonni F. Johansen, and Lars Hoff, "1-3 Microfabricated Composite Acoustic Matching Layers for High Frequency Transducers, "in *Proc. IEEE Ultrasonics Symposium*, pp. 1932-1935, 2011.

5. **Tung Manh**, Geir U. Jensen, Tonni F. Johansen, and Lars Hoff, "Modeling and Characterization of Silicon-Epoxy 2-2 Composite Material, "in *Proc. IEEE Ultrasonics Symposium*, 2012.

Bibliography

[1] G. Kovacs, *Micromachined Transducers Sourcebook*. WCB/McGraw-Hill, 1998.

[2] M. J. Madou, *Fundamentals of microfabrication: the science of miniaturization*. Boca Raton, FL: CRC Press, 2 ed., Mar. 2002.

[3] E. Mounier, "MEMS Markets & Applications," in *dMEMS 2012*, 2012.

[4] "www.memscap.com."

[5] C. Grinde, *Stacked Disks Resonators and Micro-machined Microphones: Design and Modeling*. PhD thesis, University of Oslo, 2010.

[6] S. D. Nguyen, E. Halvorsen, and I. Paprotny, "Bistable springs for wideband microelectromechanical energy harvesters," *Applied Physics Letters*, vol. 102, no. 2, p. 023904, 2013.

[7] G. Ouyang, *Hybrid Integrated Components for Optical Display Systems - Electroactive Polymer Based Micro-Opto-Electro-Mechanical Actuators*. PhD thesis, University of Oslo, 2012.

[8] E. Tenstad, A. Tourovskaia, A. Folch, O. Myklebost, and E. Rian, "Extensive adipogenic and osteogenic differentiation of patterned human mesenchymal stem cells in a microfluidic device," *Lab Chip*, vol. 10, pp. 1401–1409, 2010.

[9] T. Manh, L. Hoff, T. F. Johansen, and G. U. Jensen, "1-3 microfabricated composite acoustic matching layers for high frequency transducers," in *Ultrasonics Symposium (IUS), 2011 IEEE International*, pp. 1932–1935, 2011.

[10] A.-T. T. Nguyen, F. Tjulkins, K. E. Aasmundtveit, N. Hoivik, L. Hoff, and K. Imenes, "Miniaturization of Package for an Implantable Heart Monitoring Device ," in *DTIP Conference*, 2013.

[11] F. Chollet and H. Liu, *A (not so) short introduction to micro electromechanical systems*. http://memscyclopedia.org/introMEMS.html, 2007.

[12] C. T. C. Nguyen, "MEMS: Generalizing the Benefits of Miniaturization," in *Texas-Area MEMS Workshop*, 2003.

[13] W. Hendee and E. Ritenour, *Medical Imaging Physics*. Wiley, 2003.

[14] T. Szabo, *Diagnostic Ultrasound Imaging: Inside Out*. Academic Press Series in Biomedical Engineering, Academic Press, 2013.

[15] J. Krautkramer and H. Krautkramer, *Ultrasonic Testing of Materials*. Springer-Verlag, 1983.

[16] B. A. Angelsen, *Ultrasound Imaging: Waves, signals and signal processing*, vol. 1, ch. 3. Ematec, 2000.

[17] K. Shung, "Diagnostic ultrasound: Past, present and future," *Journal of Medical and Biological Engineering*, vol. 27, pp. 371–374, 2010.

[18] J. Jensen, O. Holm, L. Jerisen, H. Bendsen, S. Nikolov, B. Tomov, P. Munk, M. Hansen, K. Salomonsen, J. Hansen, K. Gormsen, H. Pedersen, and K. Gammelmark, "Ultrasound research scanner for real-time synthetic aperture data acquisition," *Ultrasonics, Ferroelectrics and Frequency Control, IEEE Transactions on*, vol. 52, pp. 881 –891, may 2005.

[19] A. Kurjak, G. Azumendi, W. Andonotopo, and A. Salihagic-Kadic, "Three- and four-dimensional ultrasonography for the structural and functional evaluation of the fetal face," *American Journal of Obstetrics and Gynecology*, vol. 196, no. 1, pp. 16 – 28, 2007.

[20] Y. Dai, J. Tian, D. Dong, G. Yan, and H. Zheng, "Real-Time Visualized Freehand 3D Ultrasound Reconstruction Based on GPU," *Information Technology in Biomedicine, IEEE Transactions on*, vol. 14, pp. 1338 –1345, nov. 2010.

[21] N. Hozumi, R. Yamashita, C.-K. Lee, M. Nagao, K. Kobayashi, Y. Saijo, M. Tanaka, N. Tanaka, and S. Ohtsuki, "Time-frequency analysis for pulse driven ultrasonic microscopy for biological tissue characterization," *Ultrasonics*, vol. 42, no. 1-9, pp. 717 – 722, 2004.

[22] K. Shung, J. Cannata, and Q. Zhou, "Piezoelectric materials for high frequency medical imaging applications: A review," *Journal of Electroceramics*, vol. 19, no. 1, pp. 141–147, 2007.

[23] J. Cannata, Q. Zhou, J. Williams, C. Hu, and K. Shung, "Development of High Frequency Ultrasound Transducers for Medical Imaging," vol. 36, pp. 2739–2740, AAPM, 2009.

[24] J. R. Yuan, X. Jiang, C. Pei-Jie, A. Sadaka, R. Bautista, K. Snook, and P. W. Rehrig, "High frequency piezo composites microfabricated ultrasound transducers for intravascular imaging (invited)," in *Ultrasonics Symposium, 2006. IEEE*, pp. 264–268.

[25] F. Levassort, L.-P. Tran-Huu-Hue, P. Marechal, E. Ringgaard, and M. Lethiecq, "Characterisation of thin layers of parylene at high frequency using pzt thick film resonators," *Journal of the European Ceramic Society*, vol. 25, no. 12, pp. 2985 – 2989, 2005.

[26] P. Marechal, F. Levassort, J. Holc, L. P. Tran-Huu-Hue, M. Kosec, and M. Lethiecq, "High-frequency transducers based on integrated piezoelectric thick films for medical imaging," *Ultrasonics, Ferroelectrics and Frequency Control, IEEE Transactions on*, vol. 53, no. 8, pp. 1524–1533, 2006.

[27] Q. Zhang, F. Djuth, Q. Zhou, C. Hu, J. Cha, and K. Shung, "High frequency broadband PZT thick film ultrasonic transducers for medical imaging applications," *Ultrasonics*, vol. 44, pp. 711–715, 2006.

[28] R. Waksman and P. Serruys, *Handbook of the Vulnerable Plaque*. Martin Dunitz, 2004.

[29] P. Libby, "Atherosclerosis: the new view.," *Scientific American*, vol. 286, pp. 46–55, May 2002.

[30] Y.-P. P. Huang and Y.-P. P. Zheng, "Intravascular Ultrasound (IVUS): A Potential Arthroscopic Tool for Quantitative Assessment of Articular Cartilage.," *The open biomedical engineering journal*, vol. 3, pp. 13–20, 2009.

[31] K. Shung, J. Cannata, Q. Zhou, and J. Lee, "High frequency ultrasound: A new frontier for ultrasound," in *Engineering in Medicine and Biology Society, 2009. EMBC 2009. Annual International Conference of the IEEE*, pp. 1953–1955, 2009.

[32] G. Lockwood, D. Turnball, D. A. Christopher, and F. Foster, "Beyond 30 mhz [applications of high-frequency ultrasound imaging]," *Engineering in Medicine and Biology Magazine, IEEE*, vol. 15, no. 6, pp. 60–71, 1996.

[33] C. Pavlin, M. Sherar, and F. Foster, "Subsurface ultrasound microscopic imaging of the intact eye.," *Ophthalmology*, vol. 97, no. 2, pp. 244–50, 1990.

[34] C. Pavlin and F. Foster, *Ultrasound Biomicroscopy of the Eye*. Ultrasound Biomicroscopy of the Eye, Springer-Verlag, 1995.

[35] F. Levassort, E. Filoux, M. Lethiecq, R. Lou-Moler, E. Ringgaard, and A. Nowicki, "Curved piezoelectric thick films for high resolution medical imaging," in *Ultrasonics Symposium 2006 Proceedings.*, pp. 2361–2364, 2006.

[36] I. Ladabaum, X. Jin, H. Soh, A. Atalar, and B. Khuri-Yakub, "Surface micromachined capacitive ultrasonic transducers," *Ultrasonics, Ferroelectrics and Frequency Control, IEEE Transactions on*, vol. 45, pp. 678 –690, may 1998.

[37] X. Jin, I. Ladabaum, and B. Khuri-Yakub, "The microfabrication of capacitive ultrasonic transducers," *Microelectromechanical Systems, Journal of*, vol. 7, pp. 295 –302, sep 1998.

[38] X. Jin, I. Ladabaum, F. Degertekin, S. Calmes, and B. Khuri-Yakub, "Fabrication and characterization of surface micromachined capacitive ultrasonic immersion transducers," *Microelectromechanical Systems, Journal of*, vol. 8, pp. 100 –114, mar 1999.

[39] O. Oralkan, A. Ergun, J. Johnson, M. Karaman, U. Demirci, K. Kaviani, T. Lee, and B. Khuri-Yakub, "Capacitive micromachined ultrasonic transducers: next-generation arrays for acoustic imaging?," *Ultrasonics, Ferroelectrics and Frequency Control, IEEE Transactions on*, vol. 49, pp. 1596 –1610, nov. 2002.

[40] G. G. Yaralioglu, A. S. Ergun, H. Yongli, and B. T. Khuri-Yakub, "Capacitive Micromachined Ultrasonic Transducers for Robotic Sensing Applications," in *Intelligent Robots and Systems, 2003. (IROS 2003). Proceedings. 2003 IEEE/RSJ International Conference on*, vol. 3, pp. 2347–2352 vol.3, 2003.

[41] A. S. Erguri, H. Yongli, Z. Xuefeng, O. Oralkan, G. G. Yarahoglu, and B. T. Khuri-Yakub, "Capacitive Micromachined Ultrasonic Transducers: Fabrication technology," *Ultrasonics, Ferroelectrics and Frequency Control, IEEE Transactions on*, vol. 52, no. 12, pp. 2242–2258, 2005.

[42] D. Mills, "Medical imaging with capacitive micromachined ultrasound transducer (cmut) arrays," in *Ultrasonics Symposium, 2004 IEEE*, vol. 1, pp. 384 – 390 Vol.1, aug. 2004.

[43] G. Caliano, R. Carotenuto, E. Cianci, V. Foglietti, A. Caronti, A. Iula, and M. Pappalardo, "Design, fabrication and characterization of a capacitive micromachined ultrasonic probe for medical imaging," *Ultrasonics, Ferroelectrics and Frequency Control, IEEE Transactions on*, vol. 52, pp. 2259 –2269, dec. 2005.

[44] B. Bayram, M. Kupnik, G. Yaralioglu, O. Oralkan, A. Ergun, S. Wong, and B. Khuri-Yakub, "Finite element modeling and experimental characterization of crosstalk in 1-D CMUT arrays," *Ultrasonics, Ferroelectrics and Frequency Control, IEEE Transactions on*, vol. 54, pp. 418 –430, february 2007.

[45] H. Martinussen, A. Aksnes, and H. Engan, "Investigation of charge diffusion in cmuts using optical interferometry," in *Ultrasonics Symposium, 2008. IUS 2008. IEEE*, pp. 1218 –1221, nov. 2008.

[46] S. H. Wong, M. Kupnik, R. D. Watkins, K. Butts-Pauly, and B. T. Khuri-Yakub, "Capacitive Micromachined Ultrasonic Transducers for Therapeutic Ultrasound Applications," *Biomedical Engineering, IEEE Transactions on*, vol. 57, no. 1, pp. 114–123, 2010.

[47] C. Goldsmith, J. Ehmke, A. Malczewski, B. Pillans, S. Eshelman, Z. Yao, J. Brank, and M. Eberly, "Lifetime characterization of capacitive RF MEMS switches," in *Microwave Symposium Digest, 2001 IEEE MTT-S International*, vol. 1, pp. 227 – 230 vol.1, 2001.

[48] Y.-P. Zhu, T.-L. Ren, Y. Yang, X.-M. Wu, N.-X. Zhang, L.-T. Liu, Z.-M. Tan, H.-N. Wang, J. Cai, S.-D. Wang, and Z.-J. Li, "Novel ferroelectrics-based micro-acoustic devices and their ultrasonic applications," in *Electron Devices Meeting, 2004. IEDM Technical Digest. IEEE International*, pp. 51 – 54, dec. 2004.

[49] T. Pedersen, T. Zawada, K. Hansen, R. Lou-Moeller, and E. Thomsen, "Fabrication of high-frequency pMUT arrays on silicon substrates," *Ultrasonics, Ferroelectrics and Frequency Control, IEEE Transactions on*, vol. 57, pp. 1470 –1477, june 2010.

[50] A. Safari and E. K. Akdogan, *Piezoelectric and Acoustic Materials for Transducer Applications*. Boston, MA :: Springer US, 2008.

[51] F. S. Foster, K. A. Harasiewicz, and M. D. Sherar, "A history of medical and biological imaging with polyvinylidene fluoride (PVDF) transducers," *Ultrasonics, Ferroelectrics and Frequency Control, IEEE Transactions on*, vol. 47, no. 6, pp. 1363–1371, 2000.

[52] F. Levassort, T. Bove, E. Ringgaard, L. P. Tran-Huu-Hue, J. Holc, and M. Lethiecq, "A complete range of tape-cast piezoelectric thick films for high frequency ultrasonic transducers," in *Ultrasonics, 2003 IEEE Symposium on*, vol. 2, pp. 2003–2006, 2003.

[53] Q. F. Zhou, K. K. Shung, and Y. Huang, "Fabrication of sol-gel modified piezoelectric thick films for high frequency ultrasonic applications," in *Ultrasonics Symposium, 2004 IEEE*, vol. 3, pp. 1958–1961.

[54] A. Bardaine, P. Boy, P. Belleville, O. Acher, and F. Levassort, "Improvement of composite sol-gel process for manufacturing 40μm piezoelectric thick films," *Journal of the European Ceramic Society*, vol. 28, no. 8, pp. 1649–1655, 2008.

[55] R. E. McKeighen, "Design guidelines for medical ultrasonic arrays," vol. 3341, pp. 2–18, SPIE, 1998.

[56] M. Haller and B. Khuri-Yakub, "Micromachined acoustic matching layers," in *Proceedings of SPIE, New Developments in Ultrasonic Transducers and Transducer Systems* (F. L. Lizzi, ed.), vol. 1733, pp. 72–77, 1992.

[57] A. H. Meitzler and E. K. Sittig, "Characterization of Piezoelectric Transducers Used in Ultrasonic Devices Operating Above 0.1 GHz," *Journal of Applied Physics*, vol. 40, no. 11, pp. 4341–4352, 1969.

[58] M. Haller and B. Khuri-Yakub, "Micromachined ultrasound materials," in *Ultrasonics Symposium 1991 Proceedings.*, vol. 1, pp. 403–405.

[59] Y. Uenishi, M. Tsugai, and M. Mehregany, "Micro-opto-mechanical devices fabricated by anisotropic etching of (110) silicon," *Journal of Micromechanics and Microengineering*, vol. 5, no. 4, p. 305, 1995.

[60] W. A. Smith and B. Auld, "Modeling 1-3 composite piezoelectrics: Thickness-mode oscillation," *IEEE Trans. on Ultrasonics, Ferroelectrics, and Freq. Control*, vol. 38, no. 1, pp. 40–47, 1991.

[61] M. I. Haller and B. T. Khuri-Yakub, "1-3 composites for ultrasonic air transducers," in *Ultrasonics Symposium, 1992. Proceedings., IEEE 1992*, pp. 937–939 vol.2, 1992.

[62] M. Haller and B. Khuri-Yakub, "Tapered acoustic matching layers," in *in Ultrasonics Symposium, 1993. Proceedings*, vol. 1, pp. 505–508.

[63] K. Seong-Hyok, L. Sang-Hun, L. Hyung-Taek, K. Yong-Kweon, and L. Seung-Ki, "(110) silicon etching for high aspect ratio comb structures," in *Emerging Technologies and Factory Automation Proceedings, 1997. ETFA '97., 1997 6th International Conference on*, pp. 248–252.

[64] H.-T. Lim and Y.-K. Kim, "Novel fabrication of comb drive actuator using RIE of polysilicon and [110] si anisotropic bulk etching in KOH," in *Microprocesses and Nanotechnology Conference, 1998 International*, pp. 170–171.

[65] C. David, B. Nohammer, and E. Ziegler, "Wet etching of linear Fresnel zone plates for hard X-rays," *Microelectronic Engineering*, vol. 61-62, no. 0, pp. 987–992, 2002.

[66] P. Mao, "Fabrication and characterization of nanofluidic channels for studying molecular dynamics in confined envinronments," Master's thesis, Massachusetts Institute of Technology, 2005.

[67] A. Diaz, *X-ray scattering studies of ordering phenomena in colloids confined in microcavity arrays*. PhD thesis, Eidgenössische Technische Hochschule ETH Zürich, 2006.

[68] P. Mao, *Ultra-high-aspect-ratio nanofluidic channels for high-throughput biological applications*. PhD thesis, Massachusetts Institute of Technology, 2009.

[69] X. Geng, *Numerical modeling and experimental study of piezocomposite transducers*. Ph.d dissertation, The Pennsylvania State University, 1997.

[70] L. Ruibin, K. A. Harasiewicz, and F. S. Foster, "Interdigital pair bonding for high frequency (20-50 MHz) ultrasonic composite transducers," *Ultrasonics, Ferroelectrics and Frequency Control, IEEE Transactions on*, vol. 48, no. 1, pp. 299–306, 2001.

[71] J. R. Yuan, X. Jiang, K. Snook, P. W. Rehrig, T. R. Shrout, W. S. Hackenberger, A. Cheng, P. Cao, G. Lavalelle, and X. Geng, "Microfabrication of piezoelectric composite ultrasound transducers (PC-MUT)," in *Ultrasonics Symposium, 2006. IEEE*, pp. 922–925.

[72] R. E. Newnham, D. P. Skinner, and L. E. Cross, *Connectivity and piezoelectric-pyroelectric composites*. Mater Res Bull, 1978.

[73] Y. Shui and Q. Xue, "Dynamic characteristics of 2-2 piezoelectric composite transducers," *Ultrasonics, Ferroelectrics and Frequency Control, IEEE Transactions on*, vol. 44, no. 5, pp. 1110–1119, 1997.

[74] W. P. Mason, *Electromechanical transducers and wave filters*. New York: D. Van Nostrand Co., 1948.

[75] M. Redwood, "Transient performance of a piezoelectric transducer," *The Journal of the Acoustical Society of America*, vol. 33, no. 4, pp. 527–536, 1961.

[76] R. Krimholtz, D. Leedom, and G. Matthaei, "New equivalent circuits for elementary piezoelectric transducers," *Electronics Letters*, vol. 6, pp. 398–399, 1970.

[77] T. Rommetveit, T. F. Johansen, and R. Johnsen, "Using a multi-layered transducer model to estimate the properties of paraffin wax deposited on steel," *Ultrasonics*, vol. 51, no. 1, pp. 85–93, 2011.

[78] H. Wang and W. Cao, "Characterizing ultra-thin matching layers of high-frequency ultrasonic transducer based on impedance matching principle," *Ultrasonics, Ferroelectrics and Frequency Control, IEEE Transactions on*, vol. 51, no. 2, pp. 211–215, 2004.

[79] T. D. James, G. Parish, K. J. Winchester, and C. A. Musca, "A crystallographic alignment method in silicon for deep, long microchannel fabrication," *Journal of Micromechanics and Microengineering*, vol. 16, no. 10, p. 2177, 2006.

[80] A. Holke and H. T. Henderson, "Ultra-deep anisotropic etching of (110) silicon," *Journal of Micromechanics and Microengineering*, vol. 9, no. 1, p. 51, 1999.

[81] T. L. Rhyne, "Computer optimization of transducer transfer functions using constraints on bandwidth, ripple, and loss," *IEEE Trans. on Ultrasonics, Ferroelectrics, and Freq. Control*, vol. 43, pp. 1136–1149, 1995.

[82] E. Sittig, "Effects of bonding and electrode layers on the transmission parameters of piezoelectric transducers used in ultrasonic digital delay lines," *Sonics and Ultrasonics, IEEE Transactions on*, vol. 16, no. 1, pp. 2–9, 1969.

Paper A

Microfabricated 1-3 Composite Acoustic Matching Layers for 15 MHz Transducers

Tung Manh[a], Geir Uri Jensen[b], Tonni F. Johansen[c] and Lars Hoff[a]

[a] Department of Micro and Nano Systems Technology, Vestfold University College, Horten, Norway

[b] Department of Microsystems and Nanotechnology, SINTEF ICT, Oslo, Norway

[c] Department of Circulation and Medical Imaging, Norwegian University of Science and Technology, Trondheim, Norway

This paper is published in Ultrasonics, available online 5 March 2013.

Microfabricated 1-3 Composite Acoustic Matching Layers for 15 MHz Transducers

Tung Manh[a*], Geir Uri Jensen[b], Tonni F. Johansen[c] and Lars Hoff[a]

[a]Department of Micro and Nano Systems Technology, Vestfold University College, Horten, Norway
[b]Department of Microsystems and Nanotechnology, SINTEF ICT, Oslo, Norway
[c]Department of Circulation and Medical Imaging, Norwegian University of Science and Technology , Trondheim, Norway
[*]Corresponding author. Email: tung.manh@hive.no. Phone: +47 33037928.

Abstract: Medical ultrasound transducers require matching layers to couple energy from the piezoelectric ceramic into the tissue. Composites of type 0-3 are often used to obtain the desired acoustic impedances, but they introduce challenges at high frequencies, i.e. non-uniformity, attenuation, and dispersion.

This paper presents novel acoustic matching layers made as silicon-polymer 1-3 composites, fabricated by deep reactive ion etch (DRIE). This fabrication method is well-established for high-volume production in the microtechnology industry. First estimates for the acoustic properties were found from the iso-strain theory, while the Finite Element Method (FEM) was employed for more accurate modeling. The composites were used as single matching layers in 15 MHz ultrasound transducers. Acoustic properties of the composite were estimated by fitting the electrical impedance measurements to the Mason model.

Five composites were fabricated. All had period 16 µm, while the silicon width was varied to cover silicon volume fractions between 0.17 and 0.28. Silicon-on-Insulator (SOI) wafers were used to get a controlled etch stop against the buried oxide layer at a defined depth, resulting in composites with thickness 83 µm. A slight tapering of the silicon side walls was observed; their widths were 0.9 µm smaller at the bottom than at the top, corresponding to a tapering angle of 0.3°. Acoustic parameters estimated from electrical impedance measurements were lower than predicted from the iso-strain model, but fitted within 5% to FEM simulations. The deviation was explained by dispersion caused by the finite dimensions of the composite and by the tapered walls. Pulse-echo measurements on a transducer with silicon volume fraction 0.17 showed a two-way -6 dB relative bandwidth of 50%. The pulse-echo measurements agreed with predictions from the Mason model when using material parameter values estimated from electrical impedance measurements.

The results show the feasibility of the fabrication method and the theoretical description. A next step would be to include these composites as one of several layers in an acoustic matching layer stack.

Keywords: 1-3 composite, acoustic matching layers, high frequency transducers, silicon micromachining.

1. Introduction

For applications where the imaging depth is small, e.g. less than a centimeter, and the transducer aperture size is limited, e.g. intravascular ultrasound where the sensor head diameter is limited to one or two millimeters, high frequency (10 - 60 MHz) broadband ultrasound transducers provide images with high resolution in axial and lateral directions. Most ultrasound transducers are based on a piezoelectric ceramic, often lead zirconate titanate (PZT), operating in thickness mode. To effectively couple energy into the human tissue, one or more acoustic matching layers are required. This requires matching layer materials with acoustic impedances in the range from 2 to 19 MRayl [1]-[4]. Finding a single-phase material with the optimal acoustic impedance is not always possible, and composite materials are often used. Newnham *et al.* [5] classified composite materials according to the connectivity of the constituent phases, and identified 16 different composite patterns for a bi-phase material. Among these, the 0-3, 2-2 and 1-3 connectivity composites are most common in transducer engineering. 0-3 composites are usually formed by mixing metal powder and epoxy resin, whereas the others are traditionally manufactured by mechanical dicing, using a saw to cut kerfs into a bulk substrate and filling the trenches with epoxy [6].

The 0-3 composite is the most common form of matching layers, typically containing particles with diameters around a few microns. Using these materials at high frequencies introduces some challenges. Achieving high acoustic impedance (> 8 MRayl) requires a large volume fraction of particles, which may cause particles to come into contact and change the acoustic properties of the composite. Moreover, a thin matching layer, e.g. a 100 MHz transducer requires matching layers less than 8 µm thick [1], results in only a few particles across its thickness, making it difficult to obtain uniform material parameters [1], [7]. Lastly, if the particle size is not small compare to the thickness of the matching layer, scattering on the particles will cause attenuation, which increases strongly with frequency. This limits the operating frequency of these materials to typically below 10 MHz [1], [8].

Table 1 Material properties for polymer [17] and silicon [22]

Parameter	Notation	Value	Notation	Value
	POLYMER		SILICON	
Density (kg/m^3)	ρ^p	1100	ρ^{Si}	2330
Elastic constants (GPa)	c_{11}^p	5.410	c_{11}^{Si}	166
	c_{12}^p	2.526	c_{12}^{Si}	64
	c_{44}^p	1.307	c_{44}^{Si}	80
Mechanical loss	$\tan\delta_m^p$	0.033[a]	$\tan\delta_m^{Si}$	0.0025[b]
Longitudinal wave velocity (m/s)	V^p	2200	V^{Si}	8400
Acoustic impedance (MRayl)	Z^p	2.4	Z^{Si}	19.7

[a] Estimated from pulse-echo measurements.
[b] Estimated from electrical impedance measurements on a transducer consisting of a silicon layer on a PZT disc.

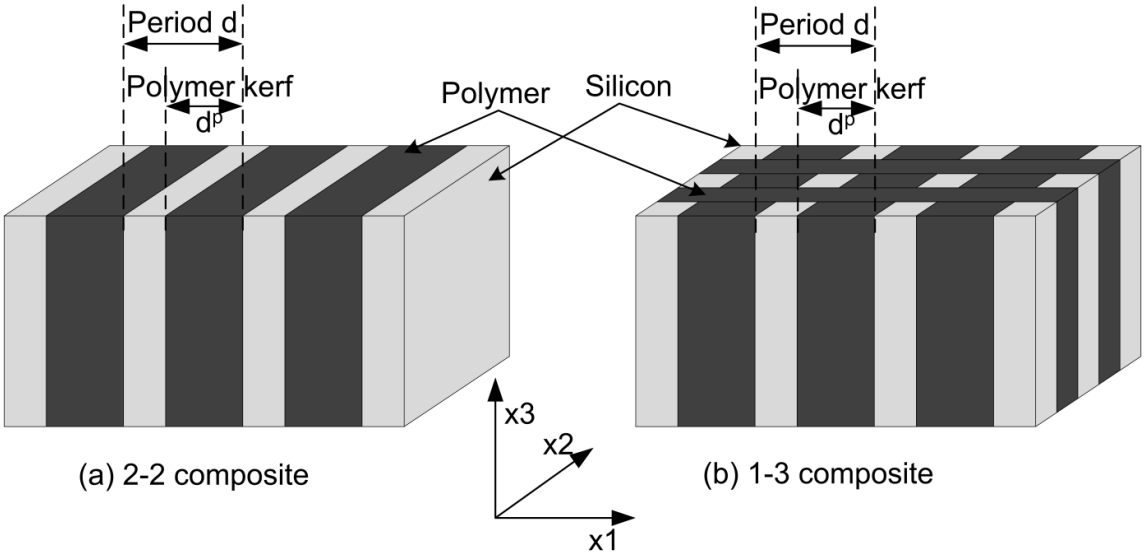

Figure 1 Schematic of silicon-polymer composite (a) 2-2 composite (b) 1-3 composite. The composites have period d and polymer kerf d^p. Only the silicon-polymer 1-3 composite is investigated in this paper.

The first and most obvious solution to these problems is to use a 0-3 composite with smaller particles, i.e. nanopowders. This method has been recently studied by numerous researchers [1], [7]-[9]. Different nanoscale particles such as alumina [1], [7], cerium oxide [8], titanium oxide [9] loaded in various polymer matrices have been explored. This method has been demonstrated to give promising matching materials for ultrasound transducers up to 100 MHz.

A different approach is using micro-fabrication tools from the MEMS-industry (Micro Electrical Mechanical Systems). This technology allows fabrication of composite structures in both 2-2 and 1-3 connectivity (Figure 1). By using lithography and etch instead of mechanical dicing to make the grooves, µm-sized structures with adjustable volume fraction can be fabricated. This method can provide composite materials with any selected acoustic impedance in a wide range limited by chosen polymer, e. g. 2.4 MRayl, and silicon, 19.7 MRayl, by just changing the volume fraction ratio between the two constituents. Moreover, with advanced lithography techniques such as electron beam or scanning-beam interference lithography and etch, it is possible to manufacture sub-micron sized structures [10], [11], suitable for transducers operating at very high frequencies (> 100 MHz). The first use of this to fabricate acoustic matching layers for ultrasound transducers was demonstrated by Haller and Khuri-Yakub [12]. They used anisotropic wet etch to fabricate a 2-2 composite (Figure 1a), etching along the crystal planes of <110> oriented silicon wafers. The resulting deep and long trenches in the silicon were subsequently filled with epoxy resin, forming the 2-2 composite to be used as acoustic matching layers in transducers operating around 5 MHz. However, the method requires accurate alignment of the long straight line features to the <111> planes in the silicon within 0.1º, which can be demanding if structures are less than 2 µm) [13]. Moreover, H_2 bubbles trapped inside the deep grooves are known to cause non-uniformity in the thickness of the layer [10]. Another work by Haller and Khuri-Yakub used plasma etch to fabricate a Kapton/air 1-3 composite to be used as acoustic matching layer for ultrasonic transducers operating in air [14]. This composite was fabricated for low

frequencies, around 1 MHz, and the measured results did not agree with the theoretical calculations, probably caused by limitations in the fabrication technique. Since then, to our knowledge, there has been no further development in the micro-machining of composite materials for use as acoustic matching layers.

In this paper, we present a new method to fabricate a composite with µm-sized features, for use as one of the layers in an acoustic matching layer stack. Instead of anisotropic wet etch, we use deep reactive-ion etch (DRIE), the *Bosch Process*, to fabricate silicon-polymer composites of 1-3 connectivity (Figure 1b). To obtain a composite layer of a defined thickness, Silicon-on-Insulator (SOI) wafers are used, stopping the etching at a buried silicon dioxide layer at a specified depth. The DRIE-process is not sensitive to crystal orientation, and is promising for mass production.

This composite is intended to be used as an intermediate layer in a stack of two or three acoustic matching layers for a piezo-ceramic ultrasound transducer [15]. In this stack, the silicon substrate would be bonded to a piezoelectric disc, or alternatively, a piezoelectric film can be deposited on the silicon substrate, to make the silicon substrate function as the first acoustic matching layer, as suggested in [15].

The aim of this paper is to explore in detail the acoustic properties of the silicon-polymer composite, how it can be made, how it can be described theoretically, and how it performs acoustically. The acoustic properties of a composite have been described by two theoretical models: The *iso-strain* approach by Smith and Auld [16] and the *dynamic* model of guided waves by Geng [17]. The iso-strain model assumes the composite lateral period to be much smaller than the acoustic wavelength and describes the composite as a homogeneous material with a set of material parameters. The dynamic model of guided waves goes one step further by considering the composite lateral dimensions. By applying the concept of guided wave propagating along the thickness direction, and coupling these waves at the interfaces between the two components, the relations between the wave vector component in the thickness direction, k_3, and the frequency, f, are obtained. The resulting curves, showing the wave vector as function of frequency, are the dispersion relations of the composite [17], [18]. A full wave solution for a three dimensional 1-3 composite is difficult to obtain mathematically [19]. Instead, we have chosen to calculate these dispersion relations from Finite Element Method (FEM) simulations. The composites in this paper were fabricated with dimensions suited to a transducer working at 15 MHz. Testing and characterization of the composites was achieved by bonding these composites to PZT discs, forming air-backed ultrasound transducers. The acoustical composite properties were determined from electrical impedance of these transducers in air. By curve-fitting the measured impedances to a one dimensional Mason model [20] consisting of a PZT discs and a composite matching layer, the acoustical properties of composite were estimated and then compared to results of pulse-echo measurements in water.

2. Methods

2.1. The iso-strain model

A composite will behave acoustically like a homogeneous material if its lateral spatial scale is much smaller than the acoustic wavelength [17]-[19]. For a piezocomposite material, the following requirement has been found to avoid interference from the lateral mode into the thickness resonance [21]

$$d^p \le \frac{V_S^p}{4\sqrt{2}\, f_c} \qquad (1)$$

where f_c is the resonance frequency of the thickness mode; V_S^p is the shear wave velocity in the polymer and d^p is the width of the polymer phase, i.e. the kerf, see Figure 1. Within this regime, the elastic parameters of the composite are approximated by the iso-strain model [16]. In this paper, we only look at passive silicon-polymer composites and there is no electromechanical coupling. According to this model, the acoustic parameters for a 1-3 composite are

$$\bar{c}_{33}^C = \Phi^{Si}\left[c_{33}^{Si} - \Phi^p \frac{2\left(c_{12}^p - c_{13}^{Si}\right)^2}{\Phi^p\left(c_{11}^{Si} + c_{12}^{Si}\right) + \Phi^{Si}\left(c_{11}^p + c_{12}^p\right)}\right] + \Phi^p c_{11}^p \qquad (2)$$

$$\bar{\rho}^C = \Phi^{Si}\rho^{Si} + \Phi^p \rho^p \qquad (3)$$

$$\bar{Z}^C = \sqrt{\bar{c}_{33}^C \bar{\rho}^C} \qquad (4)$$

$$\bar{V}^C = \sqrt{\frac{\bar{c}_{33}^C}{\bar{\rho}^C}} \qquad (5)$$

where the overbars ($\bar{x}$) with superscript ^{C} refers to parameters of the composite, superscript ^{p} refers to parameters of the polymer, and superscript ^{Si} to parameters of the silicon. c_{ij} are the elastic coefficients of the two materials, ρ are the densities, and Φ^{Si} is the volume fraction of silicon in the composite, so that $\Phi^p = 1 - \Phi^{Si}$ is the volume fraction of polymer. $\bar{Z}^C$ is the acoustic impedance and $\bar{V}^C$ is the pressure wave velocity of the composite, both measured in the thickness direction. Silicon is an anisotropic crystal with cubic symmetry so that $c_{11}^{Si} = c_{22}^{Si} = c_{33}^{Si}, c_{12}^{Si} = c_{13}^{Si}$ and $c_{12}^{Si} = c_{13}^{Si}$ [22].

The FEM model was further used to investigate the influence of deviations from vertical side walls, or tapering. This was modelled by letting the silicon post size in the FEM model decrease linearly from the top to the bottom.

2.2. FEM model

Our goal is to fabricate a silicon polymer 1-3 composite material with an acoustic impedance of about 6.3 MRayl, to be used as an intermediate layer in an acoustic matching-layer stack [15]. According to the iso-strain model, and with the material parameters given in Table 1, a 6.3 MRayl acoustic impedance corresponds to a silicon volume fraction of 0.19, giving a composite with density 1335 kg/m^3 and pressure wave velocity 4730 m/s. The iso-strain model can be used as a starting point for obtaining first estimates. But as it is a one dimensional (1D) model, it will only capture the thickness vibration mode, lateral modes are not included, and the finite lateral dimensions of the composite are ignored. Moreover, deviations from a perfect structure due to the fabrication process are not captured. E.g., the etched side walls are not perfectly perpendicular to the wafer/device surface, but exhibit a slight tapering profile.

To account for these phenomena, a 3D FEM model of the transducer was set up using *COMSOL Multiphysics*, ver. 4.1 (*Comsol AB*, Stockholm, Sweden). The FEM model

describes one composite silicon-polymer layer driven by a PZT plate. A periodic structure consisting of a quarter composite unit cell was modelled, with symmetric boundary conditions as described by Hossack and Hayward [23]. The influence of the finite dimensions of the composite was investigated by keeping the volume fraction of the silicon, Φ^{Si} constant at Φ^{Si} =0.19, while the polymer width, d^p, was varied around a range given by the constraint (1).

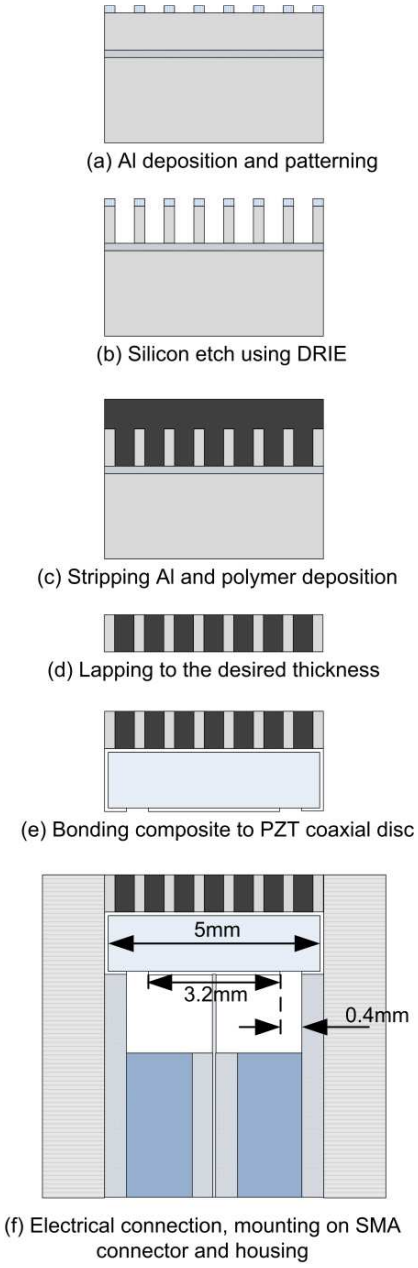

Figure 2 Main steps in fabrication of an air-backed transducer with a silicon-polymer composite as matching layer. (a) Sputtering Al and patterning by photoresist. (b) Silicon etch using DRIE. (c) Stripping Al and depositing polymer. (d) Lapping the structure to the desired thickness. (e) Bonding the composite to a PZT coaxial disc. (f) Electrical connection, mounting the transducer on SMA connector and housing.

2.3. Electrical impedance measurements

Electrical impedance measurements were used to get estimates for the acoustic material parameters of the composite. This was performed in the two-step procedure: First, the electromechanical properties of a PZT disc alone were determined. Then, a composite was bonded to that PZT disc to form an air-backed transducer. The acoustical material parameters of the composite were then extracted from the measured electrical impedance of this transducer by curve-fitting the measured data to the one dimensional Mason model. All impedance measurements were performed in air using an HP 8753D Network Analyzer (Agilent Technologies, Santa Clara, CA, USA).

2.3.1. Estimation of the PZT parameters

The electromechanical parameters of the PZT disc alone were determined from the method described by Kwok *et al.* [24]. Five discs were characterized, all from the same production batch (PZT-5A, Boston Piezo-optics, Bellingham, MA, USA), having center frequency 15 MHz. The PZT discs had a coaxial electrode pattern, chosen to allow electrical connection to both electrodes from the back side of the discs. The coaxial electrode pattern had center electrode diameter 3.2 mm, outer ring width 0.5 mm and 0.4 mm gap between them. The electrical impedances of these discs were measured over the frequency range from 12 MHz to 18 MHz using 201 data points. A non-linear regression algorithm, the Gauss-Newton method, was applied to fit the measured impedances to the Mason model. Losses were included by describing the material parameters as complex quantities, giving the three complex material coefficients as

$$\begin{aligned} c_{33}^{D*} &= c_{33}^{D}\left(1+i\tan\delta_m\right) \\ \varepsilon_{33}^{S*} &= \varepsilon_{33}^{S}\left(1-i\tan\delta_e\right) \\ k_t^{*} &= k_t\left(1+i\tan\delta_k\right) \end{aligned} \qquad (6)$$

where c_{33}^{D*} is the complex elastic coefficients at constant electric field, ε_{33}^{S*} is the complex clamped dielectric permittivity, k_t^{*} is the complex electromechanical coupling constant for thickness mode vibration, and $\tan\delta_m$, $\tan\delta_e$ and $\tan\delta_k$ are the corresponding loss tangents. Reliable results from this inversion method require initial guesses, and these were obtained from the non-iterated method by Sherrit *et al.* [25].

2.3.2. Estimation of the composite material parameters

The characterized PZT discs above then were glued to composites (fabrication process is described in section 3). This created an air-backed transducer consisting of a piezo-electric plate and a single silicon-polymer composite acoustic matching layer; see Figure 2e. Spurr's epoxy (Low viscosity embedding media Spurr's Kit, Catalog #14300, Electron Microscopy Sciences, Hatfield, PA, USA) was used for bonding adhesion. Prior to bonding to the PZT discs, microscopic images of the composite from both the top and the bottom were taken. The dimensions measured on these images were used to find initial estimates for the acoustic properties of the composite, using the iso-strain model. These parameters were inserted into the Mason model as start values. Better estimates for the three composite material parameters, acoustic impedance Z^C, longitudinal wave speed V^C, and loss tangent $\tan\delta_m^C$, were found by

fitting the measured electrical impedance curves to calculations from the Mason model. The fitting was performed using a non-linear regression scheme, the Nelder-Mead simplex method [26], implemented in MATLAB. The arithmetical mean roughness Ra, measured by an interferometer (Wyko NT9100Technical, Veeco Instruments Inc., USA), was in the range 0.5-0.6 μm for PZT discs and 0.2-0.3 μm for composites, respectively. Hence, the bonding thickness was estimated to be less than 1 μm, based upon the assumption that the total surface roughness of the PZT and the composite defined the epoxy thickness. This bonding thickness is small compared to the wavelength of the operating frequency, 15 MHz, and the influence of the bonding layer was neglected in the fit. The thickness of the composite layers is defined by the device layer thickness in the SOI wafer with the accuracy of ±1 μm. The PZT material parameters were taken from Table 2 based upon the estimation from the electrical impedance measurements on the PZT discs alone (described in subsection 2.3.1).

Table 2 Material properties for PZT coaxial discs, estimated from five discs. The electromechanical properties were estimated from curve-fitting to the measured electrical impedances; the acoustic impedance and wave velocity were calculated from the elastic constants in thickness mode

Parameter	Notation	Value	Manufacturer
Density (kg/m^3)	ρ	7800[a]	7800
Active area (mm^2)	A	8[b]	—
Thickness (μm)	t	135±1[c]	—
Acoustic impedance (MRayl)	Z	33.8±0.27	28.8
Longitudinal wave velocity (m/s)	V	4335±35	3686
Elastic stiffness constant at constant electric displacement (10^{11} N/m^2)	c_{33}^D	(1.47±0.23)	1.06
Mechanical loss tangent	$\tan\delta_m$	0.018±0.005	0.0125
Relative permittivity	$\varepsilon^S/\varepsilon_0$	916±24	1900
Electrical loss tangent	$\tan\delta_e$	0.067±0.032	0.018
Electromechanical coupling for thickness mode	k_t	0.420±0.014	0.48
Electromechanical coupling loss tangent	$\tan\delta_k$	0.020±0.010	—

[a] From manufacturer.
[b] Calculated from the electrode diameter.
[c] Direct measurement using micrometer.

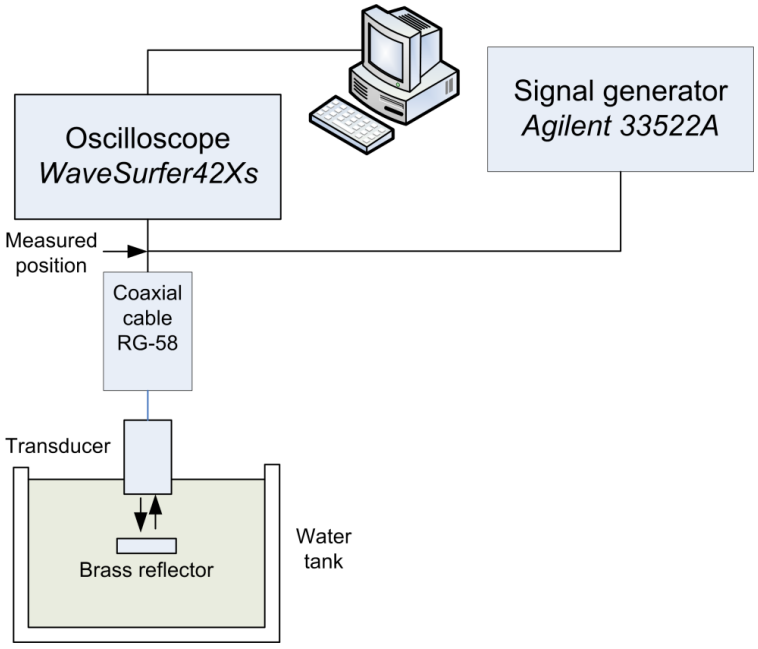

Figure 3 Schematic drawing of the acoustic pulse-echo setup. The brass target was a cylinder with 44 mm diameter and 41 mm thickness, which was placed with normal incidence to the acoustic axis at the distance of 7 mm.

2.4. Acoustic pulse-echo measurements

Pulse-echo measurements in a water tank were used to finally check the acoustic performance of the transducer with the composite as acoustic matching layer. Before these measurements the composite matching layer surface was lapped down to its desired quarter wavelength thickness ±1 µm. The transducer was mounted to an SMA electrical connector, with the center electrode connected to the SMA connector via a 0.12 mm diameter wire, using conductive epoxy (Epo-Tek EE129-4, Epoxy Technology, Inc., Bellerica, MA, USA). A Teflon tube covered the SMA to make the transducer waterproof, Figure 2f.

The pulse-echo measurement setup is shown in Figure 3. The transducer was mounted on a handler controlled by a robot motor (Physik Instrumenter, Karlsruhe, Germany) and placed in a tank containing de-ionized water. The transducer was connected to a 50 Ω signal generator (*Agilent 33522A*, Agilent Technologies, Inc., Santa Clara, CA, USA) via a 1.5 m RG-58 cable. The driving pulse was single cycle sine wave at center frequency 15 MHz, with 10 V amplitude. Echoes were received by the same transducer after reflection from a polished brass target. The brass target was a cylinder with 44 mm diameter and 41 mm thickness, which was placed with normal incidence to the acoustic axis at the distance of 7 mm. The received signals were recorded at the signal generator end of the cable using a digitizing oscilloscope (*WaveSurfer 42Xs*, LeCroy Corporation, Chestnut Ridge, NY, USA), and transferred to a PC for further investigation.

3. Fabrication of the composite

Silicon-on-Insulator, SOI, wafers (Ultrasil Corporation, USA) with diameter 100 mm were used to obtain a defined control of the thickness of the composite layer. The SOI wafers contain a thin buried oxide layer which will stop the etching at a determined depth. The

thicknesses were (83±1) µm for the device layer, 0.5 µm for the buried oxide layer, and (500±10) µm for the handle layer. Masks for processing of the silicon wafers were designed with composite period 16.0 µm and post size 7.0 µm. The wafers were patterned using DRIE. This fabrication process always causes some undercut, i.e. the etched trenches will be slightly wider than the features on the mask. To account for this, the mask was made with different openings, spanning an expected undercut range between 0.0 and 1.0 µm in steps of 0.1 µm per side. This would also make composites spanning a range of silicon volume fractions, allowing the investigation of the effect of the silicon volume fraction on the acoustic properties.

The fabrication procedure is illustrated in Figure 2. First, a 0.5 µm aluminum (Al) layer was sputtered on top of the SOI wafer. The Al layer was patterned by 1.5 µm photoresist, etched to create a mask for the DRIE process, before the photoresist was removed by plasma stripping (Figure 2a). DRIE was performed in an *AMS 200 I-Productivity* machine (Alcatel Micro Machining Systems, Annecy, France) using a low frequency bias etch option to minimized the notching/tapering at the bottom of the posts [27] (Figure 2b).

The Al mask and polymer were stripped in *piranha* etching solution, a mixture of H_2SO_4 and H_2O_2. The wafers were rinsed in DI water, air dried, and the etched structures vacuum filled by Spurr's epoxy resin to form the composite material. This particular epoxy resin was chosen due to its low viscosity (60 cP) and small heat shrinkage, to avoid damage to the silicon posts [28]. The impregnated wafers were cured at 70°C for 8 hours (Figure 2c).

The processed wafers were diced into 6mm x 6mm dies using a *Disco Abrasive Systems* dicing saw (Disco Corporation, Japan). The top polymer and bottom silicon layers of each sample were ground and polished, leaving only the composite layer. This lapping process was performed using *MultiPrep™ System* grinding and polishing equipment (Allied High Tech Products Inc., USA) using a coarse-to-fine grit scheme with precision of 1 µm in thickness and 0.01° in angular positioning. The final lapping particle diameter was 5 µm and the polishing chemical was a mixture of colloidal silica and 0.05 µm alumina (Allied High Tech Products Inc., USA) (Figure 2d). The thickness of the samples was measured by a digital micrometer (Mitutoyo 293-561, Mitutoyo America Corp., USA) with accuracy of ± 1 µm.

A microscopic image of the fabricated structures is shown in Figure 4. This verifies that the trench bottoms are homogeneous and flat, and that the etching stopped at the buried oxide layer. Optical measurements from the top show a lateral reduction in the width of the Si posts of (0.90±0.06) µm at each side, compared to the openings in the mask. This lateral displacement is as expected, and varies slightly over the wafer. Measurements also show that the post width reduction is almost constant from wafer to wafer. This indicates the repeatability of the process, which is promising for mass production.

Measurements from the bottom show post widths that are about 0.9 µm smaller than measured at the top (Figure 5b), corresponding to a tapering angle of 0.3º. This tapering of the side walls could not be eliminated in our process, but is judged as acceptable. Optimization of the DRIE process might allow reduction of this tapering. However, the chosen composite volume fraction requires approximately 80% of the silicon to be removed. This is considered a high local loading in the DRIE process, and is known to make it hard to obtain straight walls in the fabricated structures [18].

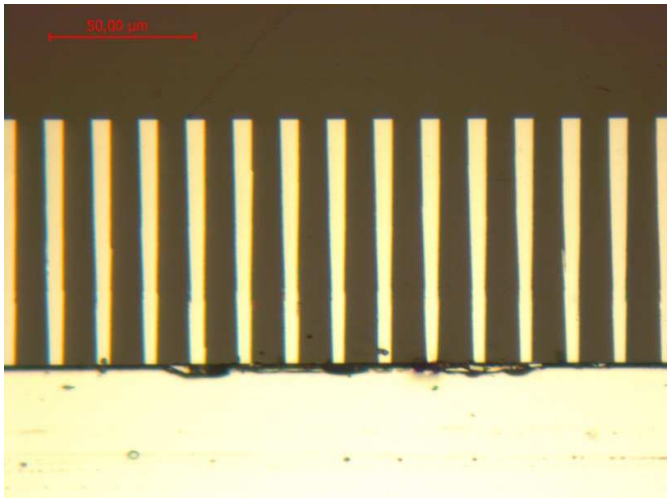

Figure 4 Microscopic image of the 1-3 composite with silicon posts (light color) in polymer matrix (dark color).

4. Results and discussions

4.1. FEM simulations

FEM simulations of electrical impedance for varying kerf sizes with Φ^{Si}=0.19 are shown in Figure 6. The highest resonance frequency is for a homogeneous material with properties predicted by the iso-strain model. The FEM simulations show how the resonance frequency shifts downwards as the kerf size increases towards $\lambda_s^p / 2$, half the shear wavelength in the polymer. This reduction in resonance frequency corresponds to a reduction in longitudinal wave velocity, and is associated with a reduction in acoustic impedance in the composite material [17]. A kerf size of 1/16 λ_s^p, or 4.5 µm, is seen to cause a small but still visible difference from the iso-strain model, the peaks were shifted downward about 0.1 MHz, as shown in Figure 6. As the kerf size reaches 1/2 λ_s^p, lateral modes start to appear within the bandwidth of the transducer. This can be related to a dispersive behavior of the composite material, as described by the dynamic model in references [17]-[19]. The dispersion relation, as the variation of the wave number in the thickness direction, k_3 as function of frequency, was found from FEM simulations giving the eigenmodes of the composite. Figure 7 shows the dispersion relations for the two lowest symmetric modes, which are assumed to be the most important ones. At large thickness ($k_3d<1$), the first branch, the 0–mode, corresponds to the longitudinal wave in the thickness direction, whereas the second branch, the 1-mode, corresponds to the lateral resonance formed by a standing wave in the polymer kerfs. For a very fine composite structure, when the period d is much smaller than the longitudinal wavelength, λ_3, the wave velocity in the thickness direction is proportional to the slope of the first branch and almost constant, with value as predicted by the iso-strain model. As k_3d increases, the coupling between the two modes gets stronger. This results in the first branch bending downwards, giving reduced wave velocity and hence, reduced acoustic impedance of the composite. The dispersion curves also show that for composites with dimensions as described in section 3, the operating range will be below the interaction zone, i.e. the zone where the two curves are close to each other (see Figure 7), preventing switching of modes [17]-[19].

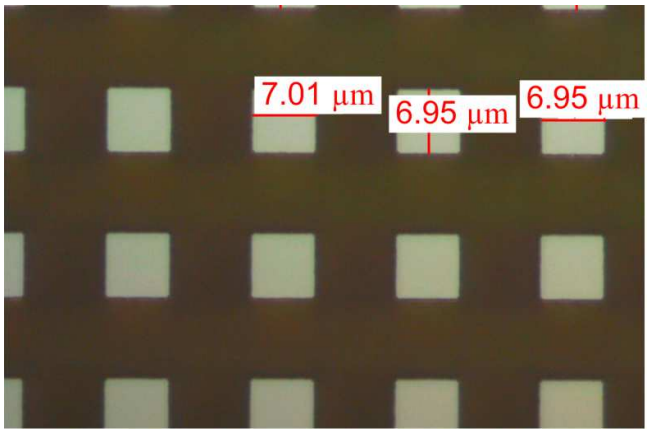

(a)

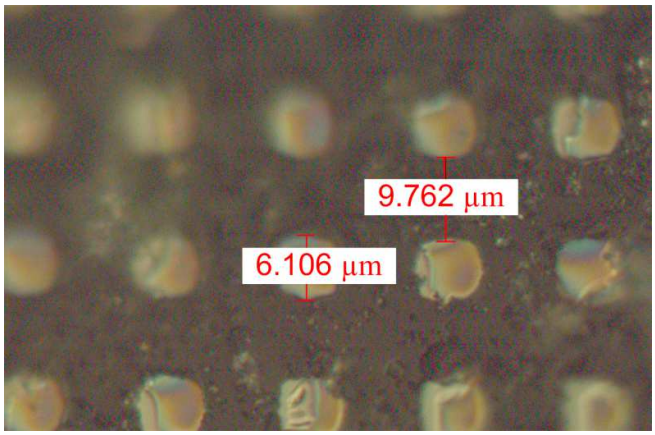

(b)

Figure 5 Microscopic images of the 1-3 composite structure used to make the air-backed transducer, top (a) and bottom (b) view. The images show the reduction of silicon volume fraction at the bottom compared to that on the top.

FEM simulations were also used to investigate the effect of non-vertical side walls, as seen in the fabricated structure in Figure 4. The simulated electrical impedances of a transducer consisting of a PZT disc bonded to a composite matching layer are presented in Figure 8. This matching layer has silicon posts 7.0 µm wide at the top, decreasing linearly to 6.1 µm at the bottom, corresponding to a tapering angle of 0.3°. Results for composites with vertical walls with post width 7.0 µm and 6.1 µm are shown for comparison. The simulations show clear differences among the three situations. For vertical walls with post width 7.0 µm, the two resonance peaks are found at 11.6 MHz and 17.1 MHz. For 0.3° tapered walls, they move to 11.2 MHz and 16.6 MHz. The impedance of the tapered structures was found to be closer to the impedance of the composite with post width as measured at the bottom of the composite, 6.1 µm, than to the impedance of the composite with post width as measured at the top, 7.0 µm.

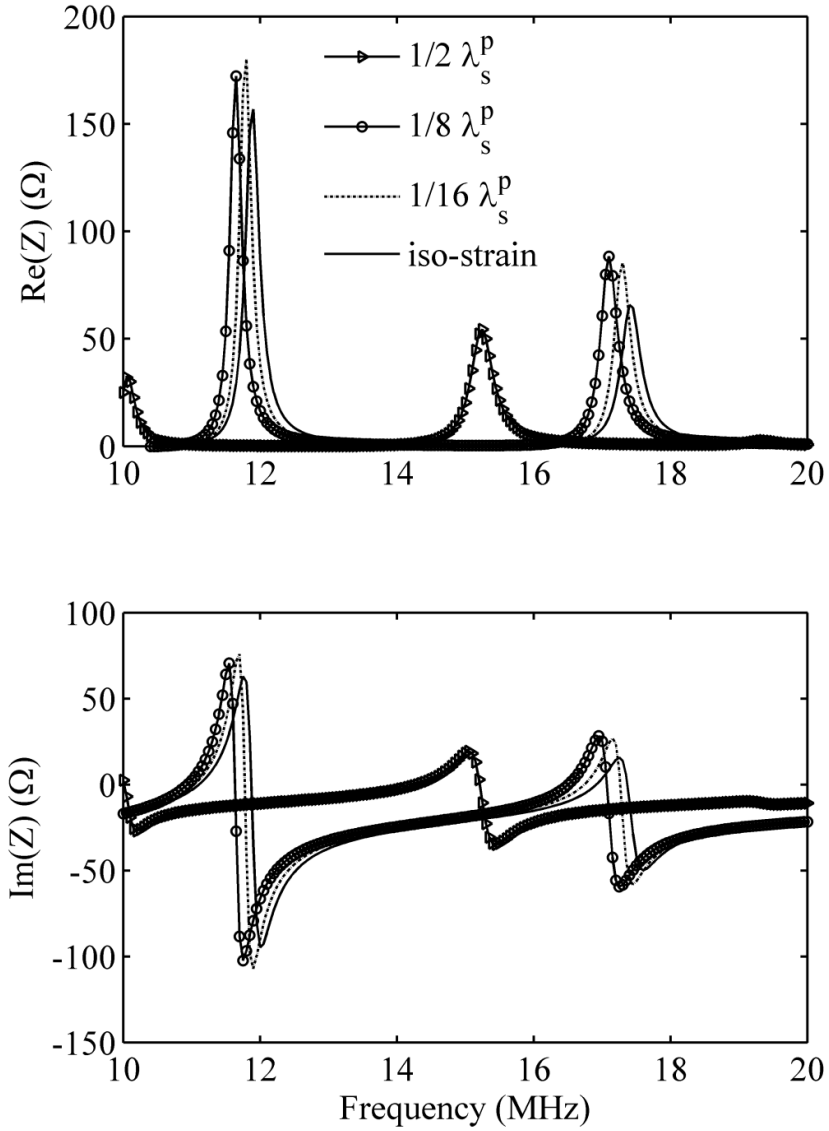

Figure 6 FEM-simulations of the electrical impedance of an air backed transducer, using a silicon-polymer composite as acoustic matching layer on top of a piezoelectric PZT-disc. Different dimensions of the composite are simulated, scaled relative to the shear wavelength in the polymer λ_s^p = 72 µm, at the center frequency, f_c=15 MHz of the piezo-electric disc. The silicon volume fraction was constant at 0.19. The curves show electrical impedance for composite material parameters calculated from the iso-strain model (solid lines), kerf size 1/16 λ_s^p (dotted lines), kerf size 1/8 λ_s^p (solid lines with circles), and kerf size 1/2 λ_s^p (solid lines with triangles).

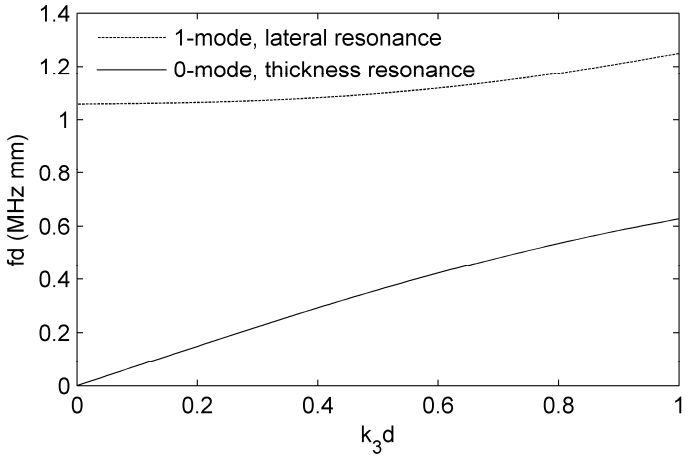

Figure 7 FEM-simulations of the dispersion curves for waves propagating in the 1-3 composite. The composite period *d*, is 16 µm with 0.19 volume fraction silicon. The frequency, *f*, and wave number, k_3, are normalized by the period d of the composite.

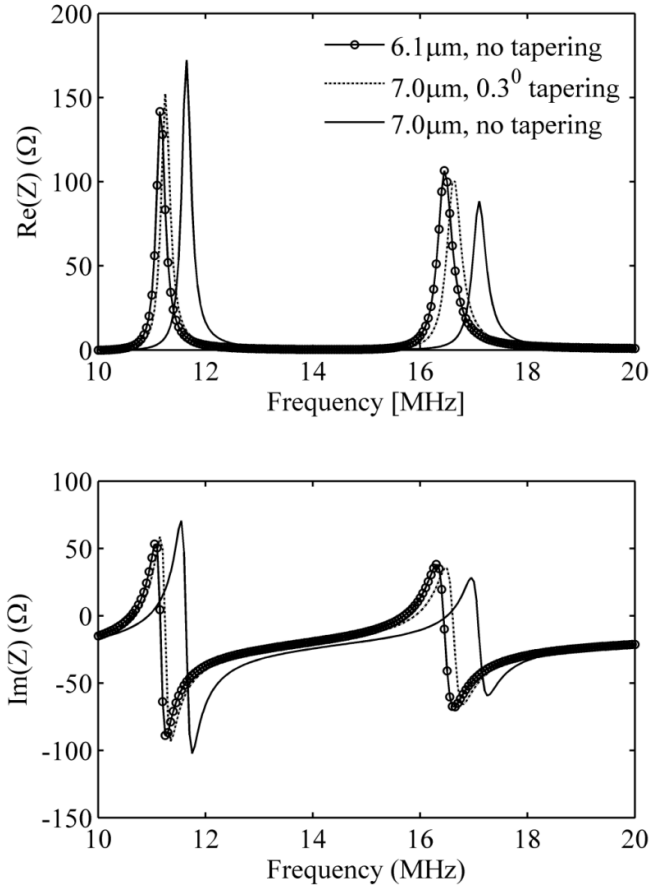

Figure 8 FEM-simulations of the electrical impedance of the same transducer as in Figure 4 with and without tapering of the side walls. The curves show the electrical impedance for post width 6.1 µm and no tapering (solid lines with circles), post width 7.0 µm and 0.3º tapering (dotted lines), and post width 7.0 µm with no tapering (solid lines).

4.2. Electrical impedance measurements

4.2.1. *Estimation of the PZT parameters*

Figure 9 shows electrical impedance measurements on the PZT disc alone in air. These measurements were fitted to the theoretical model and used to estimate the electro-mechanical parameters for the PZT. The fitted impedance curves are plotted in the same graphs for comparison. The material parameters estimated from these measurements are listed in Table 2, based on results of five different PZT samples. These results differ from the manufacturer's material data (Table 2), which are measured at 1 kHz. However, our results are consistent with the parameters from Foster *et al*. [29], who measured in the frequency range from 20 to 80 MHz.

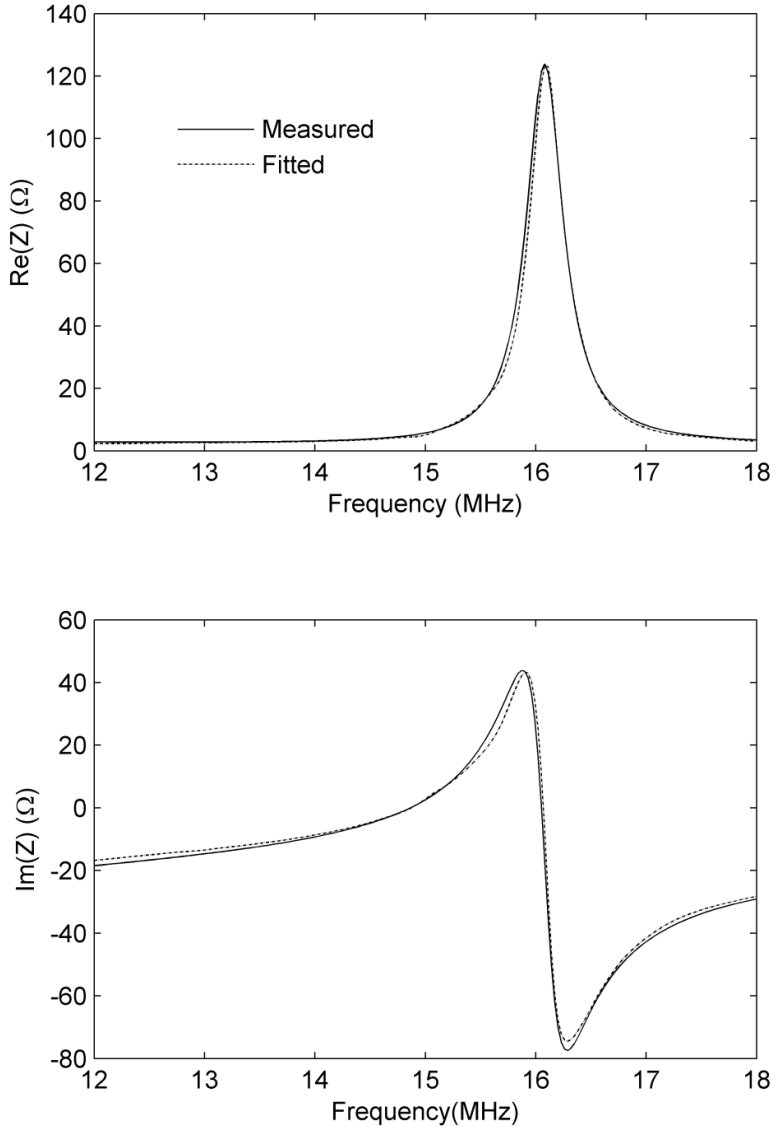

Figure 9 The measured (solid lines) and fitted (dotted lines) impedance of one of the coaxial PZT discs.

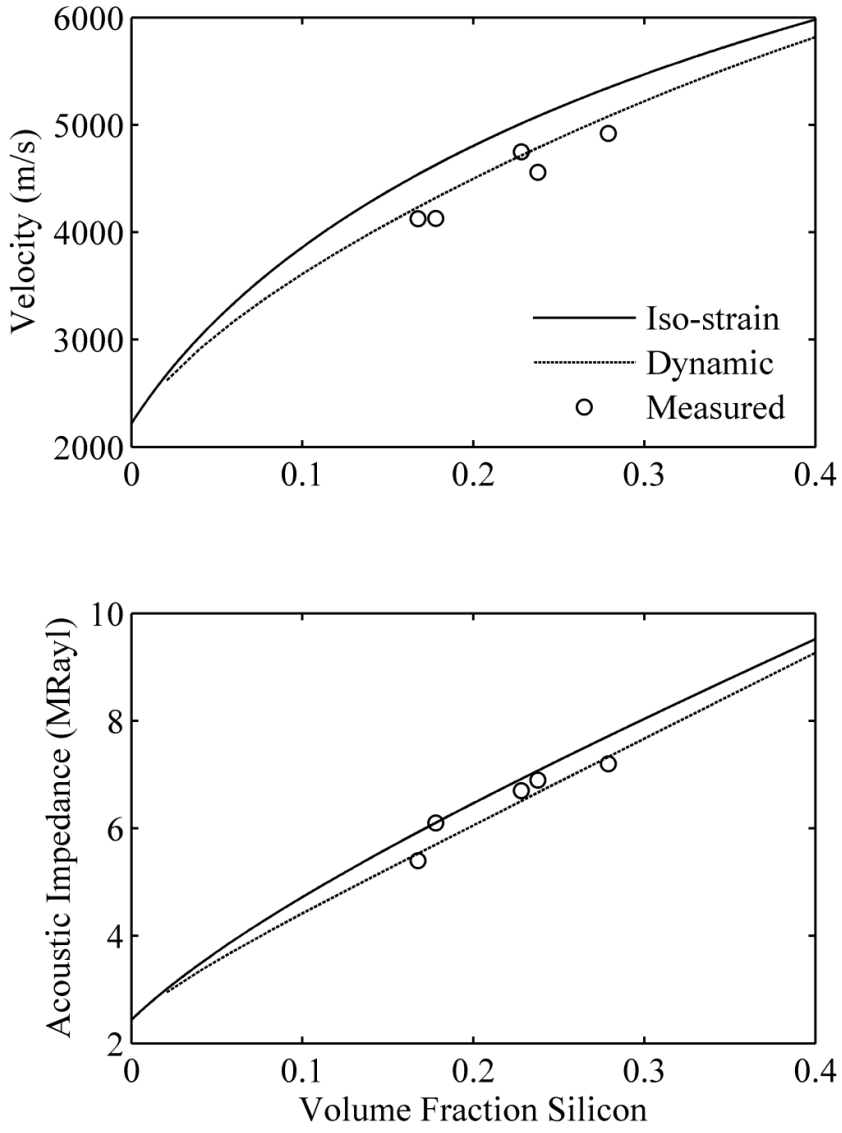

Figure 10 Longitudinal wave speed and acoustic impedance of the composite vs. silicon volume fraction. Values calculated from the iso-strain model (solid lines); and from FEM-simulations (dotted lines). Circles are values estimated from the electrical impedance measurements in air, where the silicon volume fractions are the average values computed from the dimensions observed at both the top and bottom of composites, assumed linear tapering.

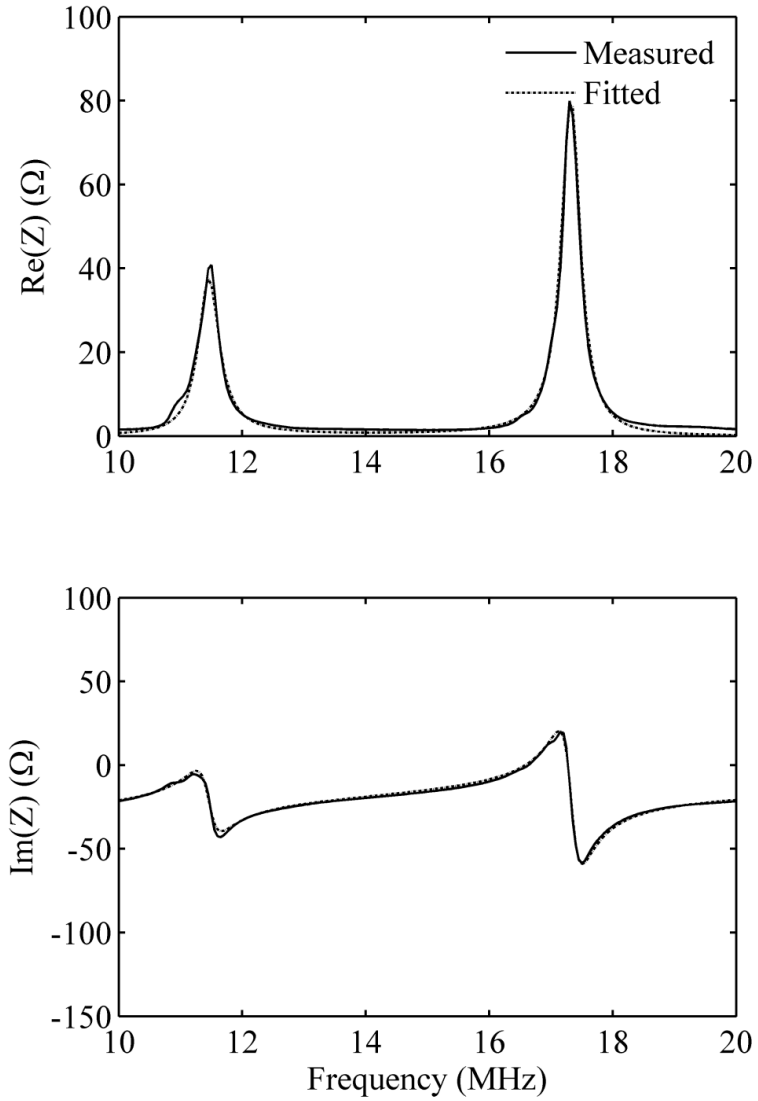

Figure 11 The measured (solid lines) and fitted (dotted lines) impedance of one of the transducers with composite post size 7 μm at top, decreasing to 6.1 μm at the bottom measured in air.

Table 3 Material properties for a 1-3 composite matching layer, estimated from electrical impedance measurements**.**

	Dimension Measured at		Fitted
Parameter	Top	Bottom	
Density (kg/m^3)	1335	1278	1309
Thickness (μm)	83	83	83
Longitudinal wave velocity (m/s)	4730	4336	4126
Acoustic impedance (MRayl)	6.32	5.54	5.40
Mechanical loss tangent	—	—	0.037

4.2.2. Characterization of the silicon-polymer composite layer

Longitudinal wave velocity and acoustic impedance estimated for 5 composite samples with different post widths are shown in Figure 10, together with theoretically calculated curves. Curves showing the measured and fitted electrical impedances of a transducer, with post width 7 µm measured at the top, are shown in Figure 11, with the estimated material parameters listed in Table 3.

The acoustic impedance of the composite, as estimated from the electrical measurements, is about 14% lower than the value predicted from the iso-strain model. We see two explanations for this: First, the finite lateral dimensions of the composite cause dispersion within the transducer bandwidth, decreasing the acoustic impedance. As seen in Figure 10 the wave velocity estimated from the FEM simulations of the real structure fits better to measured results (within 5%) than the results calculated from the iso-strain model (within 11%). In addition to this, the tapering of the side walls also reduces the acoustic impedance compared to what vertical walls would give.

The mechanical loss in the composite was found to be about 10% higher than that of the polymer alone. This can be expected, as the non-uniform structure causes some extra loss in addition to the pure material losses in the polymer and silicon. The mechanical loss in silicon is very low, the attenuation coefficient is in the range from 0.030 to 0.043 dB/mm/MHz, [30]), and gives negligible contribution to the total loss in the structure [19].

4.3. Acoustic pulse-echo measurements

Results of the pulse-echo measurements are shown in Figure 12. The upper graph is the received pulse, the lower graph shows the normalized power spectrum calculated from this pulse, giving a -6 dB relative bandwidth of 50%. For comparison, the pulse and power spectrum calculated from the Mason model using estimated material parameters from

Table 2 and Table 3 were plotted in the same graphs. The slight reduction (1.1 dB) in the measured compared to the calculated results may be caused by diffraction. The agreement between the measured and calculated acoustic pulses and between their spectra indicates that estimating the composite material parameters from electrical impedance measurements, as described here, is sufficient to predict the acoustic performance of the transducer.

The 50% relative bandwidth of the resulting transducer is typical for a transducer with one matching layer and air backing, but cannot match the bandwidth of modern transducers with two or three matching layers. However, the aim of this work was not to optimize the performance of this transducer, but to develop, test and model the composite as an acoustic matching layer, for inclusion into a multiple matching layer stack.

5. Conclusions

This study has demonstrated a method to design, fabricate and characterize a silicon-polymer 1-3 composite material for use as an acoustic matching layer in 15 MHz ultrasound transducers. The DRIE microfabrication process was shown to produce µm-sized structures with the high aspect ratio (10:1) required for such a composite. SOI wafers with a buried oxide layer gave a controlled stop of the etching at a predefined depth, with a flat, homogeneous surface in the trench bottoms.

Comparison between measurements and theory show that the acoustic parameters of the silicon-polymer layer are lower than values calculated from the iso-strain model. These deviations are attributed to the finite dimensions of the composite structure, and to a tapering

of the side walls. The iso-strain model is insufficient to reliably design and predict the acoustic properties of such a composite layer, but FEM-simulations seem to deliver results in close agreement with the measurements.

The performance of the test transducer was as expected for an air-backed transducer with a single matching layer. The result confirms the applicable feasibility of the fabrication method, which is well-established for high-volume production in the MEMS industry, into transducer manufacturing. When this has been demonstrated, a next step would be to include these composites as one of several layers in an acoustic matching layer stack.

Acknowledgments

We would like to thank Svein Mindrebøe for making the Teflon housing tube and Tormod Vinsand for his assistance in the material lab.

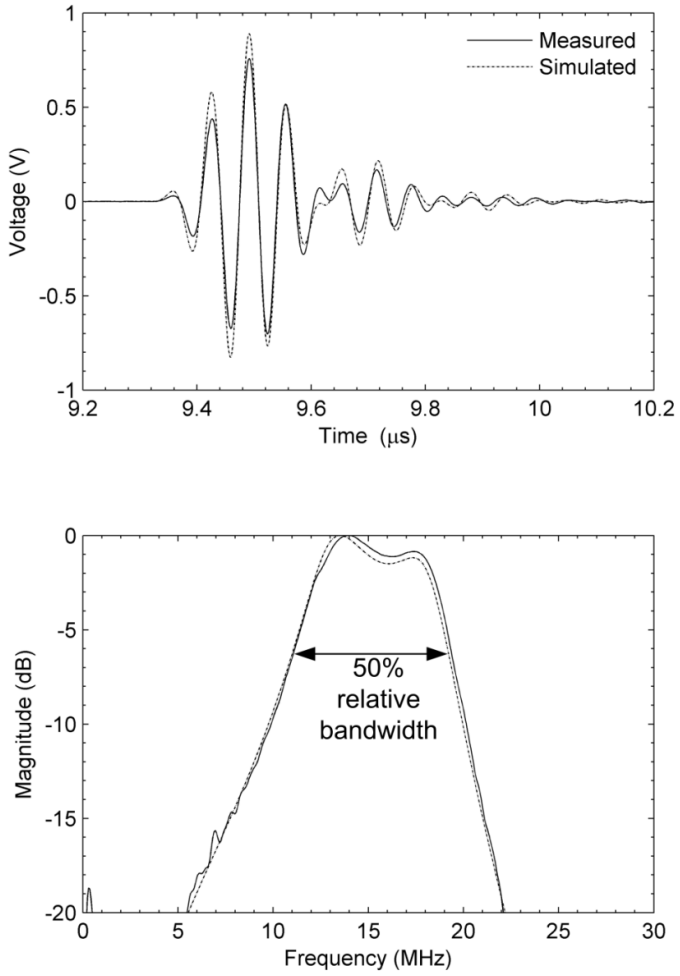

Figure 12 Pulse-echo measurement results from an air-backed transducer with composite as matching layer, measured values (solid lines) and values calculated from the Mason model (dotted lines) with the estimated acoustic material parameters. The composite used in these measurements has 16 µm period, 7 µm wide post at top and decreases to 6.1 µm at the bottom. The composite was lapped down to 67 µm thickness, or ¼λ.

References

[1] Q. Zhou, J. H. Cha, Y. Huang, R. Zhang, W. Cao, K.K. Shung, "Alumina/epoxy nanocomposite matching layers for high-frequency ultrasound transducer application," *IEEE Trans. Ultra. Ferro. Freq. Contr.*, vol. 56, pp. 213-219, 2009.

[2] L. Spicci and M. Cati, "Design and optimization of a high performance ultrasound imaging probe through FEM and KLM models," COMSOL conference, 2011.

[3] S. Rhee, T. A. Ritter, K. K. Shung, H. Wang, and W. Cao, "Materials for acoustic matching in ultrasound transducers," *Proc. IEEE Ultrason. Symp.*, pp. 1051-1055 vol.2, 2001.

[4] R. E. McKeighen, "Design guidelines for medical ultrasonic arrays," *Proc. SPIE Int. Symp.*, pp. 2-18, 1998.

[5] R. E. Newnham, D. P. Skinner, and L. E. Cross, *Connectivity and piezoelectric-pyroelectric composites,* Mater Res Bull, 1978.

[6] K. A. K. H. P. Savakas, and R. E. Newnham, "PZT-epoxy piezoelectric transducers: A simplified fabrication procedure," *Mater. Res. Bull.*, vol. 16, pp. 677-680, 1981.

[7] R. Zhang, W. Cao, Q. Zhou, J.H. Cha, K.K. Shung, Y. Huang, "Acoustic properties of alumina colloidal/polymer nano-composite film on silicon," *IEEE Trans. Ultra. Ferro. Freq. Contr.*, vol. 54, pp. 467-469, 2007.

[8] F. Tiefensee, C. Becker-Willinger, G. Heppe, P. Herbeck-Engel, and A. Jakob, "Nanocomposite cerium oxide polymer matching layers with adjustable acoustic impedance between 4 MRayl and 7 MRayl," *Ultrasonics,* vol. 50, pp. 363-366, 2010.

[9] S. Wang, P. Campistron, J. Carlier, D. Callens-Debavelaere, B. Nongaillard, A. Ndieguene, G. Nassar, C. Soyer, and X. Zhao, "Su-8-based nanocomposites for acoustical matching layer," *IEEE Trans. Ultra. Ferro. Freq. Contr.*, vol. 56, pp. 1483-1489, 2009.

[10] R. K. H. M. Ahn, and M. L. Schattenburg, "Fabrication of ultrahigh aspect ratio freestanding gratings on silicon-on-insulator wafers," *J. Vac. Sci. Technol.* , vol. 25, pp. 2593-2597, 2007.

[11] C. Chienliu, W. Yeong-Feng, K. Yoshiaki, S. Ji-Jheng, K. Yusuke, L. Chih-Kung, W. Kuang-Chong, and E. Masayoshi, "Etching submicrometer trenches by using the Bosch process and its application to the fabrication of antireflection structures," *Journal of Micromechanics and Microengineering,* vol. 15, pp. 580-585, 2005.

[12] M. I. Haller and B. T. Khuri-Yakub, "Micromachined ultrasound materials," *Proc. IEEE Ultrason. Symp.*, pp. 403-405, 1991.

[13] Y Uenishi, M Tsugai and M Mehregany, "Micro-opto-mechanical devices fabricated by anisotropic etching of (110) silicon," *Journal of Micromechanics and Microengineering,* vol. 5, pp. 305-312, 1995.

[14] M. I. Haller and B. T. Khuri-Yakub, "1-3 composites for ultrasonic air transducers," *Proc. Ultrason. Symp.*, vol.2, pp. 937-939, 1992.

[15] A.-T. T. Nguyen, T. Manh, L. Hoff, T. F. Johansen, and G. U. Jensen, "Fabrication of silicon-polymer composite acoustic matching layers for high frequency transducers," *Proc. Ultrason. Symp.*,pp. 2064-2067, 2010.

[16] W. A. Smith and B. A. Auld, "Modeling 1-3 Composite Piezoelectrics: Thickness-Mode Oscillation," *IEEE Trans. Ultra. Ferro. Freq. Contr.*, vol. 38, pp. 40-47, 1991.

[17] X. Geng, "Numerical modeling and experimental study of piezocomposite transducers," Ph.D dissertation, The Pennsylvania State University, 1997.

[18] Y. Shui, and Q. Xue, "Dynamic characteristics of 2-2 piezoelectric composite transducers," *IEEE Trans. Ultra. Ferro. Freq. Contr.*, vol. 44, pp. 1110-1119, 1997.

[19] X. Geng and Q. M. Zhang, "Resonance modes and losses in 1-3 piezocomposites for ultrasonic transducer applications," *Jour. Appl. Phys.*, vol. 85, pp. 1342-1350, 1999.
[20] W. P. Mason, *Electromechanical transducers and wave filters.* 2nd ed., New York: D. Van Nostrand Co., pp. 201-209, 399-409, 1948.
[21] H. R. Chabok, J. M. Cannata, K. Hyung Ham, J. A. Williams, P. Jinhyoung, and K. K. Shung, "A high-frequency annular-array transducer using an interdigital bonded 1-3 composite," *IEEE Trans. Ultra. Ferro. Freq. Contr.*, vol. 58, pp. 206-214, 2011.
[22] M. J. Madou, *Fundamental of Microfabrication: The Science of Miniaturization*, 2nd ed. CRC. Press, pp. 198, 2002.
[23] J. A. Hossack and G. Hayward, "Finite-element analysis of 1-3 composite transducers," *IEEE Trans. Ultra. Ferro. Freq. Contr.*, vol. 38, pp. 618-629, 1991.
[24] K. W. Kwok, H. L. W. Chan, and C. L. Choy, "Evaluation of the material parameters of piezoelectric materials by various methods," *IEEE Trans. Ultra. Ferro. Freq. Contr.*, vol. 44, pp. 733-742, 1997.
[25] S. Sherrit, H. D. Wiederick, and B. K. Mukherjee, "Non-iterative evaluation of the real and imaginary material constants of piezoelectric resonators," *Ferroelectrics*, vol. 134, pp. 111-119, 1992.
[26] A. Nelder and R. Mead, "A Simplex Method for Function Minimization," *The Computer Journal*, vol. 7, pp. 308-313, 1965.
[27] M. Hermersdorf, C. Hibert, D. Grogg, and A. M. Ionescu, "High aspect ratio sub-micron trenches on silicon-on-insulator and bulk silicon," *Microelectronic Engineering*, vol. 88, pp. 2556-2558, 2011.
[28] A. R. Spurr, "A low-viscosity epoxy resin embedding medium for electron microscopy," *Journal of Ultrastructure Research*, vol. 26, pp. 31-43, 1969.
[29] F. S. Foster, L. K. Ryan, and D. H. Turnbull, "Characterization of lead zirconate titanate ceramics for use in miniature high-frequency (20-80 MHz) transducers," *IEEE Trans. Ultra. Ferro. Freq. Contr.*, vol. 38, pp. 446-453, 1991.
[30] A. Bardaine, P. Boy, P. Belleville, O. Acher, and F. Levassort, "Improvement of composite sol-gel process for manufacturing 40 µm piezoelectric thick films," *Journal of the European Ceramic Society*, vol. 28, pp. 1649-1655, 2008.

Paper B

Modeling of Micromachined Silicon-Polymer 2-2 Composite Matching Layers for 15 MHz Ultrasound Transducers

Tung Manh[a], Geir Uri Jensen[b], Tonni F. Johansen[c] and Lars Hoff[a]

[a] Department of Micro and Nano Systems Technology, Vestfold University College, Horten, Norway

[b] Department of Microsystems and Nanotechnology, SINTEF ICT, Oslo, Norway

[c] Department of Circulation and Medical Imaging, Norwegian University of Science and Technology, Trondheim, Norway

This paper is submitted to Ultrasonics for publication.

Modeling of Micromachined Silicon-Polymer 2-2 Composite Matching Layers for 15 MHz Ultrasound Transducers

Tung Manh[a*], Geir Uri Jensen[b], Tonni F. Johansen[c] and Lars Hoff[a]

[a]Department of Micro and Nano Systems Technology, Vestfold University College, Horten, Norway
[b]Department of Microsystems and Nanotechnology, SINTEF ICT, Oslo, Norway
[c]Department of Circulation and Medical Imaging, Norwegian University of Science and Technology , Trondheim, Norway
[*]Corresponding author. Email: tung.manh@hive.no. Phone: +47 33037928.

Abstract: Silicon-polymer composites fabricated by micromachining technology offer attractive properties for use as matching layers in high frequency ultrasound transducers. Understanding of the acoustic behavior of such composites is essential for using them as one of the layers in multilayered transducer structures. This paper presents analytical and finite element modelling of the acoustic properties of silicon-polymer silicon-polymer 2-2 composites.. Analytical calculations based on partial wave solutions are applied to identify the resonance modes and estimate effective acoustic material properties. Finite Element Method (FEM) simulations were used to investigate the interaction between the composite and the surrounding load medium, including both fluids and solids, with main emphasis on the acoustic impedance of the composite. Composites with lateral periods of 20, 40 and 80 µm were fabricated and used as acoustic matching layers for air-backed transducers operating at 15 MHz. These composites were characterized acoustically, and the results compared with analytical calculations. The analytical model shows that the first lateral resonance in the silicon-polymer 2-2 composite is primarily defined by the composite period. This is in contrast to piezo-composites, where it is mainly determined by the width of the polymer phase. The first lateral resonant frequency is higher than that of a piezo-composite with the same ploymer filler. This result shows that a silicon-polymer matching layer can have lateral dimensions 1.2 times larger than a piezo-composite operating at the same frequency. FEM simulations indicate that the effective acoustic impedance of the silicon-polymer composite varies with frequency, and that it also depends on the load material, especially whether this is a fluid or a solid The estimated longitudinal sound velocities of the 20 and 40 µm period composites match to the effective values from analytical calculations within 2.7% and 2.6%, respectively. The effective acoustic impedances of the 20 and 40 µm period composites were found to be 10% and 26% lower than the values from the analytical calculations. This can be explained by the dispersion when the composites are in loaded by soft materials such as air or water. When the composites are loaded by solids, the effective acoustic impedances are increased, and were closer to the analytical calculations. This is explained by the shear stiffness in the solid, which tends to even out the surface displacements of the composites.

Keywords: 2-2 composite, acoustic matching layers, high frequency transducers, silicon micromachining.

1. Introduction

Medical transducers require acoustic matching layers to effectively couple energy from the piezoelectric active layer, often a lead zirconate titanate (PZT) plate, into the human tissue. These matching layers should have acoustic impedance between that of the PZT (>30 MRayls) and the load medium (<1.6 MRayls) [1]-[4]. Finding a single-phase material with the required impedance within this range is not always possible, and composites are often used. Typical composite matching layers are made with 0-3 connectivity, i.e. a mixture of metal particles in polymer matrix. The particle diameter is typically a few µm, and employing these materials at high frequencies, above 10 MHz, introduces challenges such as non-uniformity, high attenuation and dispersion [1], [5]. Some research groups have resolved this by reducing the particle sizes, i.e. employing nano powders. The method provides promising matching materials for ultrasound transducers up to 100 MHz [1], [5]-[7].

A different approach to manufacture composite matching materials for high frequency transducers is utilizing micro-fabrication tools from the MEMS-industry [8], [9]. The composites can be fabricated by using either anisotropic wet etch of (110) oriented silicon wafers [8] or deep reactive-ion etch (DRIE), the *Bosch process* [9], to etch trenches into the substrates and subsequently fill these grooves with epoxy resin. The method can provide composites with specific acoustic impedance in a wide range between that of silicon, 19.7 MRayls, and epoxy resin, typically around 2-3 MRayls. More advanced lithography techniques such as electron beam and scanning-beam interference, allows manufacturing composite matching layers with sub-micron sized structures, suitable for transducers operating at very high frequencies, e.g. above 100 MHz [9].

Being a bi-phase material, the acoustical properties of the composite are not only functions of the constituents' parameters but also of their dimensions and operating frequency. For composites in 2-2 connectivity, i.e. plates of silicon and polymer are periodically layered as illustrated in Figure 1, the lateral scale must be considered, as resonances caused by Lamb waves related to the periodic microstructure might influence the transducer performance. Finding the range of composite dimensions where these lateral waves do not influence the thickness mode vibrations is crucial. For ceramic-polymer piezo-composite materials, many studies have been published exploring these limits. The most common theoretical approaches use the dynamic model of guided waves [10]-[13], and numerical FEM-simulations [14], [15]. Based on the dynamic model of guided waves, it has been reported that the first lateral resonance frequency in a 2-2 piezo-composite is determined by the half-wavelength shear resonance in the polymer [10]-[13]. For a broadband transducer, the guideline is to push this lateral resonance frequency to at least twice the thickness resonance. This can be achieved by setting the polymer width less than a quarter of the shear-wavelength in the polymer, calculated at the center frequency of the transducer [13], [16]. For silicon-polymer composites being used as matching layers in medical ultrasound transducers at high frequencies, e.g. between 10 MHz and 100 MHz, this requires extremely fine structures, which are challenging to fabricate. Using this approach, a single 2-2 composite matching layer for a transducer working at 100 MHz requires a polymer width 2.75 µm and a silicon width 0.56 µm, assuming a silicon volume fraction $r = 0.17$ and material properties given in Table 1 are used. It is our aim to investigate how these guidelines for piezo-composite can be transferred to silicon-polymer matching layers, and especially, whether they can be relaxed to allow easier fabrication. This should provide new design rules for silicon-polymer composite structures, considering both the technology limitations and the requirements for acoustical performance. Moreover, it is also important to investigate the composite behavior for different load media, both fluids and solids.

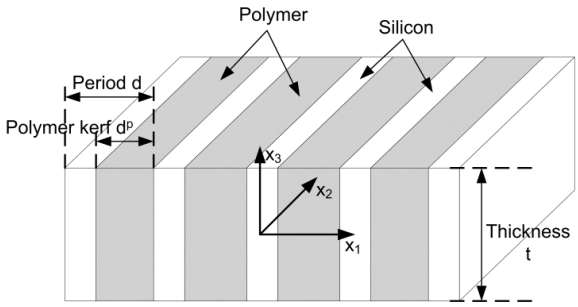

Figure 1 Schematic of a silicon-polymer 2-2 composite.

To achieve this, we have used analytical and FEM models of silicon-polymer 2-2 composites to investigate composite behavior, for different lateral dimensions and load media. Partial wave solutions in guided plates were employed to derive the dispersion curves for resonant modes in the composite, similar to what has been previously done for piezo-composites [10]-[13]. From the dispersion relations, the maximum allowable lateral dimensions and the acoustic properties of the composite can be found. The FEM simulations were used to check the analytical calculations and to investigate the interaction between the composite and the surrounding load media, both fluids and solids. Test transducers operating at center frequency 15 MHz with composite matching layer periods of 20, 40, and 80 µm were fabricated and characterized. The measured results were checked against corresponding FEM models and analytical calculations.

2. Methods

2.1. Dynamic model of guided waves

A periodic 2-2 composite with the chosen coordinate system as shown in Figure 1 can be theoretically described using a two-dimensional (2D) model in the x_1x_3 plane, where the dimension in x_1 direction is treated as infinite, if the dimensions in the x_1 and x_2-directions are much larger than the composite period *d* and thickness *t*. The elastic displacements u_i for the symmetric guided wave solutions in the silicon phase of an unbounded composite plate are [12]

$$u_1^{Si} = \sum_{n=1}^{2} B_n^{Si} A_{1n}^{Si} \sin\left(k_{1n}^{Si} x_1\right) \exp\left(jk_3 x_3\right)$$
$$u_3^{Si} = \sum_{n=1}^{2} B_n^{Si} A_{3n}^{Si} \cos\left(k_{1n}^{Si} x_1\right) \exp\left(jk_3 x_3\right) \qquad (1)$$

where $j = \sqrt{-1}$; superscripts ^{Si} denote the quantities in silicon; B_n^{Si} is the coefficient of the summation for *n*th partial wave; A_{in}^{Si} are wave amplitudes depending on wave vector components k_{1n}^{Si} in the x_1-direction and k_3 in the x_3-direction; k_{1n}^{Si} are functions of wave vector component k_3, frequency f and silicon material parameters. The solutions in the polymer phase are found by replacing x_1 in Eq. (1) by $\left(x_1 - d/2\right)$. Note that the wave vector in the x_3-direction, k_3, is common for both phases.

The four unknown parameters $B_n^{Si,p}; n=1,2$ are determined by requiring continuity in the displacements and stresses at the silicon-polymer interface $x_1 = rd/2$ where r is the silicon volume fraction in composite. This leads to the following equations

$$u_1^{Si} = u_1^p, \quad u_3^{Si} = u_3^p, \quad T_1^{Si} = T_1^p, \quad T_5^{Si} = T_5^p \qquad (2)$$

This forms a homogeneous linear system of equations that can be rewritten into matrix form as

$$\begin{pmatrix} K_{11} & K_{12} & K_{13} & K_{14} \\ K_{21} & K_{22} & K_{23} & K_{24} \\ K_{31} & K_{32} & K_{33} & K_{34} \\ K_{41} & K_{42} & K_{34} & K_{44} \end{pmatrix} \begin{pmatrix} B_1^{Si} \\ B_2^{Si} \\ B_1^p \\ B_2^p \end{pmatrix} = \mathbf{KB} = \mathbf{0}. \qquad (3)$$

where **K** is a 4 x 4 matrix and its elements are functions of k_3, f, d, r and the material properties of both the silicon and polymer phases. For example,

$$K_{11} = A_{11}^{Si} \sin\left(k_{11}^{Si} r \frac{d}{2} \right);$$

$$K_{13} = -A_{11}^p \sin\left(k_{11}^p (1-r) \frac{d}{2} \right)$$

A nontrivial solution of this system requires that the determinant vanishes, i.e.

$$|\mathbf{K}| = 0 \qquad (4)$$

For a given composite period d and silicon volume fraction r, this yields the relations between the wave vector component k_3 and the frequency f in the unbounded 2-2 composite, i.e. the dispersion relations for the composite.

When these relations are found, the effective longitudinal wave velocity can be approximated from the first branch of the dispersive curves by

$$V^C = 2\pi \frac{f}{k_3}, \qquad (5)$$

and the effective acoustic impedance is

$$Z^C = \rho^C V^C \qquad (6)$$

where $\rho^C = r\rho^{Si} + (1-r)\rho^p$ is the density of the composite. In the above formulas, superscript ^{C} refers to composite and r is the volume fraction of silicon in the composite.

2.2. FEM simulations

The FEM simulations were performed using software *COMSOL Multiphysics*, version 4.1, (*Comsol AB*, Stockholm, Sweden). The eigenvalue mode was used to extract the dispersion curves of the plate in air, to verify the calculations from the dynamic model of guided waves. By varying the composite thickness and finding the corresponding eigen-frequencies, a set of values were obtained, providing the relations between the x_3-component k_3 of the wave vector and the frequency f [14].

FEM simulations were also used to investigate the interaction between the composite and the surrounding medium. This was done using a 2D model illustrated in Figure 2. For a fluid medium, a source positioned in the surrounding fluid emitted plane waves into medium, hitting the composite interface (Figure 2a). For a solid medium, a distributed force was used as source, giving an incoming wave similar to the plane wave source in the liquid (Figure 2b). Half of the composite unit cell was modeled and symmetric boundary conditions were applied on the sides [17]. Perfectly matched layers were added to absorb incoming waves in the composite, ensuring no waves reflected back to the composite/isotropic interface [17]. The acoustic impedance was then found by the approach of Miller and Pursey [18]

$$Z_{FEM}^{C}\left(x_3\right)=\frac{\int T_3^C\left(x_1,x_3\right)dx_1}{\int v_3^C\left(x_1,x_3\right)dx_1} \qquad (7)$$

where T_3^C is the stress and v_3^C is the velocity in the composite; both in the thickness direction. The fluid was modeled as either water or ethanol. Three artificial solid materials were modeled, to investigate the importance of the shear stiffness of the load material. These solids were given identical values of the elastic constant c_{11} = 5.41GPa, but different shear stiffness: c_{44} = 2.3, 1.3 and 0.3 GPa.

Last, FEM models corresponding to the fabricated transducers were made and the results compared with results from the 1D Mason model [19] and with experiments.

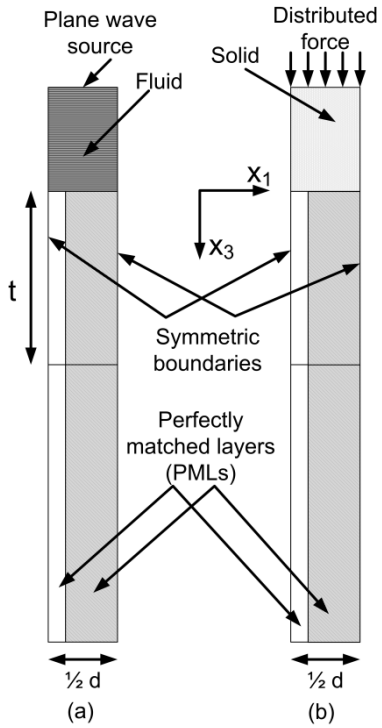

Figure 2 Schematic of a 2D FEM model set up in COMSOL.

Table 1 Material properties used in this study

Materials	**Properties Parameters**					
Active layer	Elastic constants (GPa)		Piezoelectric constants (C/m^2)		Dielectric constants	Density ρ (kg/m^3)
PZT-5A	c^E_{11} = 120.3	c^E_{33} = 113.7	e_{15} = 9.78		$\varepsilon^S_{11}/\varepsilon_0$ = 919 $\varepsilon^S_{33}/\varepsilon_0$ = 754	7800
	c^E_{12} = 75.2	c^E_{44} = 21.1	e_{31} = -1.81			
	c^E_{13} = 75.1	c^E_{66} = 22.6	e_{33} = 17.32			
Passive layer	Elastic constants (GPa)				Density ρ (kg/m^3)	
Silicon	c_{11} = 166.0	c_{12} = 64.0	c_{13} = 64.0	c_{44} = 80.0	2330	
Spurrs Epoxy	c_{11} = 5.41	c_{12} = 2.79	c_{13} = 2.79	c_{44} = 1.31	1100	
Water	c_{11} = 2.37	-	-	-	1000	
Ethanol	c_{11} = 1.10	-	-	-	789	

2.3. Experiments

Silicon-polymer 2-2 composites were manufactured by the method described in [9], where DRIE was used to etch deep trenches into Silicon on Isolator (SOI) wafers and *Spurr's epoxy* was used as filler (Low *viscosity embedding media Spurr's Kit*, Catalog #14300, Electron Microscopy Sciences, Hatfield, PA, USA). Three different composites were fabricated, with periods d = 20, 40 and 80 µm, and three samples were made for each period. The volume fraction in each set was 0.12, 0.17 and 0.18 corresponding to polymer width $d^p \sim \lambda_s^p/4$, $\lambda_s^p/2$ and λ_s^p, respectively; where λ_s^p is the shear-wavelength in polymer at 15 MHz. The silicon carrier layer and the top polymer layer of the SOI wafers were lapped off to leave only a single composite layer. The composites were bonded to PZT discs (*PZT-5A*, Boston Piezo-optics, Bellingham, MA, USA) to form test transducers operating at center frequency 15 MHz. The PZT discs have thickness (138±1) µm and diameter 3.2 mm. Material parameters for silicon, polymer and PZT discs are given in Table 1.

The composite matching layers on the fabricated transducers were ground down to the thickness corresponding to λ/4 and the surfaces were polished using a coarse to fine grit scheme. The final lapping particle was 5 µm and the polishing chemical was a mixture of colloidal silica and 0.05 µm alumina (Allied High Tech Products Inc, CA, USA). This lapping process was done using a *MultiPrep*^{TM} System (Allied High Tech Products Inc., CA, USA) with accuracy of 1 µm in thickness and 0.01° in angular positioning. The transducers were mounted on an SMA connector using conductive epoxy adhesion (*Epo-Tek EE129-4*, Epoxy Technology, Inc., Bellerica, MA, USA) and connected directly to a *HP 8753D* Network Analyzer (Agilent Technologies, Santa Clara, CA, USA) for electrical impedance measurements [9]. This was performed in air to easily identify the resonance peaks. Electrical impedance was measured as a function of frequency in the range 100 Hz – 30 MHz. Then, acoustic pulse-echo measurements in a water tank were performed on these air-backed transducers. The transducers were mounted on a robot controlled handler and immersed in water. A 50 Ω signal generator (*Agilent 33522A*, Agilent Technologies, Inc., Santa Clara, CA, USA) generated a 16 V amplitude, one cycle sine signal as the electrical transmit pulse. Reflected echoes from a 41 mm thick brass plate placed at normal angle to the acoustic axis at a distance of 7.8 mm were received and recorded by a digital oscilloscope (*WaveSurfer 42Xs*, Lecroy Corporation, Chestnut Ridge, NY, USA).

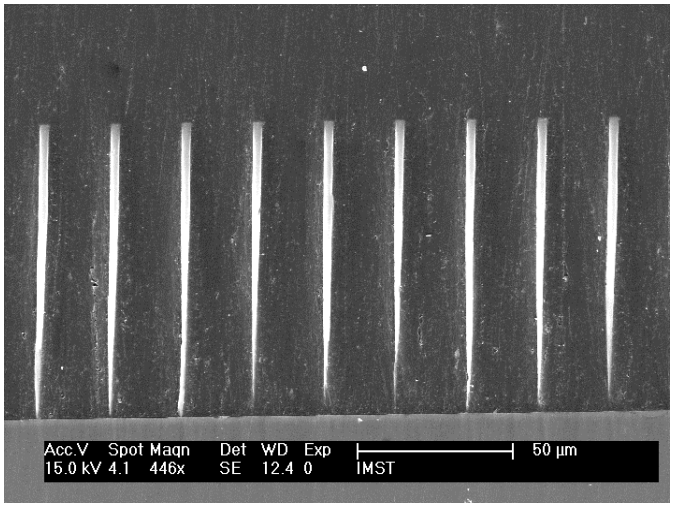

Figure 3 A SEM cross-section image of a silicon-epoxy 2-2 composite fabricated by the DRIE method. Bright is silicon and dark is Spurr's epoxy filler. Composite period d = 20 µm.

3. Results and discussions

Microscope images showed that the side walls of the fabricated silicon-polymer composites were slightly tapered as reported previously in [9]. This has previously been explained by the high local loading effect in the DRIE process, A Scanning Electron Microscopy (SEM) image of the structure is shown in Figure 3. Transducers with matching layers having different composite period were fabricated, giving differences in the measured electrical impedance spectra, as observed in Figure 4. Radial modes, arising at frequencies well below 10 MHz, are seen in all three graphs in Figure 4. These are outside the bandwidth of interest (10-20 MHz), and are not considered. The fabricated transducers consist of two layers, the PZT plate as the active layer and the silicon-polymer composite as a single acoustic matching layer. This configuration should result in two main peaks when operating in the thickness mode. In Figure 4a, with period d = 20 µm, no unwanted resonance is observed in the frequency bandwidth of interest. However, for the transducer with period d = 80 µm, the transducer performance is strongly influenced by the lateral mode where an additional peak appeared in the bandwidth of interest; see Figure 4c. For the transducer with the composite period d = 40 µm ($d^p \sim \lambda_s^p/2$), only a weak lateral resonance at about 25 MHz is seen (Figure 4b). The influence on the transducer performance from this mode is negligible, the signal level is about -20 dB, as seen from the pulse-echo measurement results in Figure 13. These different behaviors are investigated further using analytical models and FEM simulations in the following sections.

3.1. Dispersion curves, lateral resonance and interaction between modes

Dispersion curves were calculated from the dynamic model of guided waves for different silicon volume fractions. The two lowest branches, corresponding to fundamental and first lateral resonances, are shown in Figure 5. Both axes are normalized by the composite period d. The normalized operating frequencies for the fabricated transducers are f_d = 0.3, 0.6 and 1.2 corresponding to composite period 20, 40 and 80 µm, respectively. In Figure 5, they are presented by a square line, a triangle line and a circle line, respectively.

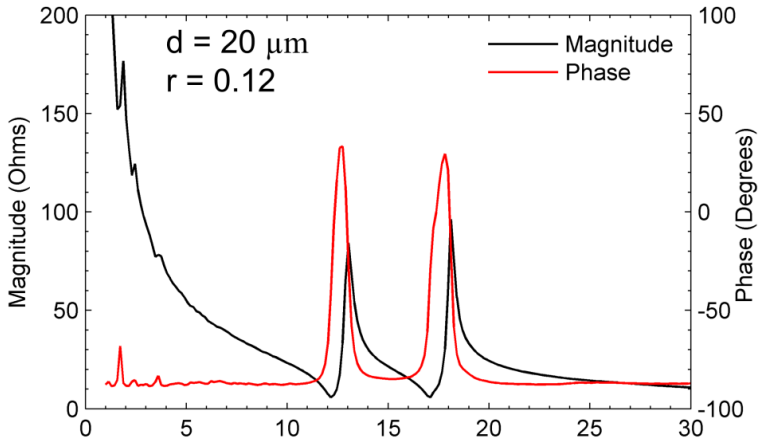

(a)

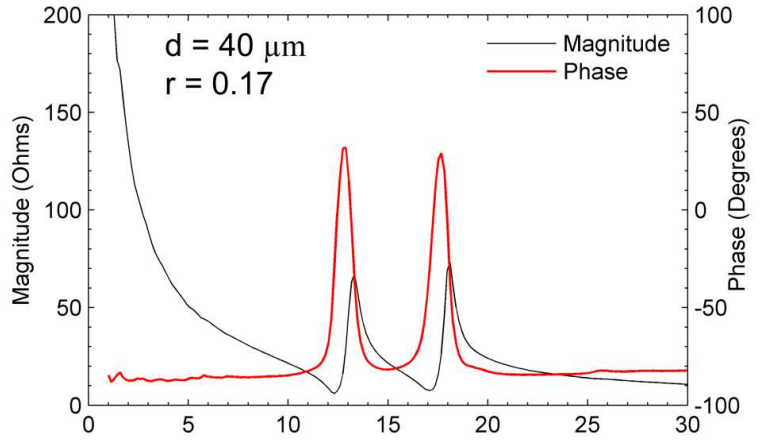

(b)

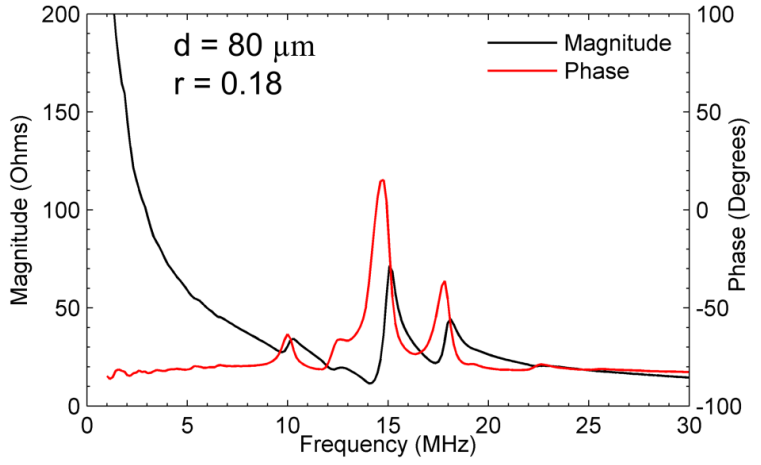

(c)

Figure 4 Measured electrical impedances of the fabricated transducers with different composites as a single matching layer (a) d = 20 μm, t = 68 μm, r = 0.12 (b) d = 40 μm, t = 64 μm, r = 0.17 (c) d = 80 μm, t = 80 μm, r = 0.18.

It is known that the gap between the fundamental and the first lateral branches in the interaction zone, i.e. the zone where two curves are close to each other, is an indication of the strength of the mode coupling [10]-[13]. From Figure 5, it is seen that the larger the silicon volume fraction *r*, the weaker coupling between the thickness and lateral modes. For example, for $r = 0.7$, the mode coupling is weak, as the two curves are close to each other; while for $r = 0.17$, they are highly separated and the coupling is stronger. The gap in the interaction zone for the silicon-polymer composite is relatively larger than what has been found in similar studies of piezoelectric composites, using the same polymer filler [11], i.e. the coupling is stronger between the two lowest modes in a silicon-polymer 2-2 composite than in a 2-2 piezo-composite. This can be explained by the coupled mode theory shown in [20]. The coupling constant between thickness and lateral modes in the piezo-composite is defined as [20]

$$\Gamma = \left[1 - \frac{\bar{c}_{33}^{D}\rho}{c_{33}^{D}\bar{\rho}}\right]^{1/2} \qquad (8)$$

where $c_{33}^{D} = c_{33}^{E} + e_{33}^{2} / \varepsilon_{33}^{S}$ is the elastic stiffness constant at constant electric displacement and ρ is the density of the piezoelectric material; $\bar{c}_{33}^{D} = \bar{c}_{33}^{E} + \bar{e}_{33}^{2} / \bar{\varepsilon}_{33}^{S}$ is the effective elastic stiffness constant at constant electric displacement and $\bar{\rho}$ is the effective density of the piezo-polymer composite. These effective constants are found from Smith's model [21] and the calculations are omitted here. Using Eq. (8) and material data for PZT, silicon and polymer given in Table 1, coupling constants for the silicon-polymer composite and for the piezo-polymer composite are plotted on the same graph in Figure 6. It is seen that when the volume fraction increases, the coupling constant decreases, as expected. For a wide range of volume fractions (r<0.75), the coupling between thickness and lateral resonances in the silicon-polymer composite is stronger than in the piezo-polymer composite. Only for volume fraction *r* above 0.75, the coupling constant of the piezo-polymer is above that of the silicon-polymer composite.

Figure 7 presents the relationship between the lateral resonance frequency and the composite dimension. The lateral cut-off frequency of a composite is defined as the first lateral resonance frequency when $k_3 d \to 0$. This was calculated from the dynamic model of guided waves as function of volume fraction, its value normalized by the period d is shown on the left. The same result normalized by the polymer width d^p is shown on the right. It is seen that, for low to medium silicon volume fractions (r <0.4), the curve normalized by the composite period d is flat, ranging from 0.99 to 1.1, i.e. $\Delta f/f$<5%. For higher silicon volume fractions, 0.4<r<0.9, this curve rises steeply from 1.1 to 5.1. In contrast, the curve normalized by the polymer width d^p decreases sharply when r<0.4, and flattens out in the region where 0.4<r < 0.9 (in the range from 0.52 to 0.67, $\Delta f/f$ <13%). This shows that for medium to high silicon volume fractions, where r = 0.4 to 0.9, the lateral resonance is mainly determined by the polymer width. However, for low to medium volume fractions, where r<0.4, the lateral resonance is primarily determined by the composite period d, rather than by the polymer width d^p. The results are in contrast with results reported for a piezo-composite using the same polymer filler [11].

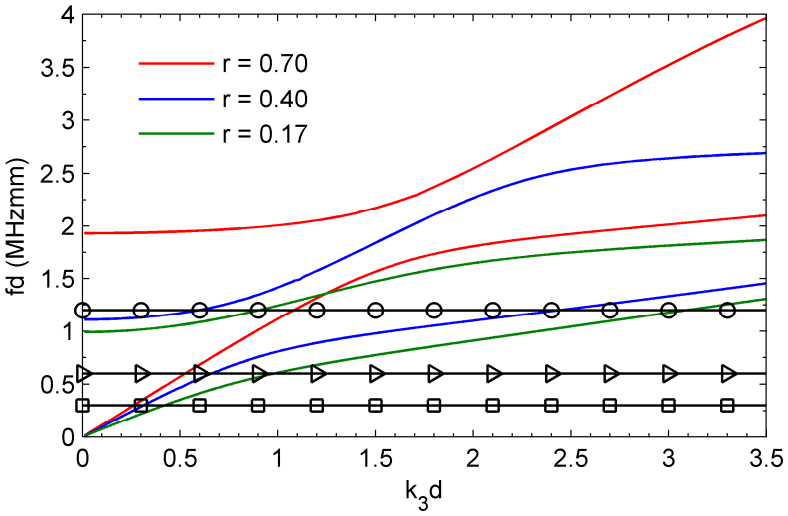

Figure 5 Dispersion curves for different silicon volume fractions calculated from the dynamic model of guided waves. Red lines are with r = 0.70, blue lines are with r = 0.40 and green lines are with r = 0.17, respectively. Square, triangle and circle lines are normalized operating frequency of transducers with composites period 20, 40 and 80 µm, respectively.

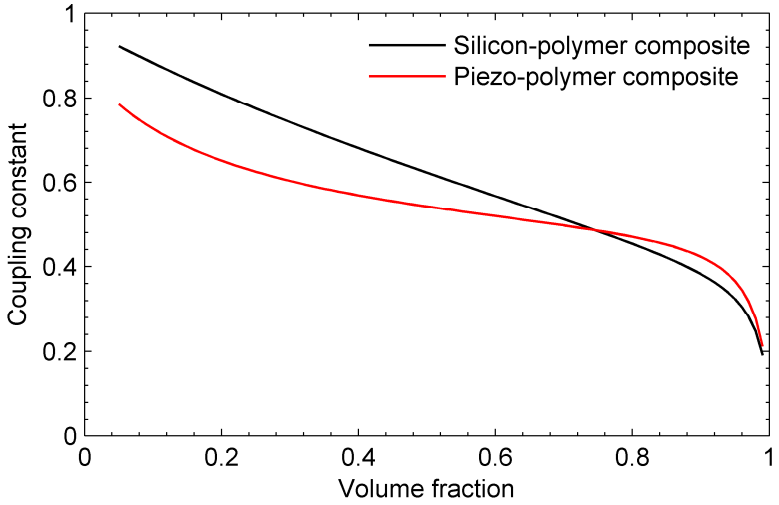

Figure 6 Coupling constant for silicon-polymer composite (black line) and piezo-polymer composite (red line) versus volume fraction r. PZT-5A was used as piezoelectric material for calculation. The polymer filler was Spurr's epoxy. The material data are given in Table 1.

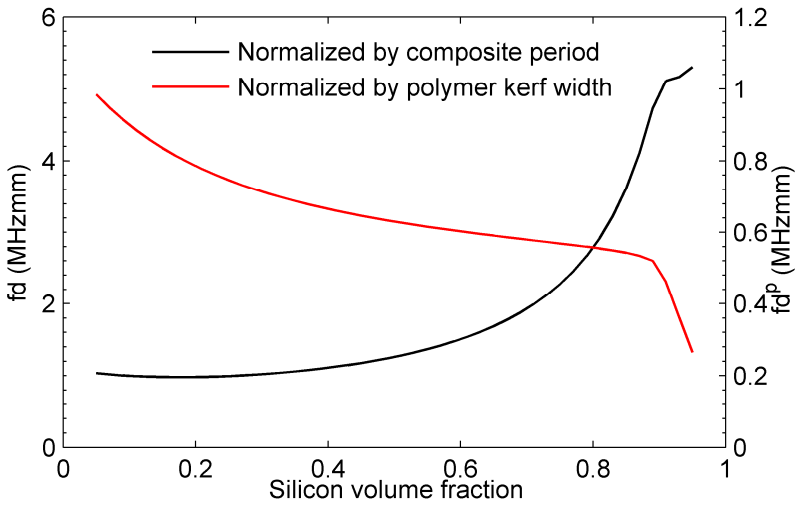

Figure 7 Lateral resonance frequency at small k_3 for various silicon volume fractions calculated from the dynamic model of guided waves, normalized by the composite period d and the polymer width d^p.

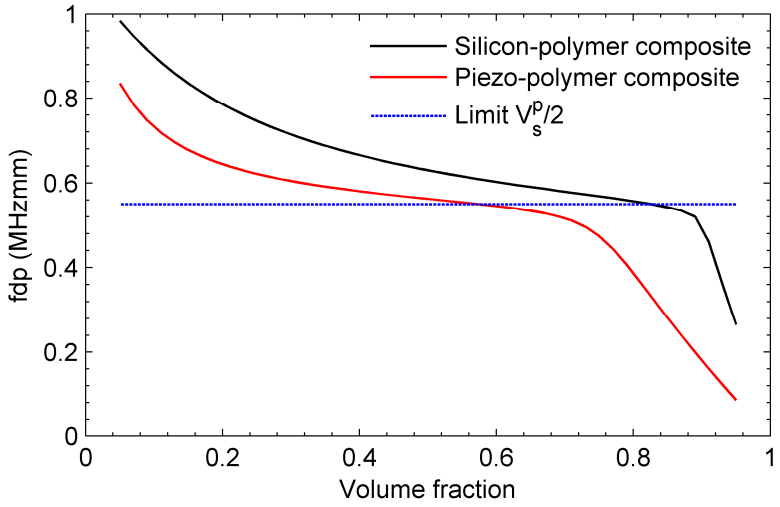

Figure 8 Lateral resonance frequency at small k_3 for silicon-polymer composite (black line) and piezo-polymer composite (red line) versus volume r, normalized by the polymer width d^p. PZT-5A was used as piezoelectric material for calculation. The polymer filler was Spurr's epoxy. The material data are given in Table 1.

From Figure 7, we also see that the three different composites have almost the same normalized lateral cut-off frequency ($fd \approx 1$) although they have different silicon volume fractions. From Figure 5 and Figure 7, it is seen that the normalized operating frequencies of the transducers with composite periods 20 and 40 µm are far below their normalized lateral cut-off frequencies ($fd \approx 1$). Only the fundamental mode will be excited in these composites at the normalized frequencies below $fd \approx 1$ and hence, the transducers can work without interference from the lateral resonances. For transducers with composite period 80 µm, the normalized operating frequency f_d =1.2 is slightly above the normalized lateral cut-off frequency ($fd \approx 1$), and hence the transducer performance is interfered by the lateral mode.

Using the material data for PZT, silicon and polymer given in Table 1, the lateral cut-off frequencies for the silicon-polymer composite and for the piezo-polymer composite are plotted on the same graph in Figure 8. They were calculated from the dynamic model of guided waves as function of volume fraction and normalized by the polymer width d^p. The normalized half-wavelength shear resonance in the polymer, $V_s^p/2 = 0.55$, where V_s^p is the shear velocity in polymer, is also included. It is seen that the normalized lateral cut-off frequency of the silicon-polymer composite is higher than that of the piezo-composite for all volume fraction and also higher than normalized half-wavelength shear resonance for *r* less than 0.8. This could be explained by the difference between the acoustic impedances of silicon and PZT. As mentioned in [10], the higher the acoustic impedance ratio between the two materials, the closer the polymer slab vibrates as a clamped half shear-wave resonance, and the closer will the lateral resonance frequency approache the value $V_s^p/2d^p$. The acoustic impedance ratio between silicon and polymer is smaller than that between PZT and polymer, in our calculations they are 8.2 and 15.4, respectively. Hence, the lateral resonance in the silicon-polymer composite must be higher than that of the piezo-polymer composite, and much higher than the value $V_s^p/2d^p$. Consequently, the maximum lateral scale in a silicon-polymer composite can be much larger than the limit achieved by setting the polymer width equal to a quarter of the shear-wavelength in the polymer, as given in Ref. [16]. From Figure 8, it is also seen that the smaller the volume fraction, the higher the lateral resonance frequency and the larger maximum allowable dimensions can be obtained. For a silicon-polymer composite with silicon volume fraction less than 0.4, corresponding to the acoustic impedance range of interest from 2.4 to 11 MRayls, our calculations show that the lateral resonance frequency is at least 1.2 time higher than that in piezo-polymer composite, and about 1.2-2 time higher than the half-wavelength shear resonance frequency $V_s^p/2d^p$. Hence, the maximum allowed dimensions can be improved by a factor 1.2 to 2 compared to the limit of a quarter of shear-wavelength in polymer. For instance, for a composite with r = 0.17, if the minimum allowed lateral resonance is set to 25 MHz, the polymer width d^p obtained by the limit in Ref. [16] must be less than 22 µm, leading to the piezoelectric composite period d less than 26.5 µm. Compared to this, our calculations presented in Figure 8 and our experiments show that a lateral resonance at 25 MHz is achieved by a composite period d = 40 µm, i.e. the maximum allowed composite period is increased by a factor 1.5.

The results of the analytical calculations were compared to the FEM simulations by plotting the two lowest dispersion curves for a composite with silicon volume fraction r = 0.17 in the same graph, see Figure 9. The black curves show the results from the dynamic model of guided waves, while the red lines are the results from FEM simulations. The graph shows that the FEM simulations produce results very similar to the analytical calculations. A slight difference is seen where the composite becomes very thin, for $k_3 d > 1$. This deviation can be explained by the difference in the boundary conditions. The dynamic model was derived under the assumption that the composite was unbounded, whereas in the COMSOL model, air was used as load on the composite surfaces. The similarity in the obtained results confirmed that our theoretical model was correctly derived.

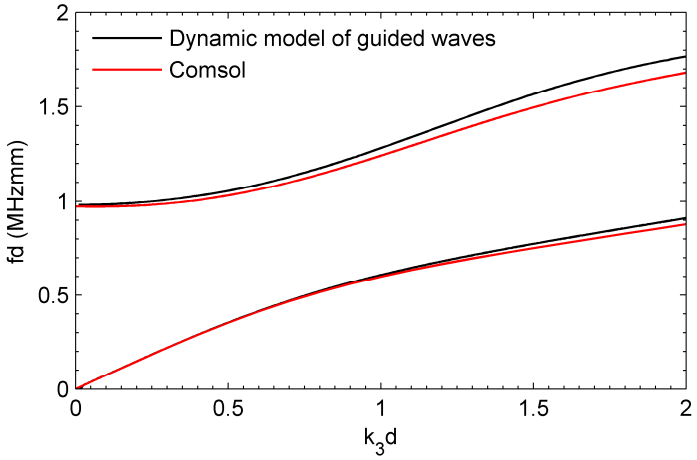

Figure 9 Dispersion relations calculated by theoretical dynamic model of guided waves (black lines) and FEM simulations in eigen-frequency mode (red lines) of silicon-polymer 2-2 composite with 0.17 silicon volume fraction. The frequency f and wave vector k_3 are normalized by composite period d.

3.2. Interaction of composite with isotropic medium

The input acoustic impedance, i.e. the acoustic impedance calculated by Eq. (7) at $x_3 = 0$, is shown to vary with frequency and with the medium the composite is in contact with [11], as shown by COMSOL simulations in Figure 10. The acoustic impedance of the composite is complex, not real as is the case for homogenous materials [11]. At low frequencies ($fd \rightarrow 0$), i.e. at fine lateral dimensions, the composite works similar to a homogeneous material; the magnitude of the acoustic impedance is close to the value calculated by Smith's model [21], and the phase of the acoustic impedance approaches zero, as expected. As the frequency increases, the magnitude of the acoustic impedance is seen to decrease monotonically to a minimum value, and undergoes a jump near the first normalized lateral resonance frequency ($fd \approx 1$). The phenomenon is directly related to the non-uniformity of the composite surface displacement, as reported in [11]. As mentioned in [21]-[22], the shear stress transferred between the two phases at their bonding interface decides the non-uniformity of the surface displacement. Because the shear stiffness of silicon is much larger than that of the piezo-ceramic (in Table 1 they are 80.0 GPa and 21.1 GPa, respectively), the silicon bars tend to move together with the polymer slabs, resulting in more uniformity deformation. Hence, a silicon-polymer composite is less dispersive than a piezo-composite with the same filler [11], and the minimum value of the acoustic impedance magnitude for silicon-polymer is larger than that of a piezo-composite.

Below the normalized lateral resonance, the input acoustic impedance of the composite is seen to be independent of the contact fluid (Figure 10a), but changes with the contact solid medium (Figure 10b). This can be explained by that the interaction between the composite and the isotropic loading medium is via the shear stiffness of the isotropic medium [11]. When composite interacts with fluids, with no shear stiffness, the movement of the two constituents is only connected via the shear stress transferred in the composite, as mentioned in [21]-[22]. When the composite interacts with solids, there is an additional stress transferred between two phases of the composite via the solid medium, and the displacement non-uniformity is reduced [22]. It can be seen that the higher the shear stiffness component c_{44}, of the solid contact material, the less dispersion of the 2-2 composite.

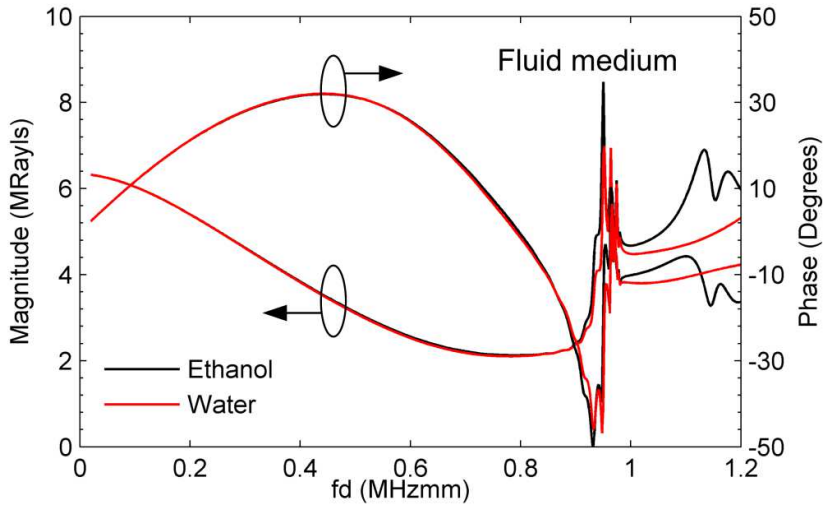

(a)

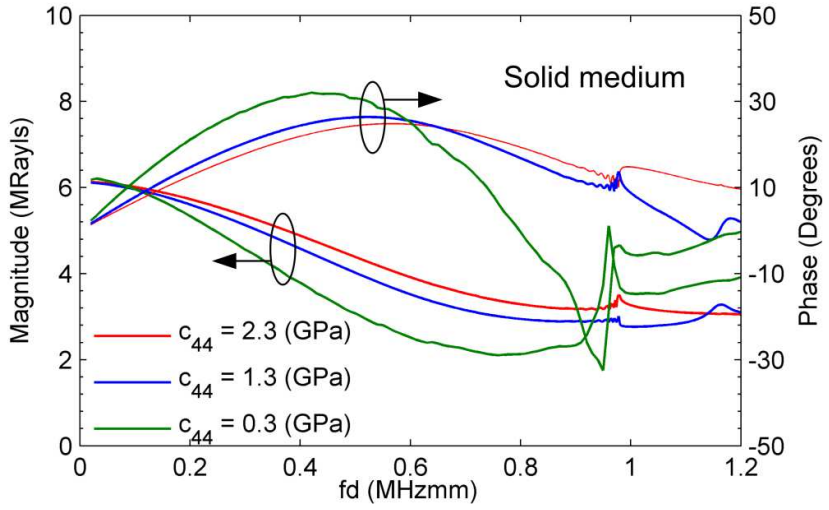

(b)

Figure 10 FEM simulations of acoustic impedance of the 2-2 composite at the composite/isotropic medium interface for different isotropic contact materials (a) Fluids: water and ethanol (b) Solids with artificial materials with c_{11} = 5.41(GPa) and c_{44} = 2.3, 1.3 and 0.3 (GPa), respectively. The silicon volume fraction is 0.17. The frequency is normalized by the period *d*.

Figure 11 shows COMSOL simulations of the acoustic impedance of the composite as a function of the depth from the composite/isotropic interface for composite with d = 20 µm, r = 0.12 (Figure 11a) and d = 40 µm, r = 0.17 (Figure 11b), respectively. The depth is normalized to the composite wavelength λ at 15MHz in the thickness direction. The isotropic medium was modeled as Spurr's epoxy for the solid, and as water for the fluid. The magnitude of the acoustic impedance is seen to be low close to the surface, and increases to a stable value deeper into the composite, where the phase also approaches a small constant value. Note that these stable impedance values can be approximately predicted from the first branch of the dynamic model as shown in Eq. (6). Figure 11 shows that the coarser structure (Figure 11b) requires longer distance (about 0.3λ) to reach the stable state compared to the finer structure (about 0.15λ) (Figure 11a). This can also be related to the displacement in the two phases, and is consistent with the results in [22], where the stress transferred is inversely

proportional to the silicon width. From Figure 10, it is also shown that, for a composite with a specified period and silicon volume fraction, its acoustic impedance at the composite/isotropic interface is lower when the composite is in contact with a fluid than when it is in contact with a solid. This can be explained by the shear stiffness in the solid material evening out the surface displacements of the composite. However, in both cases, the acoustic impedance reaches the same stable value at the same distance from the composite/isotropic interface.

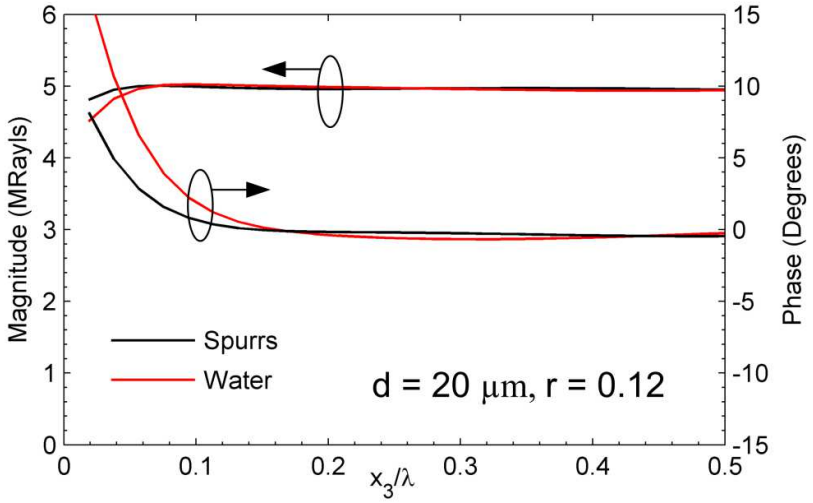

(a)

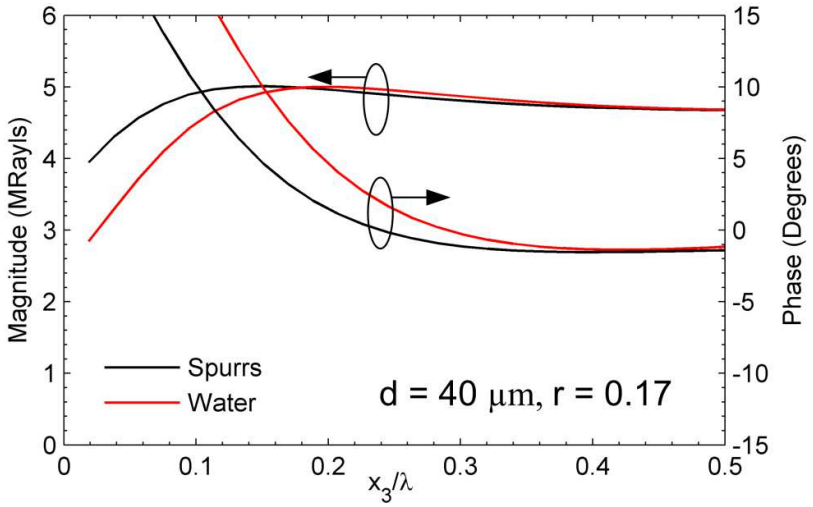

(b)

Figure 11 FEM simulations of acoustic impedance of the 2-2 composite as a function of depth from the composite/isotropic interface when interacting with different isotropic media for different composite periods (a) d = 20 μm, r = 0.12 and (b) d = 40 μm, r = 0.17. The depth is normalized to the composite wavelength λ at 15MHz in the thickness direction. The isotropic medium was modeled as Spurr's epoxy for solid and water for fluid, respectively.

3.3. Composite material estimations and transducer performance

When only the fundamental mode is excited in the composite, effective composite material properties can be estimated by fitting the measured electrical impedances of the fabricated transducers to the Mason model. Typical measured and fitted electrical impedances of a transducer with a single composite matching layer (d = 40 µm, r = 0.17) working in air are plotted in Figure 12. The electrical impedances of the corresponding transducer modelled in COMSOL were also included. The difference between the FEM simulations and the measurements can be attributed to the tapered sidewalls of the fabricated composites [9], which were not modelled in the FEM simulations.

The parameters estimated from the electrical impedance measurements; acoustic impedance and wave velocities for fabricated transducers with composite period of 20 µm and 40 µm, are listed in Table 2, together with the theoretical values calculated from Eq. (5) and Eq. (6). For fine structures (d = 20 µm, r = 0.12), the estimated velocity and acoustic impedance matched the calculations within 2.7% and 10%, respectively. For coarse structure (d = 40 µm, r = 0.17), the estimated velocity and acoustic impedance matched the calculations within 2.6% and 26%, respectively. The large deviation in the acoustic impedance of the coarse structure can be explained by the phenomenon in Figure 11b. The λ/4 thickness of the matching layer is not sufficient for the acoustic impedance to reach its stable value (~5.0 MRayls) and therefore, the estimated acoustic impedance is lower than value predicted from Eq. (6).

The pulse-echo measurement results for the transducer with electrical impedances shown in Figure 12, with d = 40 µm and r = 0.17, are shown in Figure 13, together with the results calculated from the Mason model and FEM simulations. The material parameters for the composite used in the Mason model were the estimated from the electrical measurements shown in Figure 12. The received waveforms are presented in the upper graph and their corresponding spectra are shown in the lower graph. There is an excellent agreement between the measurements, the Mason model calculations and the FEM simulations, in both pulse shape and spectrum. However, the FEM simulations provide better fit to the measured results by being able to capture the lateral resonance around 25 MHz. This lateral resonance is weak, 20 dB lower than the maximum level of the received signal, and has negligible influence on the transducer performance. Hence, fitting the measured electrical impedances to the 1D Mason model seems to be sufficient to characterize the composite velocity and impedance when working below the lateral cut-off frequency.

The measured pulses received from the fabricated transducers were lower than those in simulations, by about -3dB compared to the Mason model and -2.5 dB compared to the FEM simulations. This can be attributed to dispersion, electrical loss and diffraction. Due to dispersion, higher loss was expected for the coarser structures (d = 40 µm), but the measurements showed no significant difference in performance between transducers with fine period, low silicon volume fraction composites (d = 20 µm, r = 0.12) and coarse period, high silicon volume fraction composites (d = 40 µm, r = 0.17) used as matching layers. The measured two-way insertion loss was between -20.6 dB and -19.2 dB, while the relative -6dB bandwidth was in between 49% to 52%. This may explained by the fact that although one side of the composite layer is in contact with water, the other side is in contact with a PZT plate, which has very high shear stiffness (c_{44} = 2.11 GPa) and hence, there will be less dispersion than expected from an infinite composite plate modeled in FEM. This shows the possibility of using the 20 µm period composite as a matching layer for a transducer at higher frequencies, e.g. at 30 MHz, but the silicon volume fraction should be increased to compensate for the dispersion.

Table 2 Material Properties for Silicon-Epoxy 2-2 Composite Matching Layers Estimated from Electrical Measurements of Air-Backed Transducers

	d = 20 µm, r = 0.12		d = 40 µm, r = 0.17	
Parameter	Dynamic Model	Estimated	Dynamic Model	Estimated
Longitudinal wave velocity (m/s)	4030	4139±122	3850	3750±98
Acoustic impedance (MRayls)	5.03	4.50±0.23	5.04	3.86±0.31

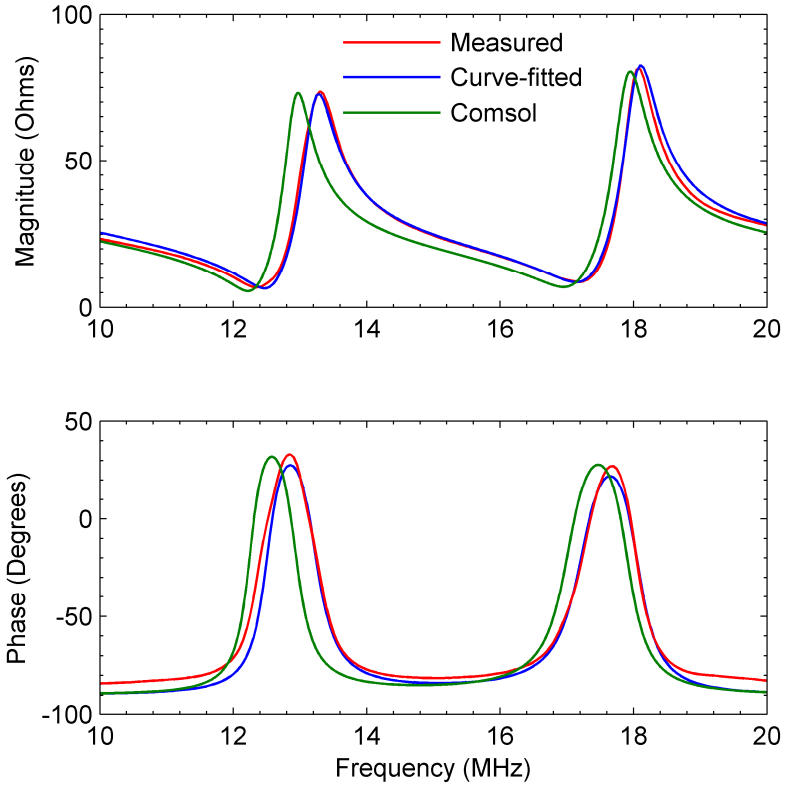

Figure 12 The measured (red lines) and curve-fitted (blue lines) electrical impedances to Mason model of the air-backed transducer operating in air. The matching layer was from sample with d = 40 µm, r = 0.17, t = 64 µm. The resulting electrical impedances of the corresponding FEM model (green lines) are also included.

4. Conclusion

This work provides an analytical model and FEM simulation of silicon-polymer 2-2 composites as matching layers for 15 MHz ultrasound transducers, emphasizing the influence from the composite lateral dimensions and from the contact media on the acoustic properties of the composite. Because the acoustic impedance of silicon is lower than that of piezoceramics, the maximum allowable lateral dimension of the silicon-polymer 2-2 composite can be increased by a factor 1.2 compared to that of piezo-composite. When a lateral scale is chosen so that the transducer bandwidth is below the lateral resonance of the composite, a 1D model can be used to characterize the 2-2 composite matching layers, though FEM simulations provide a better fit to the measured data when predicting lateral resonance.

FEM simulations of a silicon-polymer 2-2 composite in contact with fluid and solid materials show that the acoustic impedance varies with frequency, composite dimensions and the materials that the composite is in contact with. For the composites used as a single matching layer in 15 MHz ultrasound transducers, the estimated effective acoustic impedances of the composites with periods 20 and 40 µm are 10% and 26% lower than the values predicted from the analytical dynamic model of guided waves due to the high dispersion when the composite is in contact with soft materials such as air or water. In a multiple matching layer configuration, where the composite is between two solid materials, lower dispersion is expected and therefore, the analytical dynamic model may be used to estimate composite properties.

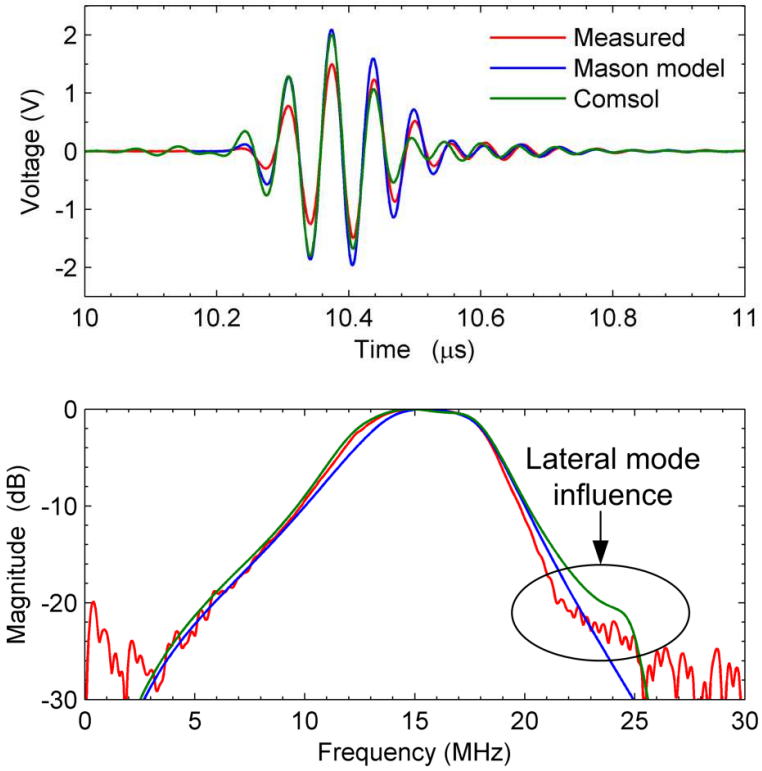

Figure 13 Measured and simulated received pulses and spectrums from Mason and FEM models of a transducer with a single composite matching layer, d = 40 µm, r = 0.17, t = 64 µm. The material parameters for the composite used in the Mason model were the estimated values from the electrical measurement shown in Fig. 12. The spectrums were normalized to their maximum values. FEM results show the resonance at 25 MHz.

References

[1] Q. Zhou, J. H. Cha, Y. Huang, R. Zhang, W. Cao, K.K. Shung, "Alumina/epoxy nanocomposite matching layers for high-frequency ultrasound transducer application," *IEEE Trans. Ultra. Ferro. Freq. Contr.*, vol. 56, pp. 213-219, 2009.

[2] L. Spicci and M. Cati, "Design and optimization of a high performance ultrasound imaging probe through FEM and KLM models," COMSOL conference, 2011.

[3] S. Rhee, T. A. Ritter, K. K. Shung, H. Wang, and W. Cao, "Materials for acoustic matching in ultrasound transducers," *Proc. IEEE Ultrason. Symp*., pp. 1051-1055 vol.2, 2001.

[4] R. E. McKeighen, "Design guidelines for medical ultrasonic arrays," *Proc. SPIE Int. Symp.*, pp. 2-18, 1998.

[5] F. Tiefensee, C. Becker-Willinger, G. Heppe, P. Herbeck-Engel, and A. Jakob, "Nanocomposite cerium oxide polymer matching layers with adjustable acoustic impedance between 4 MRayl and 7 MRayl," *Ultrasonics*, vol. 50, pp. 363-366, 2010.

[6] S. Wang, P. Campistron, J. Carlier, D. Callens-Debavelaere, B. Nongaillard, A. Ndieguene, G. Nassar, C. Soyer, and X. Zhao, "Su-8-based nanocomposites for acoustical matching layer," *IEEE Trans. Ultra. Ferro. Freq. Contr.*, vol. 56, pp. 1483-1489, 2009.

[7] R. Zhang, W. Cao, Q. Zhou, J. H. Cha, K. K. Shung, and H. Yuhong, "Acoustic properties of alumina colloidal/polymer nano-composite film on silicon," *IEEE Trans. Ultra. Ferro. Freq. Contr.*,vol. 54, pp. 467-469, 2007.

[8] M. I. Haller and B. T. Khuri-Yakub, "Micromachined ultrasound materials," *Proc. IEEE Ultrason. Symp*., pp. 403-405, 1991.

[9] T. Manh, G. U. Jensen, T. F. Johansen, and L. Hoff, "Microfabricated 1-3 composite acoustic matching layers for 15 MHz transducers," to be published in *Ultrasonics.*

[10] Y. Shui, X. Geng, and Q. M. Zhang, "Theoretical modeling of resonant modes of composite ultrasonic transducers," *IEEE Trans. Ultra. Ferro. Freq. Contr.*, vol. 42, pp. 766-773, 1995.

[11] X. Geng, "Numerical modeling and experimental study of piezocomposite transducers," Ph.D dissertation, The Pennsylvania State University, 1997.

[12] Y. Shui, and Q. Xue, "Dynamic characteristics of 2-2 piezoelectric composite transducers," *IEEE Trans. Ultra. Ferro. Freq. Contr.*, vol. 44, pp. 1110-1119, 1997.

[13] A. Abbate, G. Elfbaum, Y. Shui, and H. Wu, "A highly efficient 20 MHz piezo-composite transducer for nondestructive characterization of multilayer plastics," *Proc. IEEE Ultrason. Symp*., vol.1, pp. 707-710, 2002.

[14] M. Yamaguchi, K. Y. Hashimoto, and H. Makita, "Finite Element Method Analysis of Dispersion Characteristics for 1-3 Type Piezoelectric Composites," *Proc. IEEE Ultrason. Symp*., pp. 657-662, 1987.

[15] S. Ballandras, G. Pierre, F. Blanc, P. F. Edoa, and W. Steichen, "A periodic finite element formulation for the design of 2-2 composite transducers," *Proc. IEEE Ultrason. Symp*., vol.2, pp. 957-960, 1999.

[16] T. S. T. Ritter, R. Tutwiler and K. K. Shung, "A 30-MHz Piezo-Composite Ultrasound Array for Medical Imaging Applications," *IEEE Trans. Ultra. Ferro. Freq. Contr.*, vol. 49, pp. 217-230, 2002.

[17] M. E. Frijlink and H. Torp, "Simulation of acoustic fields from arbitrary transducer stacks using a FEM transducer model and nonlinear wave propagation," *Proc. IEEE Ultrason. Symp*., pp. 2340-2343, 2009.

[18] G. F. Miller and H. Pursey, "The field and radiation impedance of mechanical radiators on the free surface of a semi-infinite isotropic solid," in *Proc. Royal Soc. Of London*, vol. 223, pp. 521, 1954.

[19] W. P. Mason, *Electromechanical transducers and wave filters.* 2nd ed., New York: D. Van Nostrand Co., pp. 201-209, 399-409, 1948.

[20] F. Craciun, L. Sorba, E. Molinari, and M. Pappalardo, "A coupled-mode theory for periodic piezoelectric composites," *IEEE Trans. Ultra. Ferro. Freq. Contr.*, vol. 36, pp. 50-56, 1989.

[21] W. A. Smith and B. A. Auld, "Modeling 1-3 Composite Piezoelectrics: Thickness-Mode Oscillation," *IEEE Trans. Ultra. Ferro. Freq. Contr.*, vol. 38, pp. 40-47, 1991.

[22] W. Cao, Q. M. Zhang and L. E. Cross, "Theoretical study on the static performance of piezoelectric ceramic-polymer composites with 2-2 connectivity", *IEEE Trans. Ultra. Ferro. Freq. Contr.*, vol. 40, pp. 103-109, 1993.

[23] W. Cao, Q. M. Zhang, J. Z. Zhao and L. E. Cross, "Effects of face plates on surface displacement profile in 2-2 piezoelectric composites", *IEEE Trans. Ultra. Ferro. Freq. Contr.*, vol. 42, pp. 37-41, 1995.

Paper C

Fabrication of High Aspect Ratio, Vertical Microtrenches using Anisotropic Wet Etching of Silicon

Tung Manh[a], Anh-Tuan T. Nguyen[a], Tonni F. Johansen[b,c] and Lars Hoff[a]

[a] Department of Micro and Nano Systems Technology, Vestfold University College, Horten, Norway

[b] Department of Acoustic, SINTEF ICT, Trondheim, Norway

[c] Department of Circulation and Medical Imaging, Norwegian University of Science and Technology, Trondheim, Norway

This paper is being prepared as a Technical Report for use at IMST lab.

Fabrication of High Aspect Ratio, Vertical Micro-trenches using Anisotropic Wet Etching of Silicon

Tung Manh[a*], Anh-Tuan Thai Nguyen[a], Tonni F. Johansen[b,c] and Lars Hoff[a]

[a]Department of Micro and Nano Systems Technology, Vestfold University College, Horten, Norway
[b]Department of Acoustic, SINTEF ICT, Trondheim, Norway
[c]Department of Circulation and Medical Imaging, Norwegian University of Science and Technology , Trondheim, Norway
[*]Corresponding author. Email: tung.manh@hive.no. Phone: +47 33037928.

Abstract: High aspect ratio, vertical sidewall trenches are desired microstructures for a wide variety of applications in Micro Electrical Mechanical System (MEMS) such as microcavity arrays and micro grating patterns in optical sensors, micro/nanofluidic channels in BioMEMS sensors, and comb fingers in electromechanical systems. This paper presents the manufacturing of these structures using anisotropic wet etching of (110)-oriented silicon wafer in KOH etchant. The etched structures were substantially filled with epoxy resin to form a silicon-polymer 2-2 composite material, intended to be used as a matching layer in a stack of multiple layers for ultrasound transducers working at 15 MHz. Detailed fabrication steps are listed. Two different etchant concentrations were tried: KOH 25 wt% at 80ºC and 40 wt% at 70ºC. Two types of silicon wafers were used: Normal (110)-oriented wafer and Silicon on Insulator (SOI) wafer with (110)-oriented device layer. The properties of the fabricated structures (etched trench uniformity, etched profile, and alignment issue) were investigated.

Keywords: High frequency transducers, silicon-polymer composite, silicon micromachining, matching layer.

1. Introduction

Silicon-polymer composites are manufactured by forming high aspect ratio trenches into silicon substrates and filling these deep grooves with epoxy resin. To be used as matching layers at high frequencies, instead of conventional dice-and-fill method, micromachining techniques, i.e. lithography and etch, are utilized to form µm-sized structures [1]-[2]. Anisotropic wet etching of silicon is one of the oldest techniques used in MEMS to form such desired structures in crystalline materials. By choosing appropriate etchants, anisotropic wet etching results in geometric structures bounded by slowest etching crystal planes. Typical aqueous etchants for anisotropic etching of silicon are potassium hydroxide (KOH), tetramethyl ammonium hydroxide (TMAH) and ethylenediamine (EDP) based solutions [3]-[4]. The etching rate of silicon in these etchants significantly depends on the crystallographic orientation of the etched planes. Generally, they are {111} < {100} < {110} in silicon, where the {111} planes are etched extremely slower than the others [3]-[11]. The etching rate of each crystal plane, the selectivity, i.e. the etching ratio between planes, the surface roughness and the etching profiles in silicon are greatly dependent on multiple factors including silicon types (p-doped or n-doped), etchants, etchants' concentration, etching temperatures and etching systems (with/without stirring/ultrasound systems, etc…) and so forth [5]-[11]. Though considered as time-consuming and sensitive process, anisotropic wet etching of (110) silicon wafers still obtains numerous attractions for fabrication of deep, narrow, high aspect ratio trenches with smooth, vertical sidewalls due to the high selectivity between {111} and {110} planes. With the ability to provide low-cost, mass produced, precise miniaturized structures, wet etching of (110) silicon wafers has been widely used to fabricate small devices, especially sensors and actuators, in numerous applications across multiple fields such as microcavity arrays and micro grating patterns in optical sensors [9], micro/nanofluidic channels in BioMEMS sensors [10], and comb fingers in electromechanical systems [11].

In this paper, we describe the wet-etching fabrication strategy for making the high aspect ratio structures into (110) silicon wafers. By aligning the long straight line features along the {111} planes in silicon, deep and long vertical sidewall trenches can be made. Line patterns were defined by contact mask and standard ultraviolet (UV) lithography. Anisotropic wet etching of silicon was performed in KOH etchants using silicon dioxide as mask. Two different kinds of wafers were tested: normal (110) wafers and silicon on insulator (SOI) wafers with (110) device layer. Two different etching conditions were tried: KOH 25 wt% at 80ºC and KOH 40 wt% at 70ºC. In normal (110) wafers, the former showed trenches with rectangular profile, but with a certain roughness at the bottom, whereas the latter resulted in wedge shaped profile. The SOI wafers with buried oxide layer helps to stop the etching process at a defined thickness with flat bottom trenches. The resulting deep and long trenches were then subsequently filled with epoxy resin, forming the 2-2 composite to be used as acoustic matching layers in transducers operating around 15 MHz.

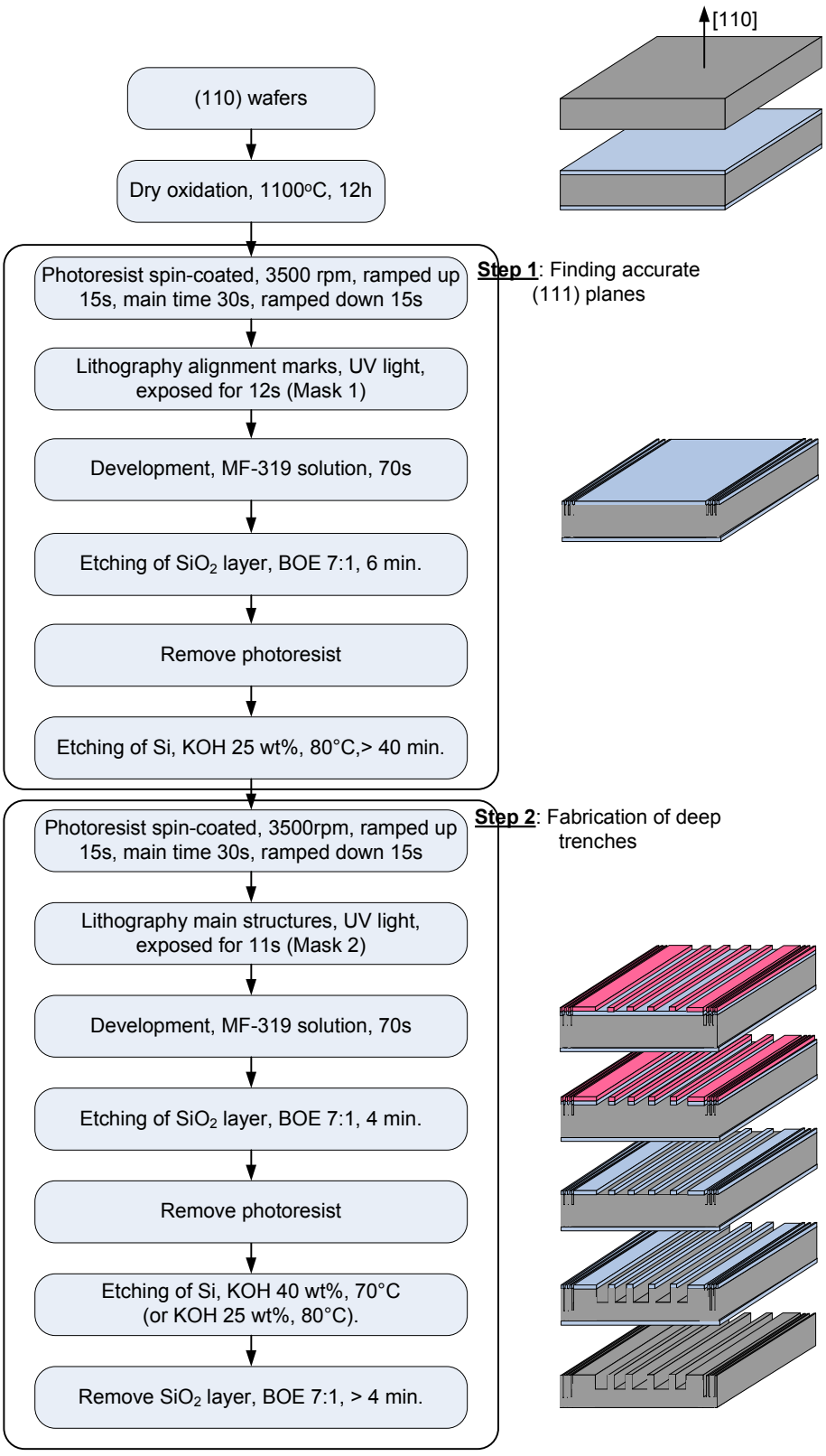

Figure 1 Wet etching fabrication procedure

2. Fabrication process

The general fabrication process for wet etching features in silicon wafers is outlined in Figure 1. First, a (110) Si wafer is thermally oxidized to give an oxide thickness of 0.5 µm. The fan-shaped patterns and circles alignment marks for finding the accurate {111} planes within 0.1 degree were transferred to oxide layer, patterned and silicon wafer was etched in KOH 25 wt% at 80°C for at least 40 min to reveal the {111} planes (described in subsection 2.1). Then, a 1.5/2.5 µm thick layer of positive photoresist (S1813/S1828, Shipley Company, MA, USA) was spin coated on top of the oxide layer. The features on the mask were transferred to the photoresist and patterned to make openings using standard photolithography with contact mask exposure. The line features were aligned to the {111} planes used the previous etched alignment marks. The oxide layer was patterned at room temperature, using buffered oxide etch, BOE 7:1, solution with etching rate 110 nm/min. The oxide layer then performed as mask for the anisotropic wet-etch of silicon in either KOH 25 wt% at 80°C or KOH 40 wt% at 70°C. Then, the oxide mask was removed by BOE solution. After etching, the wafers were rinsed in de-ionized (DI) water and air dried.

To form the 2-2 composite, the etched structures were vacuum impregnated with epoxy resin (Spurrs, Electron Microscopy Sciences, PA, USA) to form the composite material. This was done under vacuum, to improve the filling ability of the polymer into the very deep trenches and to eliminate undesirable air bubbles generated while mixing the epoxy components. The sample was cured at 70°C for 8 hours.

The details of the fabrication process to manufacture 2-2 composite by wet etching method together with guides for trouble shooting can be found in Appendix A.

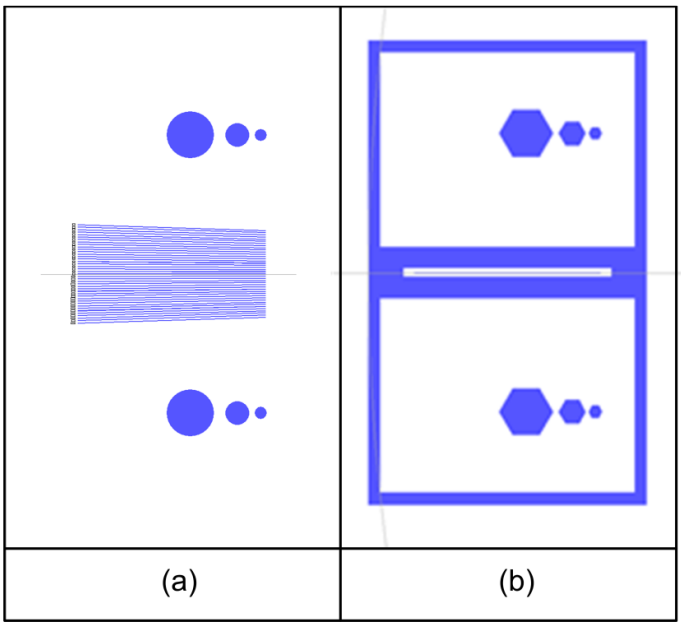

Figure 2 Alignment features on (a) Mask 1 for finding the accurate {111} planes (b) Mask 2 to align to the etched patterns from Mask 1.

2.1. Alignment technique for finding {111} planes

In order to form trenches with vertical sidewalls into (110) silicon wafers, precise alignment of the line features along the true {111} planes are crucial. Even small mis-orientation will cause skewed sidewalls [3]. The requirement to obtain μm-sized trenches in KOH is that the precision of the alignment of the patterned lines to the {111} planes must be within 0.1º [5]. The wafer primary flat indicates the <111>-direction with the accuracy of ± 0.5º along the exact <111>-direction and this is not sufficiently fulfilled the requirement. Therefore, prior to the etching process to form the vertical trenches, the first etch step was to find the correct {111} planes and its resulting patterns was used as alignment marks for etching main structures. We used both fan-shaped patterns by Uenishi *et al.* [5] and circles alignment marks by James *et. al.*[6], respectively, to find the accurate {111} planes, as shown in Figure 2. For the fan-shaped alignment patterns, two set of lines 10 μm wide and 4 mm long, fanned out to ± 2.0° with 0.1° angle between lines are designed on the mask. The {111} planes were determined by examining the etched line with minimum undercut after etching. For the circle alignment marks, a series of circles with diameter of 1 mm, 0.5 mm and 0.25 mm, respectively; were designed on the mask. These circles resulted in hexagonal patterns with the edges aligned along the {111} crystal planes after wet etching in aqueous KOH solution (Figure 4) and would be matched to hexagons on the mask of the second step (Figure 2b). The alignment marks were placed on both left and right sides of the mask, as shown in Figure 3 for the purpose of easy manual processing. Moreover, eight lines 40 μm wide and 3.5 mm long with 80 μm apart were placed to coarsely align to the main flat of the wafers.

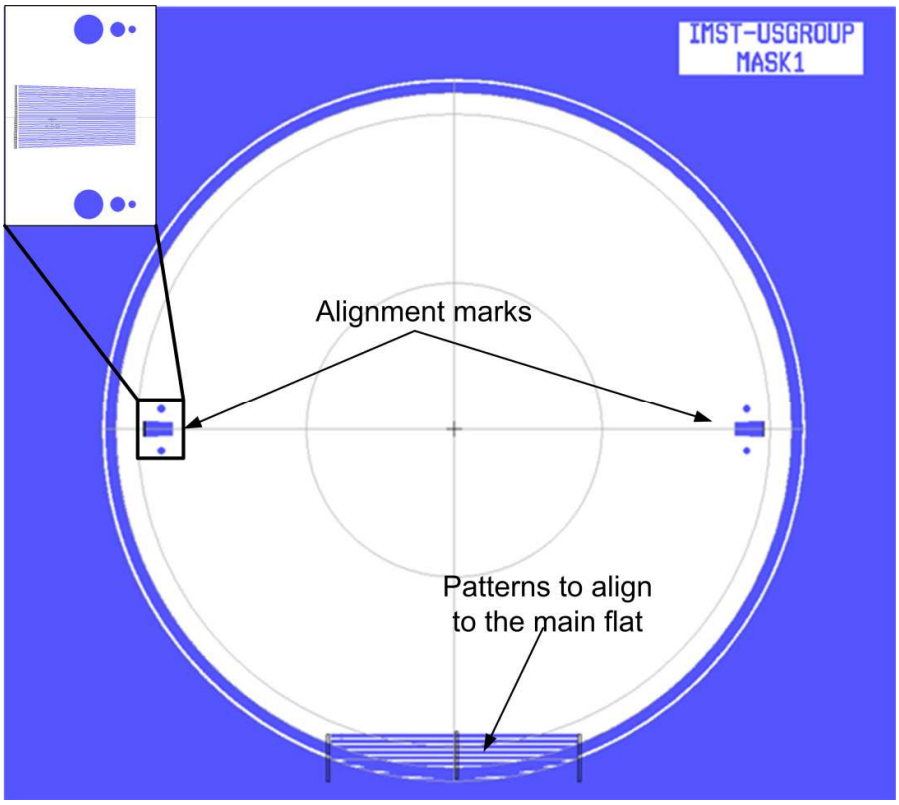

Figure 3 Mask for etching of the first step

2.2. Patterning of the photoresist

Exposure and development of the photoresist layer have shown great influence on the lateral dimensions of the patterned features. Overexposed photoresists result in undercut resist bars, which consequently form thin oxide and silicon bars which may be completely destroyed during the wet-etch process of silicon. In contrast, underexposed resists lead to overcut-resist bars with jagged borders (Figure 5). In the purpose of minimum of the line-width errors, we have experimentally characterized two different positive photoresists, S1813 and S1828, which are available in IMST lab. It is shown that with the Karl Suss MA56 mask aligner and UV light wavelength 365 nm at 10 mW/cm², the optimal exposure time is about 10-12 s for the grating silicon bars within the range of 10-20 μm. The resulting line-width error vs. exposure time is shown in Figure 6 [12]. A SEM picture of a good resist profile after exposure time of 11 s and development time of 70 s in MF-319 is shown in Figure 7.

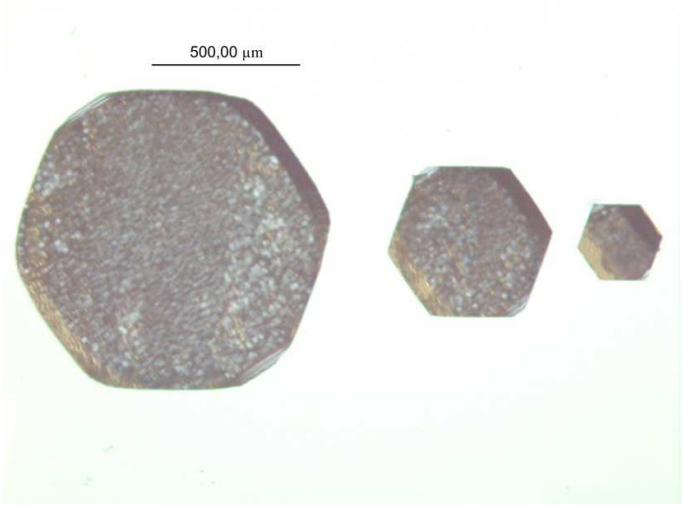

Figure 4 The results of the circle patterns after wet etching in KOH 25% at 80ºC for 40 min.

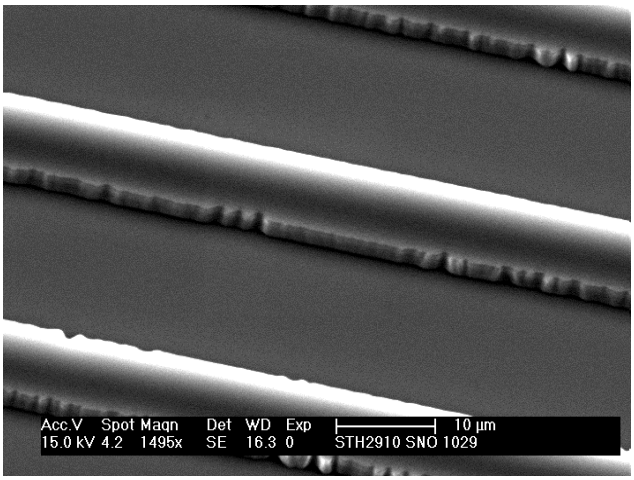

Figure 5 Underexposed resist bars with jagged edges.

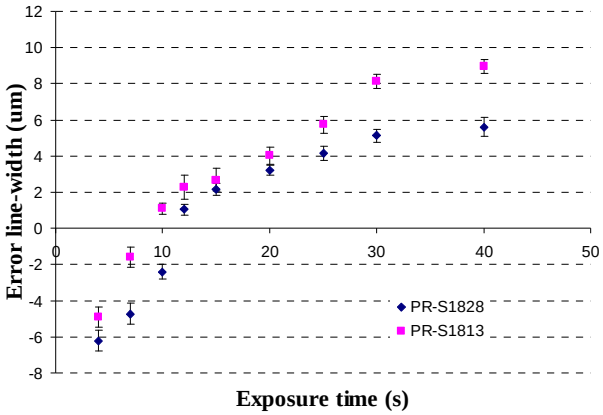

Figure 6 Error line width vs. Exposure time

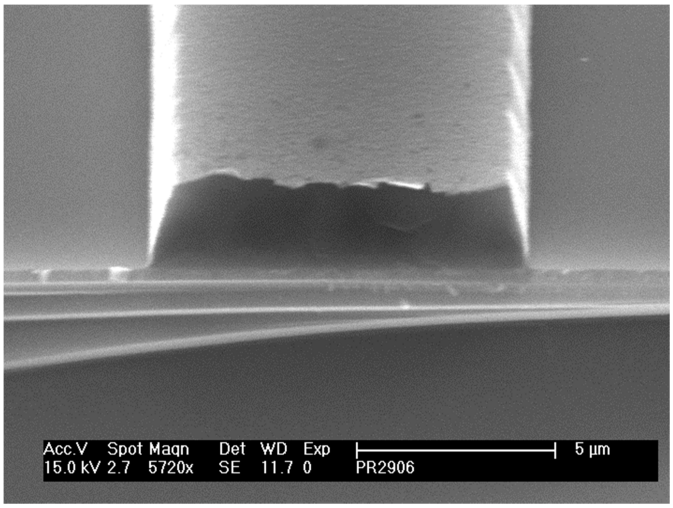

Figure 7 Photoresist 1813 profile after exposed for 11 s and then developed for 70 s.

2.3. Etching of the silicon dioxide layer

Etching of the SiO_2 layer in BOE 7:1 is quite stable with the etching rate 110 nm/min. For smaller structures, e.g. silicon bars less than 5 µm, it is advised to use reactive ion etch (RIE) to pattern SiO_2 layer. By adjusting etching parameters with different gaseous species, one might obtain an optimal recipe to be used for their own purposes.

In the wet etching process, it should also be noted that there is always a thin native oxide layer grown on top of the silicon wafer. Therefore, to reduce non-uniform silicon depth trenches, a quick etch of this native oxide layer in BOE 7:1 for 5-10 s should be performed before silicon etch in KOH (See more details in Appendix A).

2.4. Etching of the silicon layer

Etching of silicon wafer was performed under two different conditions: KOH 25 wt%, 80°C and KOH 40 wt%, 70°C, respectively. A wafer holder (Figure 8) was used to protect the backside of the wafer during wet etching process. The wafer surface should also be placed facing upwards to eliminate H_2 bubbles trapped between the grating bars, which reduces the uniformity of the etched trenches [7].

By using a Dektak 150 profilometer (Veeco, NY, USA) as well as observing the structures by a XL-30 SEM (Philips, AMS, NL), height measurements can be performed. Height measurements at different etching time are shown in the graph of Figure 9. The slopes found by linear regressions of the data show an average etching rate of 1.45 µm/min for KOH 25 wt% at 80°C and 0.91 µm/min for KOH 40 wt% at 70°C, respectively. The etching rate R<111> was found experimentally by comparing the under-etch of etched silicon bars to their corresponding silicon dioxide mask sizes. The etching rate R<110> and selectivity R<110>/R<111> of the (110)-silicon wafer in two different etching conditions were summarized and presented in Table 1. It can be seen that under condition KOH 40 wt%, 70°C, the etching of silicon is more stable and reproducible compared to that under the other condition. The results are consistent with what found in [8]. From this reference, it is also recommended to use the condition KOH 40 wt%, 70°C to form smaller structures. The etching rate in the vertical direction R<110> under condition KOH 25 wt%, 80°C is about one half of the etching rate in the other condition. However, this also resulted in much rougher bottom surface, as shown in Figure 14. The vertical etching rate only depends on the etchant concentration and temperature, while the lateral etching rate also depends on the accuracy of alignment line features along {111} planes. The more accurate alignment along the {111} planes, the higher vertical/lateral selectivity is observed [6].

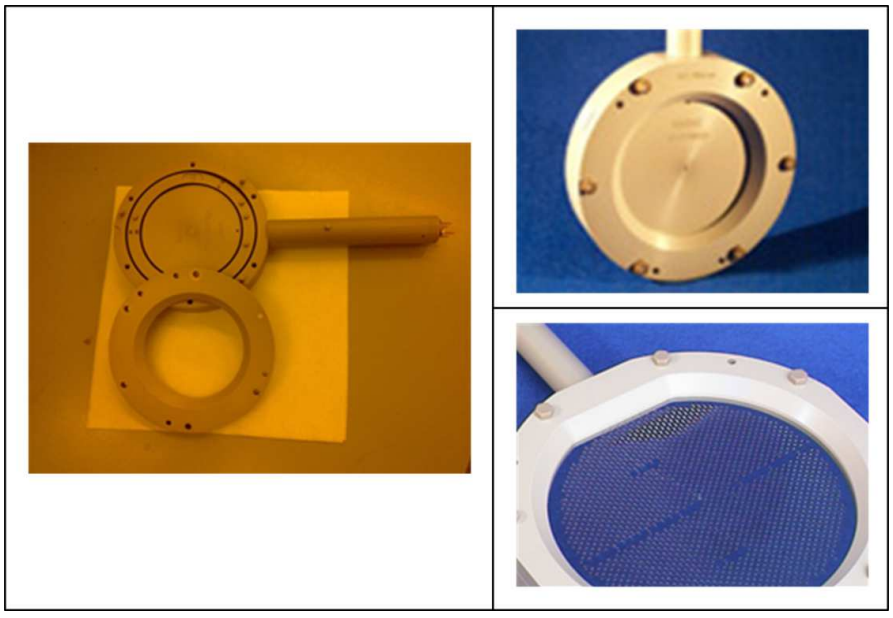

Figure 8 Wafer holder used to protect etching of silicon from the backside.

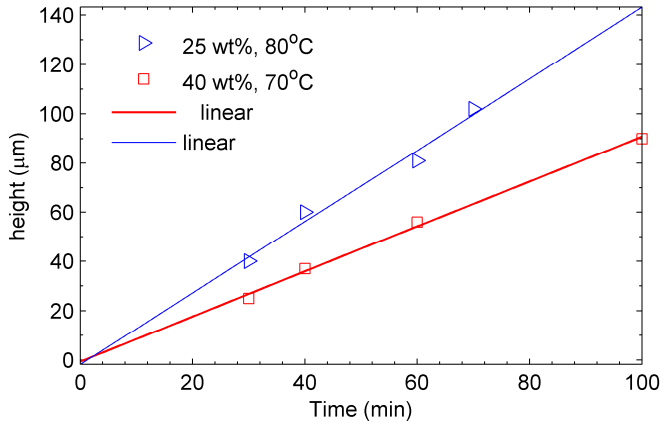

Figure 9 Experimental etched depths of (110) silicon wafer in KOH under different conditions: 25 wt%, 80°C and 40 wt%, 70°C. The slopes of the linear regressions indicate the average etching rates.

Table 1 Etching rate and selectivity between the vertical/lateral directions on (110) wafer – The parameters were found experimentally.

Condition	KOH 25 wt%, 80°C	KOH 40 wt%, 70°C
Etching rate R<110> (μm/min)	1.45 ± 0.12	0.91 ± 0.07
Selectivity R<110>/R<111>	50-90	130-140

2.5. Adhesion promoter, photoresist removal, rinsing and drying issues

Using adhesion promoter, e.g. hexamethyldisilazane (HMDS), for wafer surface treatment before coating photoresist is remarkably important, especially when starting the second step to build high aspect-ratio trenches. After the first step for finding the correct {111} planes, rinsing the wafer in water and then drying it with N_2 guns should be treated carefully in order to produce clean-surface wafer for the next step. Then, HMDS should be applied to enhance adhesion of photoresist layer to the wafer surface. This layer avoids developer to penetrate between the photoresist layer and the wafer surface, stripping of small photoresist structures in the developing process.

As high aspect ratio structures are formed in silicon, rinsing and drying must be delicate treated to avoid surface tension in the cavities, which may cause silicon walls collapse. It is recommended to flush the wafer with a water shower after dipping it in a water bath to remove remnants between lines. For thinner silicon walls, freeze drying in cyclo-hexane or critical point drying in carbon dioxide must be applied to avoid collapsing [13]. It is also recommended to use appropriate photoresist removal to strip the photoresist layer, especially after the first step (forming the alignment marks). Acetone is NOT recommended to be used as stripper in this delicate process because it promotes resist residuals on the wafer surface due to the fast evaporation [14]. This causes poor resist homogeneity in the second step to form the main structures, which consequently reduce the repeatability of the anisotropic wet etched silicon bars.

3. Characterization of the etched structures

3.1. The uniformity of the silicon bar widths

We have used both plastic and glass masks for patterning the main structures in the wet-etching process. The critical dimensions of the lines on the plastic mask (Infinite Graphics, Minnesota, USA) are 10 μm, which consequently limit the silicon bar dimensions and the operating frequency of the composite to about 15 MHz. Moreover, its poor resolutions lead to resist patterns with different widths and jagged edges. This then resulted in silicon bars with non-uniform widths (Figure 10), which are not our initial purpose. However, one may turns this into advantage as random bars can help to suppress the lateral resonance excited by periodic patterns [14].

With the glass mask (Photoplot Store, Colorado, USA) and the precision alignment of line patterns to the {111} planes within 0.1º, this resulted in silicon bars with appreciate uniform widths (Figure 11). The critical dimensions on the glass mask could down to (2±0.3) μm, which can potentially provide composite with silicon bars less than 1 μm and hence, can be used as matching layer in ultrasound transducer at frequency above 100 MHz.

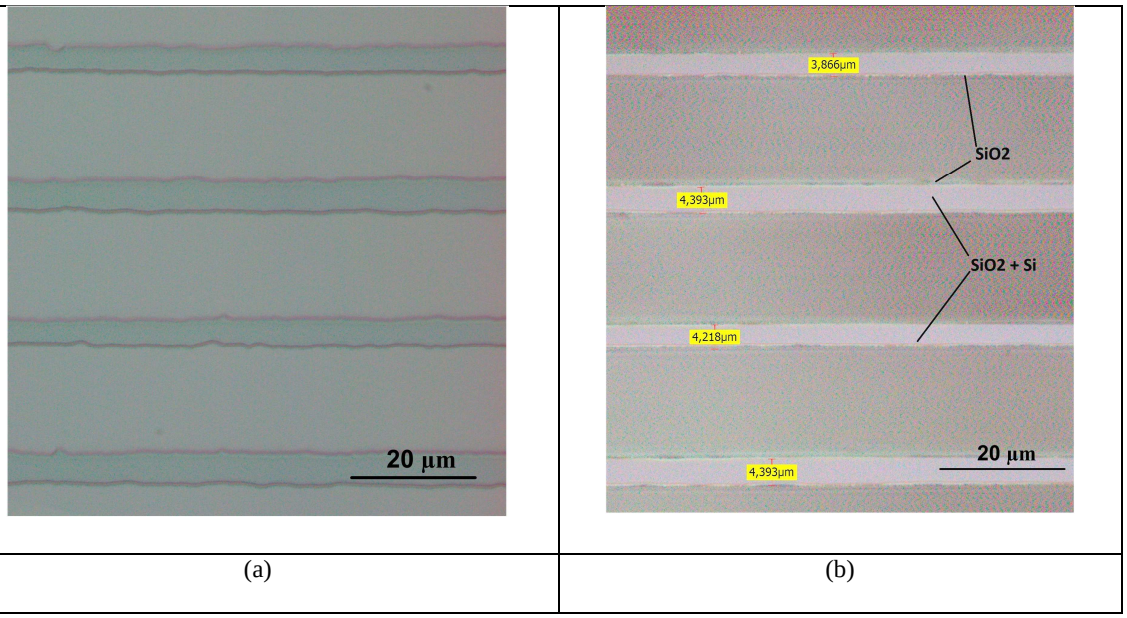

(a) (b)

Figure 10 Top view of (a) photoresist bars and (b) silicon etched structures with plastic mask.

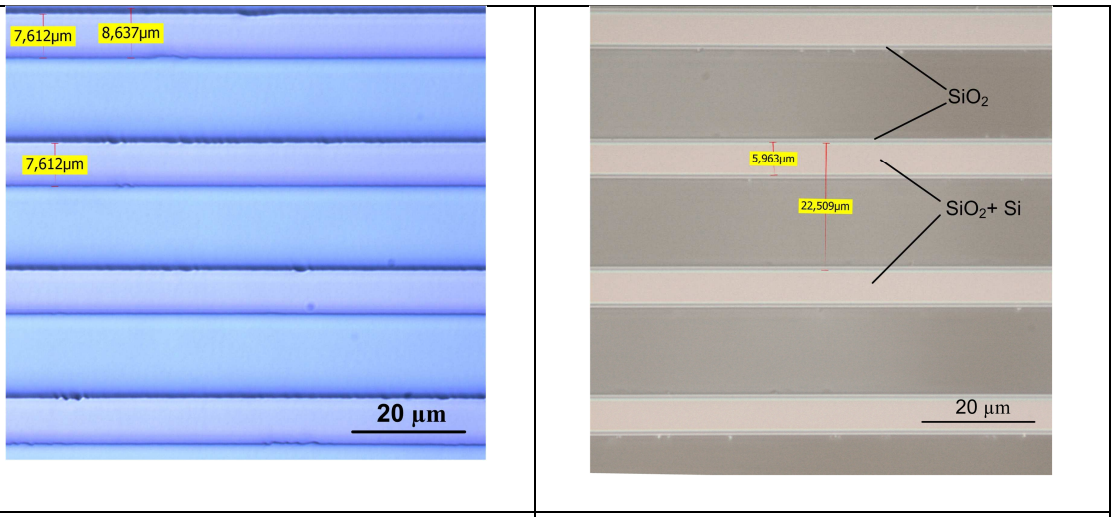

(a) (b)

Figure 11 Top view of (a) photoresist bars and (b) silicon etched structures with glass mask.

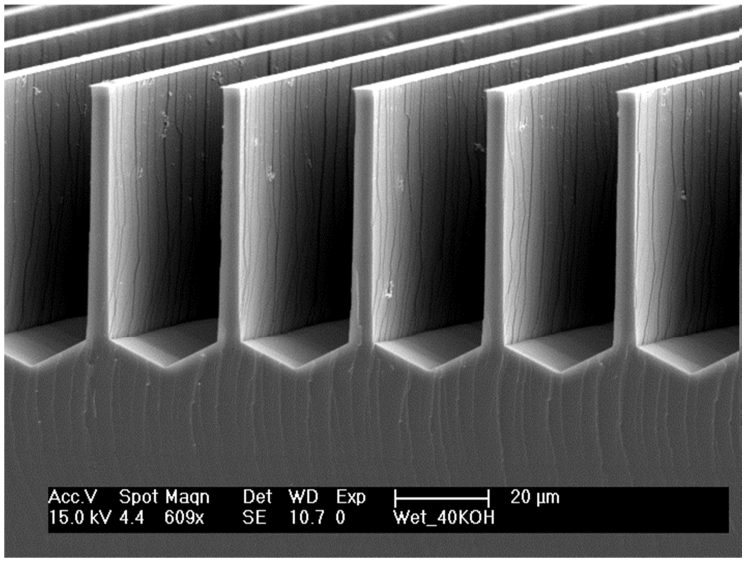

Figure 12 The resulting trenches of small misaligned structures. The sidewalls have steps on their surface. The wafer was etched in KOH 40 wt% at 70°C.

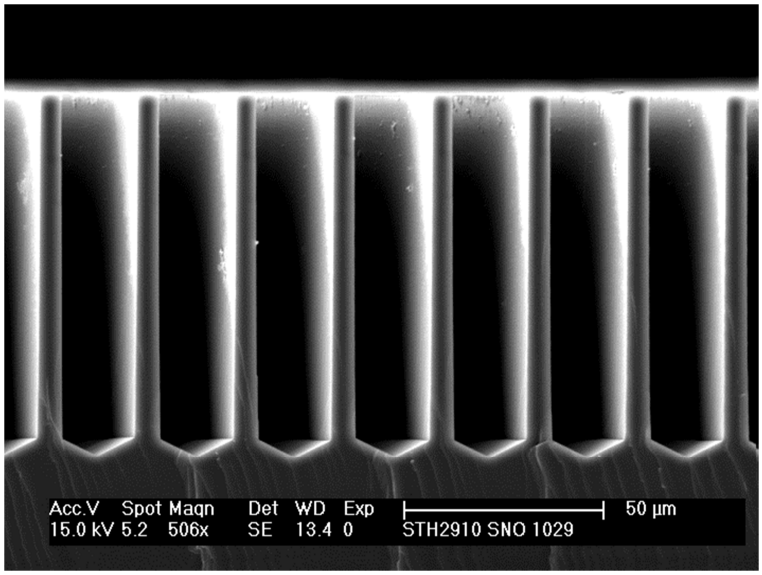

Figure 13 The resulting trenches with precision alignment along {111} planes within 0.1°. The sidewalls are nearly vertical with smooth surfaces. The wafer was etched in KOH 40 wt% at 70°C.

3.2. Alignment issue

Even small misalignment will result in structures with skewed sidewalls and steps on the surfaces (Figure 12). This might introduce extra loss in the resulting 2-2 composite. Moreover, misalignment also degrades the vertical/lateral selectivity, leading to thinner sidewalls than what was expected. This consequently changes the silicon volume fraction in 2-2 composite from batch to batch. In contrast, nearly vertical, smooth sidewalls were achieved with precision alignment along {111} planes within 0.1° (Figure 13). Therefore, it is crucial in the step 1 for finding the {111} planes that the (110) wafer should be etched sufficiently long to reveal the {111} planes clearly.

3.3. Surface roughness

Surface roughness of different planes is also an important factor should be considered if the composite is used as matching layer of an ultrasound transducer, since it may scatter the acoustic waves and introduce extra loss, especially at high frequencies. The bottom trench roughness is greatly dependent on time, temperature and etchant concentration, which define what planes are reached [15]. Etching of (110) wafer in KOH 25 wt%, 80°C resulted in very rough bottom surface, see Figure 14. For etched structures in KOH 40 wt%, 70°C, the bottom trenches are wedged but remarkable smooth (see Figure 13 and Figure 14).

The roughness of the sidewalls, however, primarily depends on how precise of the alignment of features lines to the accurate {111} planes. With the accuracy of less than 0.1°, the obtained structures showed notably smooth, vertical sidewalls (see Figure 13 and Figure 14).

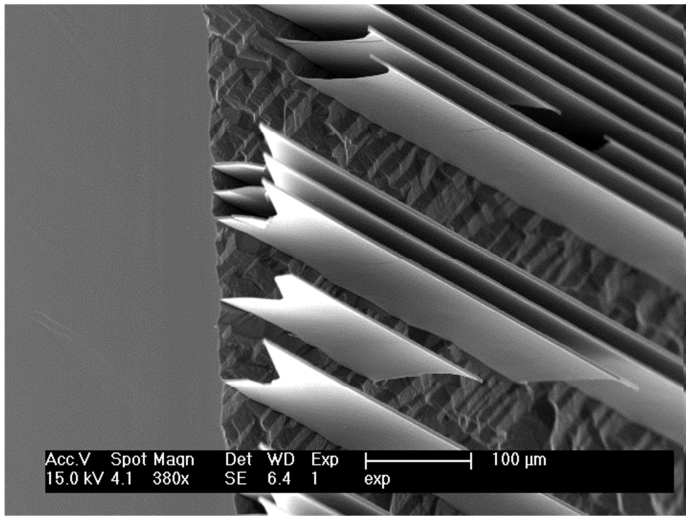

Figure 14 A SEM picture of an etched structure in KOH 25 wt% at 80°C present rough surface at the bottom trenches.

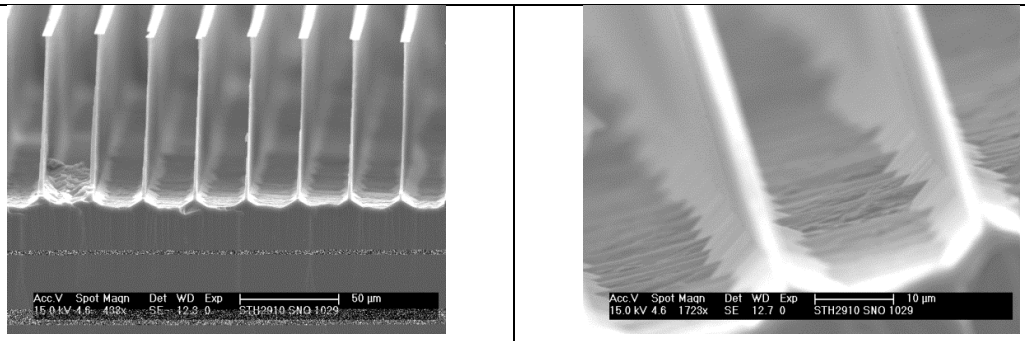

(a) (b)

Figure 15 (a) SEM image of etched front profile in KOH 40 wt%, 60°C with additive alcohol, (b) Close-up picture shows rough bottom.

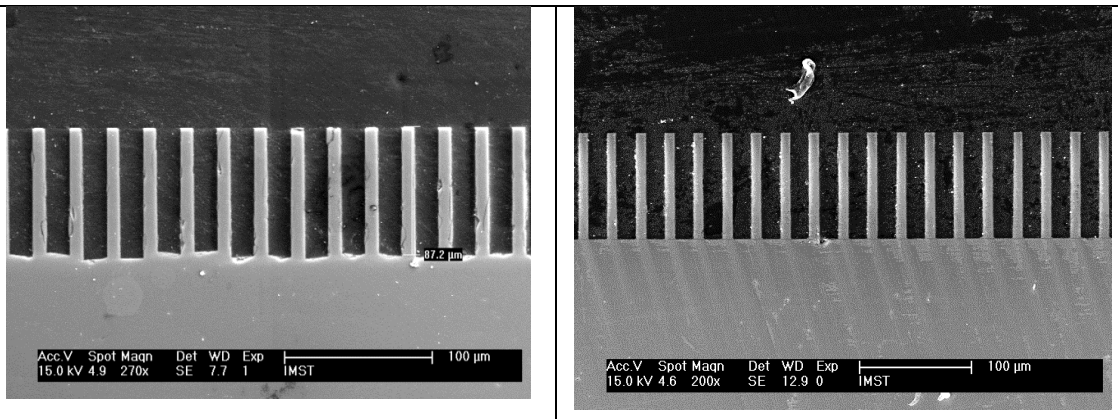

(a) (b)

Figure 16 Cross-section SEM images show etched profile structures under condition 25 wt%, 80°C with (a) Normal wafer (b) SOI wafer.

3.4. Etching profile, depth uniformity

Etching of (110) silicon wafer in KOH concentration ≤ 30 wt% was known to provide trenches with flat etched front profile, whereas the bottom of the grooves would be wedged if (110) silicon wafer were etched in KOH concentration ≥ 40 wt% [16]-[17]. However, under etching condition of 25 wt%, 80°C, we haven't achieved trenches with uniform, flat etched front profile (see Figure 15a). Etching at high temperature, though producing high etching rate, tends to cause non-uniform, rough depth with the same widths due to trapping of H_2 bubbles [7], [10]. This might affect transducer performance if the composite is used in a stack multiple matching layers. There are two solutions for this: Adding alcohol or/and reducing etching temperature [7]. We have tried to add isopropanol so that it saturated and formed a thin layer on top of the KOH etchant [4]. Since isopropanol is flammable, the temperature was also set down to 60°C. As a consequence, the vertical etching rate degrades considerably (to about 0.3 µm/min) and is considered ineffective.

Under etching condition of 40 wt% at 70°C, the etched front profile was wedged with remarkably uniform bottom trenches; see Figure 12 and Figure 13. We have also tried to turn wedged profile to flat by adding alcohol and set down the etching temperature to 60°C. However, the result roughness at the bottom showed textile profile and not as good as what achieved without alcohol, see Figure 15. This is reasonable as the wedge profile at the bottom is formed by (331) planes, and they are smoother than (110) planes [15].

One simple solution to obtain flat etched front profile was to use Silicon-On-Insulator (SOI) wafer, which has a buried dioxide layer that stops the etching process at a defined thickness [7]. The resulting structures on SOI wafer is shown in Figure 15b. However, the cost factor must be considered since SOI wafer is about 4-5 times more expensive than the normal (110) silicon wafer.

4. Conclusion

An in-house fabrication process to form high aspect ratio, vertical trenches into (110)-oriented silicon wafers was developed. The resulting structures fulfil the requirements to be used as a composite layer in 15 MHz transducers in terms of surface roughness, vertical sidewalls, silicon bar uniformity and flat bottom trenches. The process is useful for fabrication of structures used in other applications such as BioMEMS, optical MEMS, etc…

Appendix A

<table>
<tr><th>STEP</th><th>DESCRIPTION</th><th>NOTE</th></tr>
<tr><td>1</td><td>THERMAL OXIDATION
<table><tr><th>O_2 flow rate (slm)</th><th>O_2 flow rate (slm)</th><th>Temperature (°C)</th><th>Duration (h)</th><th>Thickness (µm)</th></tr><tr><td>3</td><td>1</td><td>1100</td><td>12</td><td>0.5</td></tr></table></td><td>1. Dry oxidation is less pinholes, which is better compared to wet oxidation.
2. Thickness of the oxide layer can be approximately identified by its colors.</td></tr>
<tr><td>2</td><td>STEP 1 – FORMING ALIGNMENT MARKS
1. Bake the wafer @200°C for 10 min. on contact hotplate to dehydrate the wafer, let it cool down to room temperature.
2. Prime the wafer with HMDS (use the same recipe for photoresist).
3. Pouring the photoresist 1813 (1828) on the wafer, ramp up for 15 s and accelerate it to 3500 (4000) rpm for 30 s. Then, ramp down for 15 s. The thickness of the photoresist should be about 1.5 (2.5) µm.
4. Softbake the wafer at 110°C for 60 s on contact hotplate.
5. Expose the wafer using the MA 56 mask aligner for 10 (12) s with UV light wavelength 365 nm at exposure dose of 10 mW/cm^2. The plastic MASK 1 with alignment marks is used.
6. Develop the wafer with MF-319 Developer for 70 s, dump rinse the wafer with DI water for 10 min. and dry with N_2 gun.
7. Inspect the wafer under optical microscope to determine if the desired patterns on the mask have been transferred to the photoresist.
8. Hardbake the wafer at 110°C for 60 s on contact hotplate.
9. Measure the thickness of the photoresist layer using profilometer. The thickness should be about 1.5 (2.5) µm.
10. Etch the SiO_2 using Buffered Oxide Etch (BOE) 7:1 with the etching rate of 110nm/min at room temperature. The etching time should be about 6 min.
11. Inspect the wafer under optical microscope to make sure the patterns are completely etched.
12. Strip photoresist with the Phranha solution for 5 min., dump rinse the wafer with DI wafer for 10 min and dry with the N_2 gun.
13. Insert the wafer into the holder to protect the backside of the wafer. Then quickly etch in BOE 7:1 for 5 s-10 s to etch the native oxide layer of 0.5 to 1 nm on top of the wafer. After a quick rinse in DI water, the wafer is put into KOH solution 25% by weight at 80°C for 40 min. or more to find the (111) planes. The Si etching rate is about 1.45 µm/min.
14. Dump rinse the wafer with DI water for 10 min., and dry it with the N_2 gun.
15. Inspect the wafer under the profilometer to see the patterns. The circular patterns should become the hexagons and the fan shape structure should be revealed to be undercut.

STEP 2 – FORMING DEEP LONG TRENCHES INTO SILICON WAFERS
1. Bake the wafer @200°C for 10 min. on contact hotplate to dehydrate the wafer, let it cool down to room temperature.
2. Prime the wafer with HMDS (use the same recipe for photoresist).
3. Pouring the photoresist 1813 on the wafer, ramp up for 15 s and accelerate it to 3500 rpm for 30 s. Then, ramp down for 15 s. The thickness of the photoresist should be about 1.5 µm.
4. Softbake the wafer at 110°C for 60s on contact hotplate.</td><td>1. HMDS is a flammable liquid and vapor. It is harmful if inhaled or absorbed through skin. Handle it in a vented chemical hood with care.
2. The wafer should be coated with photoresist as quickly as possible after HDMS. It is recommended that this should be performed no later than 60 min after the priming step.
3. UV intensity should be checked before exposure step to make sure the right intensity dose and uniform distribution across the whole wafers.
4. The after-develop-inspection step is critical for monitoring if a) the correct mask has been used; b) the qualities of the photoresist film are acceptable; c) the critical dimensions are within the specified tolerances; d) the registration or mask alignment is within specified limits.
5. BOE and KOH are extremely toxic and corrosive. Wearing proper gloves, goggles, and aprons… during operation.
6. In step 13, quickly etch the wafer in BOE 7:1 to remove native oxide layer is important. The process between BOE and KOH etch should be short and thorough.
7. Step 15 should be long enough to reveal the hexagonal patterns.
8. Aceton is not recommended to strip photoresist because it may cause residue photoresist on the wafer surface and is difficult to remove afterwards.</td></tr>
</table>

	5. Expose the wafer using the MA 56 mask aligner for 11 s with UV light wavelength 365 nm at exposure dose of 10 mW/cm^2. The glass MASK 2T with alignment marks is used. 6. Develop the wafer with MF-319 Developer for 70 s, dump rinse the wafer with DI water for 10 min. and dry with N_2 gun. 7. Inspect the wafer under optical microscope to determine if the desired patterns on the mask have been transferred to the photoresist. 8. Hardbake the wafer at 110°C for 60 s on contact hotplate. 9. Measure the thickness of the photoresist layer using profilometer. The thickness should be about 1.5 µm. 10. Etch the SiO_2 using Buffered Oxide Etch (BOE) 7:1 with the etching rate of 110nm/min at room temperature. The etching time should be about 4 min. 11. Inspect the wafer under optical microscope to make sure the patterns are completely etched. 12. Strip photoresist with the Phranha solution for 5 min., dump rinse the wafer with DI wafer for 10 min. and dry with the N_2 gun. 13. Insert the wafer into the holder to protect the backside of the wafer. Then quickly etch in BOE 7:1 for 5 s-10 s to etch the native oxide layer of 0.5 to 1 nm on top of the wafer. After a quick rinse in DI water, the wafer is put into KOH solution 25% by weight at 80°C (40% by weight at 70°C) for 50 – 65 (90-100) min. or more to find the (111) planes. The Si etching rate is about 1.45 (0.91) µm/min. 14. Dump rinse the wafer with DI water for 10min, and dry it with the N_2 gun. 15. Strip the remaining SiO_2 mask using Buffered Oxide Etch (BOE) 7:1. The etching time is about 1-2 min. 16. Dump rinse the wafer with DI water for 10min, and dry it with the N_2 gun. 17. Inspect the wafer under the profilometer to see the patterns. The final structures should have long trenches with vertical sidewalls.	9. Using PRIMER in STEP 2 is EXTREMELY IMPORTANT. Otherwise, the photoresist will stick on the wafer and is hard to remove!

References

[1] M. I. Haller and B. T. Khuri-Yakub, "Micromachined ultrasound materials," *Proc. IEEE Ultrason. Symp.*, pp. 403-405, 1991.

[2] T. Manh, G. U. Jensen, T. F. Johansen, and L. Hoff, "Microfabricated 1-3 composite acoustic matching layers for 15 MHz transducers," to be published in *Ultrasonics.*

[3] M. J. Madou, *Fundamental of Microfabrication: The Science of Miniaturization*, 2nd ed.: CRC,Press, 2002..

[4] G. T. A. Kovacs, *Micromachined Transducers Sourcebook*: WCB/McGraw-Hill, 1998.

[5] Y Uenishi, M Tsugai and M Mehregany, "Micro-opto-mechanical devices fabricated by anisotropic etching of (110) silicon," *Journal of Micromechanics and Microengineering,* vol. 5, pp. 305-312, 1995.

[6] T. D. James and et al., "A crystallographic alignment method in silicon for deep, long microchannel fabrication," *Journal of Micromechanics and Microengineering,* vol. 16, p. 2177, 2006.

[7] R. K. H. Minseung Ahn, and Mark L. Schattenburg, "Fabrication of ultrahigh aspect ratio freestanding gratings on silicon-on-insulator wafers," *J. Vac. Sci. Technol. ,* vol. 25, pp. 2593-2597, 2007.

[8] P. K. a. E. Obermeler, "Etch rate and surface roughness of deep narrow U-grooves in (110)-oriented silicon," *Micromech. Microeng.,* vol. 5, pp. 112-114, 1995.

[9] A. Diaz, "X-ray scattering studies of ordering phenomena in colloids confined in microcavity arrays," Ph.D dissertation, Eidgenössische Technische Hochschule ETH Zürich, 2006.

[10] P. Mao, "Ultra-high-aspect-ratio nanofluidic channels for high-throughput biological applications," Ph.D dissertation, Department of Mechanical Engineering, Massachusetts Institute of Technology, 2009.

[11] K. Seong-Hyok, L. Sang-Hun, L. Hyung-Taek, K. Yong-Kweon, and L. Seung-Ki, "(110) silicon etching for high aspect ratio comb structures," in *Emerging Technologies and Factory Automation Proceedings, 1997. ETFA '97., 1997 6th International Conference on*, 1997, pp. 248-252.

[12] A. T. T. Nguyen, T. Manh, and Lars Hoff, "Acoustic matching layer for high frequency ultrasound transducers made by anisotropic wet etching of silicon", in *Proc. of IMAPS Nordic*, Gorteborg, Sweden, 2010.

[13] H. Namatsu, K. Yamazaki, and K. Kurihara, "Supercritical drying for nanostructure fabrication without pattern collapse," *Microelectronic Engineering,* vol. 46, pp. 129-132, 1999.

[14] http://sindhu.ece.iisc.ernet.in/nanofab/twikii/pub/Main/Lithography/Lithography%20TroubleShooter_Microchem.pdf.

[15] K. Sato, M. Shikida, T. Yamashiro, M. Tsunekawa, and S. Ito, "Roughening of single-crystal silicon surface etched by KOH water solution," *Sensors and Actuators A: Physical,* vol. 73, pp. 122-130, 1999.

[16] K. Sato, M. Shikida, Y. Matsushima, T. Yamashiro, K. Asaumi, Y. Iriye, and M. Yamamoto, "Characterization of anisotropic etching properties of single-crystal silicon: effects of KOH concentration on etching profiles," in *Micro Electro Mechanical Systems, 1997. MEMS '97, Proceedings, IEEE., Tenth Annual International Workshop on*, 1997, pp. 406-411.

[17] K. Sato, M. Shikida, Y. Matsushima, T. Yamashiro, K. Asaumi, Y. Iriye, and M. Yamamoto, "Characterization of orientation-dependent etching properties of single-crystal silicon: effects of KOH concentration," *Sensors and Actuators A: Physical,* vol. 64, pp. 87-93, 1998.

Paper D

Microfabrication of Stacks of Acoustic Matching Layers for 15 MHz Ultrasonic Transducers

Tung Manh[a], Anh-Tuan T. Nguyen[a], Tonni F. Johansen[b,c] and Lars Hoff[a]

[a] Department of Micro and Nano Systems Technology, Vestfold University College, Horten, Norway

[b] Department of Acoustic, SINTEF ICT, Trondheim, Norway

[c] Department of Circulation and Medical Imaging, Norwegian University of Science and Technology, Trondheim, Norway

This paper has been accepted and available online in Ultrasonics, 2013.

Microfabrication of Stacks of Acoustic Matching Layers for 15 MHz Ultrasonic Transducers

Tung Manh[a*], Anh-Tuan Thai Nguyen[a], Tonni F. Johansen[b,c] and Lars Hoff[a]
[a]Department of Micro and Nano Systems Technology, Vestfold University College, Horten, Norway
[b]Department of Acoustic, SINTEF ICT, Trondheim, Norway
[c]Department of Circulation and Medical Imaging, Norwegian University of Science and Technology , Trondheim, Norway
[*]Corresponding author. Email: tung.manh@hive.no. Phone: +47 33037928.

Abstract: This paper presents the design, manufacture and testing of novel 15 MHz broadband piezoelectric single-element ultrasonic transducers with acoustic matching layers fabricated by silicon micromachining. To effectively couple energy from the piezoelectric layer to the load, a stack of acoustic matching layers with descending acoustic impedances was built, starting with a silicon substrate and using lithography and etch to design silicon and polymer layers with the desired properties. Two matching layer configurations were tested: a double layer structure with composite and polymer and a triple layer structure with silicon, composite, and polymer. The composite is a biphase material of silicon and polymer in 2-2 connectivity. The structures were manufactured by anisotropic wet etch of a (110)-oriented Silicon-on-Insulator wafer. The wafer was etched by KOH 40 wt%, to form deep, long trenches that were subsequently filled with epoxy. This resulted in a stack of three layers: The silicon substrate, a silicon-polymer composite intermediate layer, and a polymer layer on the top. These stacks were bonded to PZT disks to form acoustic transducers. The acoustic performance of the fabricated transducers was tested in a pulse-echo setup, where center frequency, -6 dB relative bandwidth and insertion loss were measured. The transducer with two matching layers was measured to have a relative bandwidth of 70.2%, two-way insertion loss 18.4 dB and pulse length 196 ns. The transducers with three matching layers had fractional bandwidths from 90 to 93%, two-way insertion loss ranging from 18.3 to 25.4 dB, and pulse lengths 326 and 446 µs. The long pulse lengths of the transducers with three matching layers were attributed to ripple in the passband.

Keywords: High frequency transducers, silicon-polymer composite, silicon micromachining, matching layer.

1. Introduction

Ultrasonic investigation of microstructures in soft tissues, e.g. composition of small tumors or a vessel wall, requires an imaging system that can provide high resolution in both the lateral and the axial direction. Such a system requires a high frequency (10-100 MHz) broadband ultrasound transducer, as the axial resolution is dependent on the bandwidth and the lateral resolution is inversely proportional to the center frequency of the transducer [1]. Most of the current transducers are based on a piezoelectric ceramic or a ceramic/polymer composite as the active layer, normally working in thickness mode. To operate in the frequency range from 10 to 100 MHz, the thickness of this layer must be between 20 and 200 µm. This is difficult and expensive to achieve by conventional fabrication methods, e.g. lapping [2]. Moreover, the acoustic impedance of the active layer, 20 to 40 MRayl for a ceramic, or 15 to 20 MRayl for a composite, is much higher than that of the human tissue, 1.6 MRayl. To enhance transmission of acoustic energy from the piezoelectric element into the tissue, acoustic matching layers with acoustic impedances between that of the active layer and the load are required [3]-[6]. Several matching approaches are available [3]-[5], but finding single materials with optimal acoustic impedances for these configurations are in general not possible, and composites are often used [6]. Typical composites used as matching layers are mixtures of metal particles in a polymer matrix. However, employing these materials at high frequencies, e.g. 30-100 MHz, introduces some challenges such as non-uniformity, high attenuation and dispersion [6].

We have previously proposed a novel design for high frequency broadband ultrasound transducers. By using silicon micromachining, i.e. lithography and etch, to fabricate composite acoustic matching layers, we have shown that some of these problems may be resolved [7]. In these designs, the active piezoelectric layer can be manufactured by thick-film technology, which is able to produce the ceramic layer in the range of interest (20-200 µm). The ceramic film can be made either by tape casting methods [8] and subsequently bonded to a silicon substrate, or by screen-printing or spin-coating directly on a platinum-coated silicon substrate [2], [9], [10]. The substrate is micromachined to build a stack of multiple matching layers with descending acoustic impedance from the piezoelectric layer to the tissue, while the transducer is left air backed. Instead of performing alternately deposition and lapping layer by layer as in conventional transducer manufacturing, the proposed structure allows us to build a stack of multiple layers in one process, which is a great advantage when the transducers become thin, e.g. less than 100 µm. These fabrication methods are well established for mass-production in the MEMS industry, and applying this technology to manufacture ultrasound transducers may open for mass production of low cost high frequency broadband transducers.

This paper demonstrates the feasibility of manufacturing these transducers. Two configurations of matching layers were tested: A two layer design, where the inner layer is a silicon-polymer composite and the outer layer is a polymer, and a three layer design, where the inner layer is silicon, the intermediate layer is a silicon-polymer composite and the outer layer is a polymer. The active element used in this feasibility study was a standard PZT piezoelectric ceramic disc. The silicon-polymer composite was made as 2-2 connectivity, i.e. consisting of long, narrow lines of alternately silicon and polymer. The transducer prototypes were fabricated for operating at 15 MHz. Their performance was tested by pulse-echo measurements in a water tank. Center frequency, bandwidth and insertion loss were measured and compared with simulation results from the Mason model [11]. These measurements showed good agreement with the simulations.

2. Materials and methods

2.1. Manufacturing process

The fabrication process illustrated in was used to build the transducers. First, a 0.5 µm thick layer of thermal silicon dioxide, SiO_2, was grown on top of a 100 mm diameter SOI wafer (Ultrasil Corporation, USA). The SOI wafer consist of an (83±1) µm thick (110)-oriented Si device layer, a 0.5 µm thick buried SiO_2 layer, and a (500±10) µm thick (100)-oriented Si handle layer (Figure 1a). The (110)-orientation of the Si device layer was chosen to allow use of anisotropic wet-etch to form deep, long, vertical sidewall trenches along the {111} crystal planes [12]. In contrast, anisotropic wet etch on the more common (100)-oriented Si wafers causes structures with 54.7º sidewalls. A 1.5 µm thick layer of positive photoresist (*S1813*, Shipley Company Inc., Boston MA, USA) was spin coated on top of the oxide layer. A glass mask (The International Phototool Company, LLC, CO, USA) with parallel line features, tolerance ± 0.3 µm, was used. These features were transferred to the photoresist using standard photolithography with contact mask exposure. The feature lines were aligned to the {111} crystal planes of the silicon wafer with an accuracy of 0.1º, using a fan-shaped structure and the method described in [13]. The SiO_2 was first patterned in buffered oxide etch, BOE 7:1. The patterned oxide then served as mask for the anisotropic wet-etch of the silicon device layer (Figure 1b). Silicon wet etch was performed with KOH 40% wt etchant at 70°C for 100 minutes, forming deep grooves into the substrate (Figure 1c). The SiO_2 mask was then stripped in BOE 7:1. The wafer was rinsed in de-ionized (DI) water and air dried. Then the grooves in the etched wafer were filled by Spurr's epoxy (*Low viscosity embedding media Spurr's Kit*, Electron Microscopy Sciences, Hatfield, PA, USA), and cured at 70°C for 8 hours to form a stack of silicon, composite and polymer (Figure 1d). The processed wafers were diced into 6mm x 6mm dies using a *Disco Abrasive Systems* dicing saw (Disco Corporation, Tokyo, Japan). The top polymer and bottom silicon layers of each sample were ground to their target thicknesses and their surfaces were polished. This forms a stack of multiple matching layers. The lapping process was done using *MultiPrep™ System* grinding and polishing equipment (Allied High Tech Products Inc., CA, USA) with a coarse to fine grit scheme with accuracy of 1 µm in thickness and 0.01° in angular positioning. The final lapping particle diameter was 5 µm and the polishing chemical was a mixture of colloidal silica and 0.05 µm alumina (Allied High Tech Products Inc., CA, USA).

The finished stack was glued to a 6 mm x 6 mm PZT plate (*3195HD*, Boston Piezo-optics, Bellingham, MA, USA) using Spurr's epoxy, to form a transducer (Figure 1e). The roughness was investigated by an interferometer (*Wyko NT9100 Technical*, Veeco Instruments Inc., USA), giving an arithmetic mean roughness R_a of about 0.5-0.6 µm for PZT and 0.2-0.3 µm for the final lapped samples. From this, the glue bonding layer thickness was estimated to be less than 1 µm, based upon the assumption that this thickness was defined by the total surface roughness of the PZT and the composite [14]. The PZT is (140±1) µm thick. The electrodes were processed to form a coaxial pattern on the back side, to allow electrical connection from the back side of the disc. This is described in section 2.3. The coaxial electrode pattern has a center circle diameter 3.2 mm, and the gap between the center and the ring is 0.4 mm. The transducer was mounted on an SMA connector using conductive epoxy (*Epo-Tek EE129-4*, Epoxy Technology, Inc., Bellerica, MA, USA). A 0.12 mm diameter wire connected the transducer electrode to the center connector of the SMA. A Teflon tube was designed to cover the SMA and make the transducer waterproof (Figure 1f).

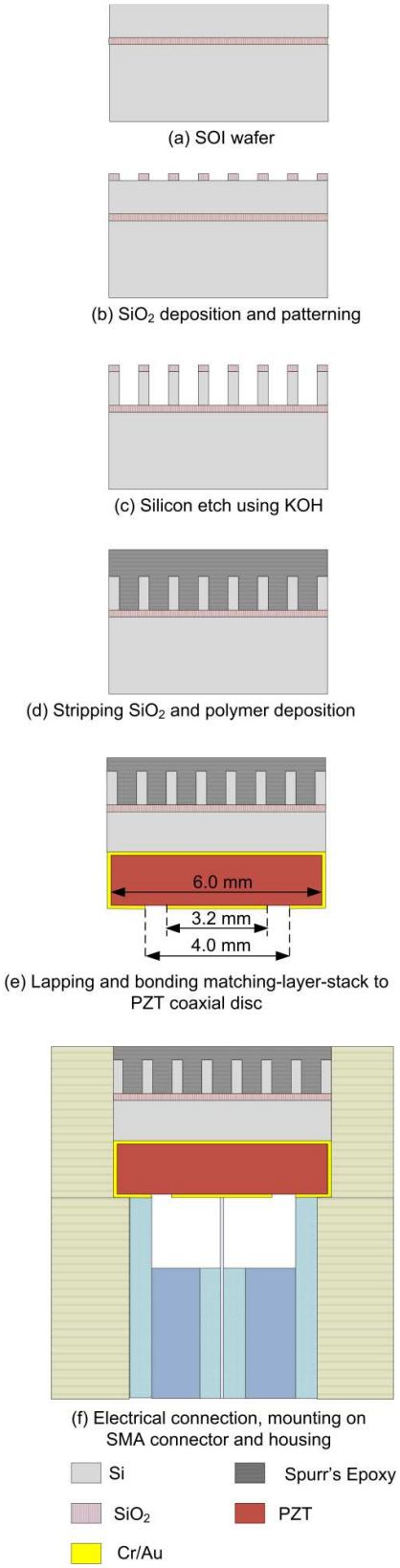

Figure 1 Main fabrication steps to manufacture multiple micromachined ultrasound transducers.

Table 1 Design specifications of the transducers in this study. The values given in parentheses are the theoretical values to achieve a transfer function of Chebyshev bandshape, calculated from [17] for acoustic impedance Z_{PZT} = 37.1 MRayl and Z_{load} = 1.54 MRayl. Material properties for Spurr's epoxy and silicon are from [15].

Parameter	Active layer	ML_1[b]	ML_2	ML_3
Two-matching layer	PZT[a]	Composite	Spurr's epoxy	
Acoustic impedance (MRayl)	37.1	9.5	2.4	—
Longitudinal velocity (m/s)	4760	6230	2200	—
Target thickness (μm)	140	83	36	—
Mechanical loss tangent	0.012	0.03	0.03	
Three-matching layer	PZT	Silicon	Composite	Spurr's epoxy
Acoustic impedance (MRayl)	37.1	19.7 (24.9)	7.6 (7.6)	2.4 (2.3)
Longitudinal velocity (m/s)	4760	8440	5400	2200
Target thickness (μm)	140	130	83	36
Mechanical loss tangent	0.012	0.0025	0.03	0.03

[a]PZT : PZT properties were estimated by curve-fitting method.
[b]ML : matching layer.

2.2. Acoustic impedance matching

Acoustical matching the high impedance of the piezoelectric material (~37 MRayl) to the relatively low impedance of human tissue (~1.6 MRayl) is challenging. For the two matching layer configuration, we followed the guidelines recommended by Desilets *et al*. [3] to achieve a maximally flat response. According to this theory, the optimal acoustic impedance values for the inner and outer matching layers are 9.5 and 2.4 MRayl (Table 1). Spurr's epoxy, with acoustic impedance 2.4 MRayl, was chosen as the outer matching layer and as the filler in the silicon-polymer composite matching layer. To achieve an acoustic impedance of 9.5 MRayl, a 2-2 composite with 35% silicon volume fraction is required, according to the dynamic model of guided waves [15], [16]. Due to the risk of cracking the composite material along the silicon crystal orientations during the grinding process, we kept a thin additional layer of silicon, about 10 μm thick, underneath the composite layer. As silicon has a high longitudinal sound velocity (8440 m/s) and low mechanical loss (loss tangent 0.0025 [15]), this layer has almost no influence on the transducer performance. Simulations with and without this thin silicon layer predict less than 1% difference in both bandwidth and sensitivity.

For the triple matching layer configuration, we used a different set of acoustic impedance values, shown in Table 1. Starting at the inner layer, close to the PZT disc, and proceeding outwards, the layers consist of silicon (19.7 MRayl), 2-2 composite with 24% silicon volume fraction (7.6 MRayl) and Spurr's epoxy (2.4 MRayl). These values were designed to approximate a Chebyshev bandshape transfer function, which ideally consists of layers with impedances 24.9, 7.6 and 2.3 MRayl [17].

2.3. Piezoelectric active element

A 1.54 cm x 1.54 cm PZT plate with 0.3 μm chrome/gold (Cr/Au) electrodes was processed to form a coaxial electrode pattern, to gain access to the front electrode from the back side. A 1.5 μm layer of photoresist S1813 was spin-coated on top of the PZT plate and patterned by standard lithography. The Cr and Au layers were etched using *Nickelkromets MC2* (Sunchem AB, Partille, Sweden) and *Guldets 22196* (Sunchem AB). The photoresist was stripped and the etched patterns were diced into 6mm x 6mm dies. A layer of Cr/Au was sputtered on the

sides of the PZT dies to create an electrical connection from the front to the back electrode. Electrical impedance of the diced plates, in air, was measured using an *HP 8753D* Network Analyzer (Agilent Technologies, Santa Clara, CA, USA). The impedance measurements were used to estimate the electromechanical properties of the PZT discs in the thickness mode, by fitting the measured impedances to calculations from the Mason model using the Nelder-Mead simplex method [19]. This fitting was done using 201 data points over the frequency range from 10 to 20 MHz [15], [18].

2.4. Silicon-polymer 2-2 composite

The silicon-polymer 2-2 composite is the key layer in our ultrasound transducer designs. The composites have a constant period, 22.5 µm, designed according to the guidelines in [18] to avoid lateral resonances. Composites with two volume fractions were made: Composite A, with 35% silicon volume fraction, was used in the two-layer acoustic matching configuration, while composite B, with 24% silicon volume fraction, was used in the three-layer configuration. Hence, the target silicon bar widths are 7.9 µm for composite A and 5.4 µm for composite B. The two composites were designed and fabricated on the same silicon wafer. The uniformity of the fabricated silicon and polymer composites was evaluated by taking Scanning Electron Microscopy (SEM) cross-sections of several randomly selected samples from each set. To evaluate the composite properties, two samples from each set were chosen and the silicon and polymer layers were removed by lapping, leaving the composites layer alone. These composites were glued to PZT plates (as described in section 2.3) using Spurr's epoxy. This gave a set of testing transducers, consisting of a single composite layer on top of a coaxial PZT plate. The bonding thickness of the epoxy was not determined, but estimated to less than 1 µm, based upon the assumption that the total surface roughness of the PZT and the composite define the epoxy thickness [14]. The acoustic properties of the composite, i.e. acoustic impedance and longitudinal velocity were estimated from electrical impedance curves measured on these transducers, using the same procedure as for the PZT discs. As the bonding epoxy layer between the PZT disc and the composite is much thinner than the wavelength at the operating frequency, this glue layer is not included in the fit. The estimated properties were compared with those calculated from the dynamic model of guided waves [15], [16] and the iso-strain theory [20].

2.5. Transducer characterization

Acoustic pulse-echo measurements were performed in a water tank to investigate the transducers' bandwidth and sensitivity. One two-matching-layer transducer and two three-matching-layer transducers were tested. The transducers were connected to a 50 Ω signal generator (*Agilent 33522A*, Agilent Technologies, Inc., Santa Clara, CA, USA) via a 2 m RG-58 cable. A single cycle 16 V amplitude sine wave with center frequency f = 15 MHz was used to drive the transducers. Received echo responses were acquired from a polished brass plate, sampled on a digital oscilloscope (*WaveSurfer 42Xs*, LeCroy Corporation, Chestnut Ridge, NY, USA) and transferred to a PC for further analysis. The brass target was a cylinder with 44 mm diameter and 41 mm thickness, placed at normal incidence to the acoustic axis in the near field zone (about less than 1 cm from the transducer surface). The insertion loss was calculated as the ratio between the received echo and the transmitted signal. A fast Fourier transform (FFT) was performed on the received waveforms to obtain the frequency response. The bandwidth was defined from the frequencies where the power spectrum was reduced 6 dB relative to its peak value. The pulse length was determined from the duration where the amplitude was reduced 20 dB below its peak value.

3. Results

3.1. Piezoelectric active element

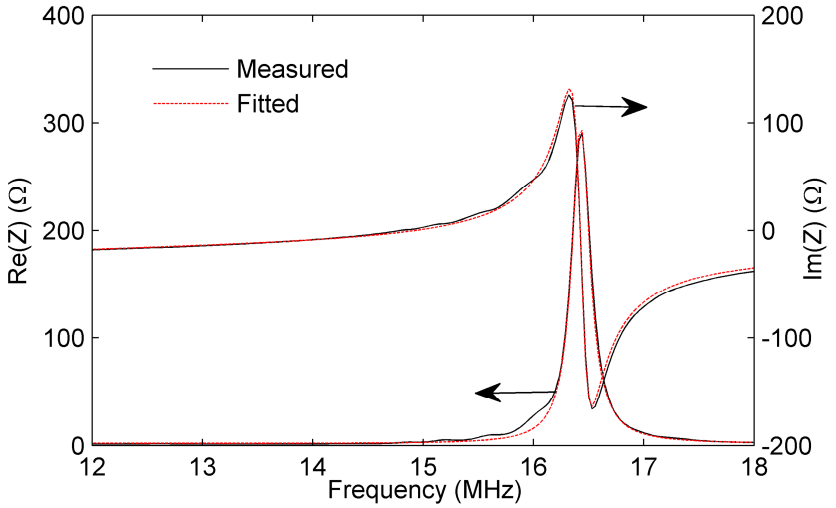

Figure 2 The measured and curve-fitted impedances of the PZT disc alone in air to estimate the active element of the transducers.

Table 2 The estimated material properties for the proceed PZT coaxial discs

Parameter	Notation	Value	Manufacturer
Density (kg/m^3)	ρ	7800[a]	7800
Elastic stiffness constant at constant electric displacement ($\times 10^{11}$ N/m^2)	c_{33}^D	(1.77±0.25)	1.06
Mechanical loss tangent	$\tan\delta_m$	0.012±0.001	0.0125
Relative permittivity	$\varepsilon^S/\varepsilon_0$	763±69	1900
Electrical loss tangent	$\tan\delta_e$	0.078±0.057	0.018
Electromechanical coupling for thickness mode	k_t	0.465±0.005	0.48
Electromechanical coupling loss tangent	$\tan\delta_k$	0.020±0.010	—

The measured and curve-fitted impedances of a typical PZT disc operating in air are shown in Figure 2. Table 2 lists the material properties estimated from the impedance measurements, based on measurements on five samples from the same batch. The material data given by manufacturer are given for comparison.

3.2. Silicon-polymer composite

The polymer kerf and silicon widths for the obtained composite structures are shown in Table 3, with the target dimensions given in parentheses. A SEM image of the cross-section of a composite of type B is shown in Figure 3. The electrical impedance measured on a transducer operating in air is shown in Figure 4, together with impedance curves fitted to the Mason model. This transducer consisted of a single composite B matching layer bonded on top of a 15 MHz PZT plate. These impedance measurements were used to estimate the composite acoustic properties, the resulting parameter estimates are shown in Table 4.

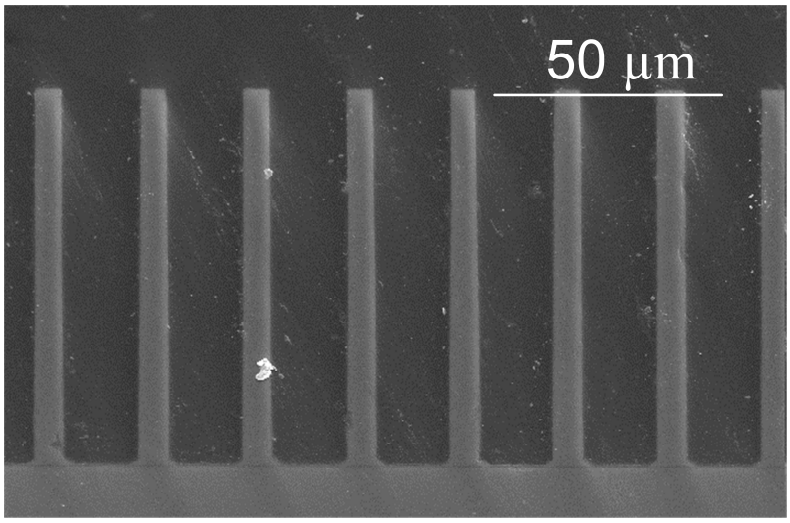

Figure 3 A cross-section image of one of the 2-2 composite B structures fabricated by wet etching and used in the three-matching-layer configuration. The bright parts in the image are silicon, the dark parts are epoxy. The white dots are from the solutions to prepare the sample cross-sections. The composite period is 22.5 μm.

Table 3 Polymer kerf and silicon width measurements for the fabricated silicon-polymer 2-2 composite

Parameter	Dimensions (μm)	
	Composite A	Composite B
Period	22.50	22.50
Polymer kerf width	15.00 (14.6)[a]	16.80 (17.10)
Silicon width	7.50 (7.90)	5.70 (5.40)
Silicon σ (standard deviation)	0.50	0.50

[a]The target design dimensions are depicted between parentheses.

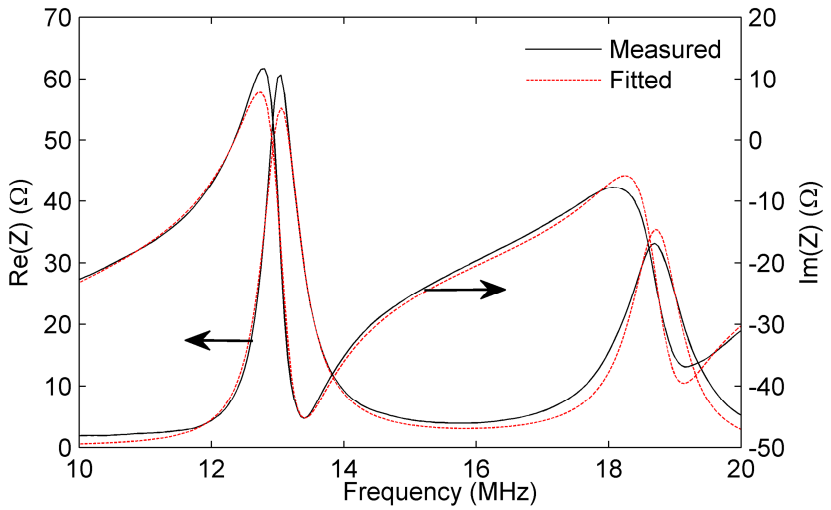

Figure 4 The measured and curve-fitted impedances of one typical transducer including a single composite layer bonded on top of a 15 MHz PZT disc operating in air. These results were used to estimate the acoustic properties of the composite. This measurement is on a composite from set B with thickness 70 µm.

Table 4 The estimated material properties for silicon-polymer 2-2 composites from curve-fitting the electrical measurements to the mason model. The modeled values calculated from dynamic model of guided waves [15] using the measured dimensions from Table 3.

Parameter	Composite A			Composite B		
	Modeled		Estimated	Modeled		Estimated
	Iso-strain	Dynamic		Iso-strain	Dynamic	
Longitudinal wave velocity (m/s)	6420 ± 138	5900 ± 91	5818 ± 300	5865 ± 173	5609 ± 225	4886 ± 166
Acoustic impedance (MRayl)	9.7 ± 0.4	8.9± 0.3	7.85 ± 0.65	8.30 ± 0.40	7.92 ± 0.47	7.4 ± 0.70

3.3. Transducer characterization

The measured pulse-echo results for one two-matching-layer transducer and two three-matching-layer transducers are shown in Figure 5, Figure 6, and Figure 7, respectively; together with the simulation results from the Mason model. The received waveforms are shown in the upper graphs, whereas their corresponding spectra are presented in the lower graphs. The spectra were normalized to their maxima for the ease of comparison between simulated and measured results. The comparison between the simulated and measured results is summarized in Table 5.

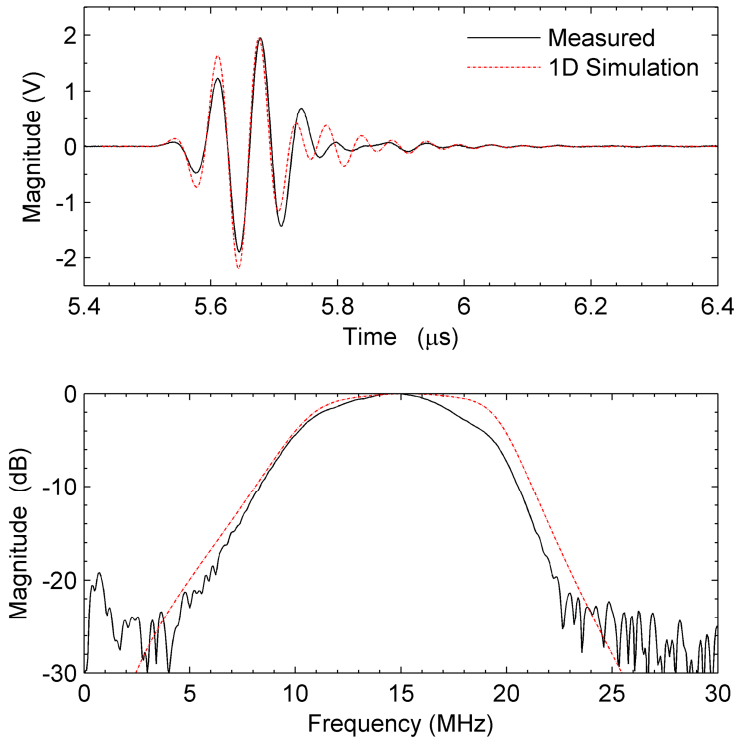

Figure 5 Pulse-echo responses for a two-matching transducer working at 15 MHz, measured (solid lines) and calculated from the Mason model (dotted lines).

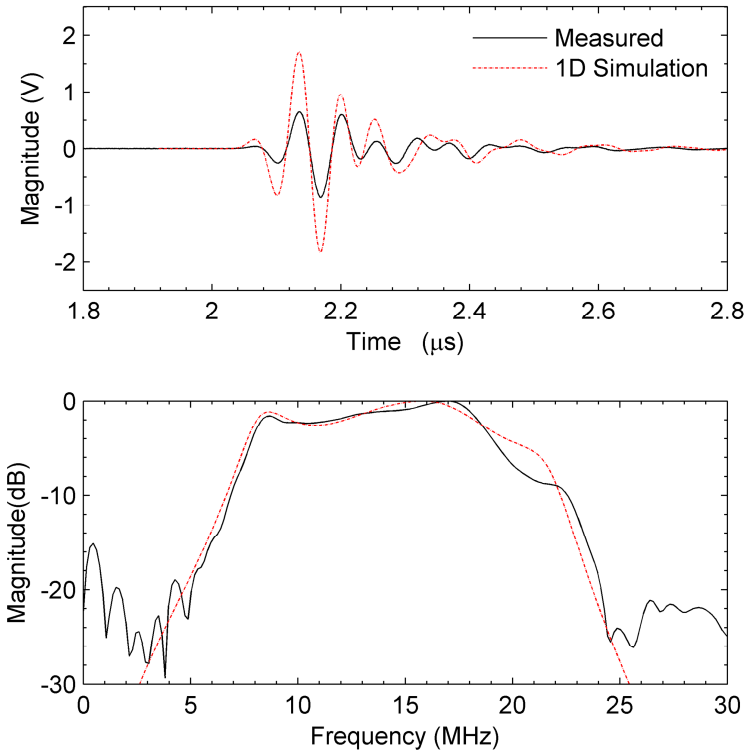

Figure 6 Pulse-echo responses for a three-matching transducer working at 15 MHz (No.1), measured (solid lines) and calculated from the Mason model (dotted lines).

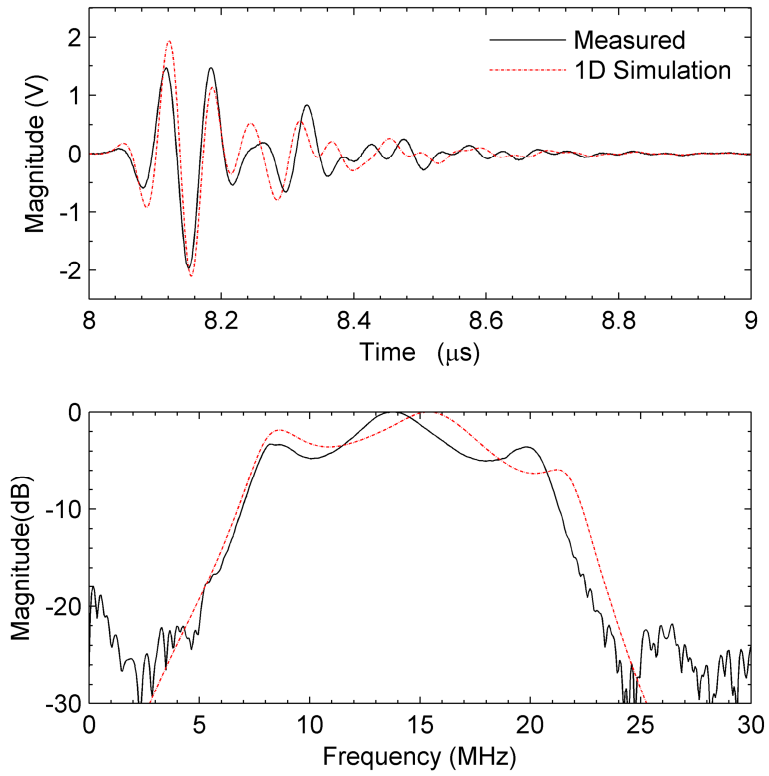

Figure 7 Pulse-echo responses for a three-matching transducer working at 15 MHz (No.2), measured (solid lines) and calculated from the Mason model (dotted lines).

4. Discussion

The electromechanical properties of the fabricated PZT plates differ from the material data given by the manufacturer. This can be expected, as the manufacturer gives values measured at 1 kHz. Our results are consistent with the parameters from Foster *et al.* [20], who measured in the frequency range 20 to 80 MHz.

The SEM image of the fabricated 2-2 composite illustrated in Figure 3 show vertical sidewalls and flat bottom trenches, suited to be used as one matching layer in multiple-layer stacks. The obtained silicon widths matched to the desired dimensions within 5%, as shown in Table 3. The uniformity of the silicon bars is highly dependent on the tolerance of the glass mask. In this work, the tolerance on the glass mask was 0.3 µm, causing a tolerance in the silicon bar width of 0.5 µm after etching. Reducing the mask tolerance would provide better uniformity. When using this fabrication process, the minimum obtainable lateral dimensions of the silicon-polymer 2-2 composite are primarily limited by the resolution of the features on the mask and the lithography technology. With better mask resolution, e.g. less than 1 µm, and more sophisticated lithography, such as electron beam, it is possible to achieve composites with sub-micron silicon bars [22], [23], suited to be used as matching layers in ultrasound transducers at frequencies above 100 MHz. The estimated material parameters of the micromachined composites are closer to the values calculated from the dynamic model of guided waves than those from the iso-strain model, as mentioned in [24] . The deviations between the estimated and calculated values from the dynamic model of guided waves for velocity and acoustic impedance are 1.4% and 11.8% for composite A and 12.9% and 6.6%

for composite B. The difference can be attributed to the dispersion in the composite and to an influence from the bonding layer between the matching layers and the PZT disc. Due to the high acoustic impedance mismatch between the Spurr's epoxy used for bonding and the composite, the acoustic properties of the complete stack are sensitive to the bonding thickness [25]. We found that the velocity estimate will increase about 10% when the thickness of the epoxy bonding layer increases from 0.1 µm to 1 µm. A different approach to accurately estimate the thin composite matching layer might be considered, e.g. the method based on the impedance matching principle by H. Wang [26]. By transmitting plane waves through a silicon substrate with and without a quarter-wavelength composite layer on top and taking the ratio of these two transfer functions in the frequency domain, one may deduce the velocity of the composite layer at the frequency where this ratio is maximum [26].

Pulse-echo measurements on the transducer with two matching layers shows close agreement with the simulations from the Mason model (see Table 5). A large -6 dB fractional bandwidth (70.2%), low insertion loss (18.4 dB) and a short pulse (196 ns) are achievable. The performance of this transducer demonstrates the feasibility of using silicon micromachining to manufacture high frequency broadband ultrasound transducers.

Pulse-echo measurements on the three-matching-layer transducers show very large fractional bandwidths, 90% to 93%, but display long pulse duration, 326 to 446 ns. The reason for the difference in echo level between simulated and measured results in one of the transducer measurements was not determined, but it might be attributed to a poor electrical connection between the transducer and the SMA connector. The long pulse durations directly link to the level of ripples in the transducers spectra [5]. The measured ripple levels for the three-layer transducers were 2.3 and 4.7 dB, see Figure 6 and Figure 7, and less ripple in the transducer spectrum means a shorter pulse. The performance of this three-matching-layer configuration can be improved by optimizing the matching layers impedances and thicknesses under constraints to bandwidth, ripple and loss [5].

Silicon is a crystal with cubic symmetry, and the acoustic impedance depends on its orientation. Commercially available silicon wafers have crystal orientations (100), (110) and (111) with corresponding acoustic impedances of 19.7, 21.3 and 21.7 MRayl, respectively [27]. When a specific polymer and silicon orientation has been chosen, the properties of the intermediate layer can be adjusted and optimized by changing the volume fraction of silicon in the composite material. The microfabrication processes presented in this paper, the anisotropic wet etch; can only be used on (110)-oriented silicon wafers.

Due to the high acoustic impedance mismatch between Spurr's epoxy, PZT and silicon (2.4, 37.1 and 19.7 MRayl) as well as the low velocity of Spurr's epoxy (2200 m/s), the bonding thickness between the PZT plates and the matching stacks must be kept thin. The bonding layer was found to have higher influence on the three-matching-layer configuration than on the two-layer configuration. According to our calculations, the bonding thickness could be tolerated to be 2 to 3 µm for the two-matching- layer transducers. However, in the three-matching-layer configuration, this layer must be less than 1 µm, to keep the ripple level less than 6 dB in the transducer spectra. The maximum acceptable thickness of the bonding layer scales with frequency, hence, to make a transducer working at higher frequencies, a thinner epoxy bonding layer must be used. For example, a Spurr's epoxy thickness must be less than 0.15 µm for a transducer operating at 100 MHz, and this is not achievable by the described technology. To resolve this, thermo-compression bonding with indium could be used, at a thickness about 0.65 µm [25]. As indium has higher acoustic impedance than epoxy, a thicker bonding layer would be tolerated. Alternatively, the bonding layer problem would be eliminated by using a PZT thick-film printed directly on a platinum-coated silicon wafer [9], [10].

5. Conclusion and outlook

This paper describes how double- and triple-matching-layer transducers operating at 15 MHz have been designed, built and tested. Silicon micromachining technology from the MEMS industry was used to fabricate silicon-polymer composite layers with specified acoustic properties. Transducers with large bandwidth (>70%), and low insertion loss (<25.5 dB) were obtained. The resulting two-matching-layer transducer showed good performance, with pulse length 195 ns. For the three-matching-layer, the bandwidth was larger, but the pulses longer. This was attributed to ripple in the passband. However, the three-matching-layer transducer performance can be improved by optimizing the design. Transducers operating at 15 MHz were fabricated, but higher frequencies can be obtained by scaling down the dimensions. By combining the wet etching of (110)-oriented silicon with thick-film PZT, the process described can be used to manufacture broadband ultrasound transducers working at frequencies up to 100 MHz.

Table 5 Comparison between the simulated and measured transducer performance

Transducer	Mason modeling				Measured results			
	f_c (MHz)[a]	BW (%)	IL (dB)	PL (ns)	f_c (MHz)	BW (%)	IL (dB)	PL (ns)
Two-matching layer	14.9	74.3	17.8	258	14.6	70.2	18.4	196
Three-matching layer No.1	14.3	97.7	19.2	331	13.6	90	25.4	326
Three-matching layer No.2	14.0	97.2	18.1	393	14.2	93	18.3	446

[a] f_c is the center frequency; BW is the -6dB bandwidth; IL is the insertion loss; and PL is the 20 dB pulse length.

References

[1] B. A. Angelsen, *Ultrasound Imaging: Waves, signals and signal processing*, Trondheim, Norway: vol. 1, Ematec 2000, ch.3.

[2] Q. Q. Zhang, F. T. Djuth, Q. F. Zhou, C. H. Hu, J. H. Cha, and K. K. Shung, "High frequency broadband PZT thick film ultrasonic transducers for medical imaging applications," *Ultrasonics*, vol. 44, pp. 711-715, 2006.

[3] C. S. Desilets, J. D. Fraser and G. S. Kino, "The design of efficient broadband piezoelectric transducers," *IEEE Trans. on sonics and ultrasonics*, vol SU 25, no. 3, pp. 115-125, 1978.

[4] T. Inoue, M. Ohta and S. Takahashi, "Design of ultrasonic transducers with multiple acoustic matching layers for medical application," *IEEE Trans. Ultra. Ferro. Freq. Contr*., vol. 14, pp. 8-15, 1987.

[5] T. L. Rhyne, "Computer optimization of transducer transfer functions using constraints on bandwidth, ripple, and loss", *IEEE Trans. Ultra. Ferro. Freq. Contr*., vol. 43, pp. 1136-1149, 1996.

[6] S. Rhee, T. A. Ritter, K. K. Shung, H. Wang, and W. Cao, "Materials for acoustic matching in ultrasound transducers," *Proc. IEEE Ultrason. Symp*., pp. 1051-1055 vol.2, 2001.

[7] A.-T. T. Nguyen, T. Manh, L. Hoff, T. F. Johansen, and G. U. Jensen, "Fabrication of silicon-polymer composite acoustic matching layers for high frequency transducers," *Proc. Ultrason. Symp.*, pp. 2064-2067, 2010.

[8] F. Levassort, T. Bove, E. Ringgaard, L. P. Tran-Huu-Hue, J. Holc, and M. Lethiecq, "A complete range of tape-cast piezoelectric thick films for high frequency ultrasonic transducers," *Proc. Ultrason. Symp.*,pp. 2003-2006, 2003.

[9] T. Hedegaard, T. Pedersen, R. L. Moeller, K. Hansen, T. Zawada, and E. V. Thomsen, "Screen printed thick film based pMUT arrays," *Proc. Ultrason. Symp.*,pp. 2126-2129, 2008.

[10] A. Bardaine, P. Boy, P. Belleville, O. Acher, and F. Levassort, "Improvement of composite sol-gel process for manufacturing 40 µm piezoelectric thick films," *Journal of the European Ceramic Society*, vol. 28, pp. 1649-1655, 2008.

[11] W. P. Mason, *Electromechanical transducers and wave filters.* 2nd ed., New York: D. Van Nostrand Co., pp. 201-209, 399-409, 1948.

[12] M. I. Haller and B. T. Khuri-Yakub, "Micromachined ultrasound materials," *Proc. IEEE Ultrason. Symp*., pp. 403-405, 1991.

[13] Y Uenishi, M Tsugai and M Mehregany, "Micro-opto-mechanical devices fabricated by anisotropic etching of (110) silicon," *Journal of Micromechanics and Microengineering*, vol. 5, pp. 305-312, 1995.

[14] H. J. Vos, M. E. Frijlink, E. Droog, D. E. Goertz, G. Blacquiere, A. Gisolf, N. De Jong and A. F. W. Van Der Steern, "Transducer for harmonic intravascular ultrasound imaging," *IEEE Trans. Ultra. Ferro. Freq. Contr*., vol. 52, pp. 2418-2422, 2005.

[15] T. Manh, G. U. Jensen, T. F. Johansen and L. Hoff, "Modeling of micromachined silicon-polymer 2-2 composite matching layers for 15 MHz ultrasound transducers," submitted for publication.

[16] X. Geng, "Numerical modeling and experimental study of piezocomposite transducers," Ph.D dissertation, The Pennsylvania State University, 1997.

[17] T. Gudra and K. J. Opielinski, "Influence of acoustic impedance of multilayer acoustic systems on the transfer function of ultrasonic airborne transducers," *Ultrasonics*, vol. 40, pp. 457-463, 2002.

[18] T. S. T. Ritter, R. Tutwiler and K. K. Shung, "A 30-MHz Piezo-Composite Ultrasound Array for Medical Imaging Applications," *IEEE Trans. Ultra. Ferro. Freq. Contr.*, vol. 49, pp. 217-230, 2002.

[19] J. A. Nelder and R. Mead, "A Simplex Method for Function Minimization," *The Computer Journal*, vol. 7, pp. 308-313, 1965.

[20] W. A. Smith and B. A. Auld, "Modeling 1-3 Composite Piezoelectrics: Thickness-Mode Oscillation," *IEEE Trans. Ultra. Ferro. Freq. Contr.*, vol. 38, pp. 40-47, 1991.

[21] F. S. Foster, L. K. Ryan, and D. H. Turnbull, "Characterization of lead zirconate titanate ceramics for use in miniature high-frequency (20-80 MHz) transducers," *IEEE Trans. Ultra. Ferro. Freq. Contr*., vol. 38, pp. 446-453, 1991.

[22] A. Diaz, "X-ray scattering studies of ordering phenomena in colloids confined in microcavity arrays," Ph.D dissertation, Eidgenössische Technische Hochschule ETH Zürich, 2006.

[23] R. K. H. M. Ahn, and M. L. Schattenburg, "Fabrication of ultrahigh aspect ratio freestanding gratings on silicon-on-insulator wafers," *J. Vac. Sci. Technol.* , vol. 25, pp. 2593-2597, 2007.

[24] T. Manh, G. U. Jensen, T. F. Johansen, and L. Hoff, "Microfabricated 1-3 composite acoustic matching layers for 15 MHz transducers," to be published in *Ultrasonics.*

[25] E. K. Sittig, "Effects of bonding and electrode layers on the transmission parameters of piezoelectric transducers used in ultrasonic digital delay lines," *IEEE Trans. Sonics and Ultrasonics*, vol. SU-16, No. 1, 1969.

[26] Haifeng Wang and Wenwu Cao, "Characterizing ultra-thin matching layers of high frequency ultrasonic transducer based on impedance matching principle", *IEEE Trans. Ultra. Ferro. Freq. Contr*., vol. 51, pp. 211-215, 2004.

[27] D. Royer amd E. Dieulesaint, *Elastic waves in solids I: Free and Guided Propagation*, Springer, Verlag-Berlin Heidelberg, pp. 200, 2000.